THE EUROPEAN
PHYSICAL JOURNAL C

Regular Article - Experimental Physics

Measurement of the top quark-pair production cross section with ATLAS in pp collisions at $\sqrt{s} = 7$ TeV

The ATLAS Collaboration[*]

CERN, 1211 Geneva 23, Switzerland

Abstract A measurement of the production cross-section for top quark pairs ($t\bar{t}$) in pp collisions at $\sqrt{s} = 7$ TeV is presented using data recorded with the ATLAS detector at the Large Hadron Collider. Events are selected in two different topologies: single lepton (electron e or muon μ) with large missing transverse energy and at least four jets, and dilepton (ee, $\mu\mu$ or $e\mu$) with large missing transverse energy and at least two jets. In a data sample of 2.9 pb^{-1}, 37 candidate events are observed in the single-lepton topology and 9 events in the dilepton topology. The corresponding expected backgrounds from non-$t\bar{t}$ Standard Model processes are estimated using data-driven methods and determined to be 12.2 ± 3.9 events and 2.5 ± 0.6 events, respectively. The kinematic properties of the selected events are consistent with SM $t\bar{t}$ production. The inclusive top quark pair production cross-section is measured to be

$$\sigma_{t\bar{t}} = 145 \pm 31 (\text{stat.})^{+42}_{-27}(\text{syst.}) \text{ pb}.$$

The measurement agrees with perturbative QCD calculations.

1 Introduction

The observation of top quark pair ($t\bar{t}$) production is one of the milestones for the early LHC physics programme. The measurement of the top quark pair production cross-section ($\sigma_{t\bar{t}}$) in the various decay channels is interesting for several reasons. Uncertainties on the theoretical predictions are now at the level of 10% and a comparison with experimental measurements performed in different channels will ultimately allow a precision test of the predictions of perturbative QCD. In addition, the abundant $t\bar{t}$ sample which is expected to be produced in the first years of data-taking can be exploited for improving many aspects of detector performance. Finally, $t\bar{t}$ production is an important background

in various searches for physics beyond the Standard Model, and new physics may also give rise to additional $t\bar{t}$ production mechanisms or modification of the top quark decay channels.

In the Standard Model (SM) [1–3] the $t\bar{t}$ production cross-section in pp collisions is calculated to be 164.6 $^{+11.4}_{-15.7}$ pb at approximate NNLO precision [4, 5][1] at a centre of mass energy $\sqrt{s} = 7$ TeV assuming a top mass of 172.5 GeV, and top quarks are predicted to decay to a W boson and a b-quark ($t \rightarrow Wb$) nearly 100% of the time. Events with a $t\bar{t}$ pair can be classified as 'single-lepton', 'dilepton', or 'all hadronic' by the decays of the two W bosons: a pair of quarks ($W \rightarrow q\bar{q}$) or a lepton-neutrino pair ($W \rightarrow \ell\nu$), where ℓ refers to a lepton. At the Tevatron the dominant production mechanism is $q\bar{q}$ annihilation, and the $t\bar{t}$ cross section at $\sqrt{s} = 1.8$ TeV and at $\sqrt{s} = 1.96$ TeV have been measured by D0 and CDF [6–9] in all channels. The production of $t\bar{t}$ at the LHC is dominated by gg fusion. Recently, the CMS collaboration has presented a cross-section measurement, $\sigma_{t\bar{t}} = 194 \pm 72$ (stat.) ± 24 (syst.) ± 21 (lumi.) pb in the dilepton channel using 3.1 pb^{-1} of data [10].

The results described in this paper are based on reconstructed electrons and muons and include small contributions from leptonically decaying tau leptons. The single-lepton mode, with a branching ratio[2] of 37.9% (combining e and μ channels), and the dilepton mode, with a branching ratio of 6.5% (combining ee, $\mu\mu$ and $e\mu$ channels), both give rise to final states with at least one lepton, missing transverse energy and jets, some with b flavour. The cross-section measurements in both modes are based on a straightforward counting method. The number of signal events is

---

[1] Predictions in the paper are calculated with Hathor [52] with $m_{\text{top}} = 172.5$ GeV, CTEQ66 [19], where PDF and scale uncertainties are added linearly.

[2] The quoted branching ratios are based on the values reported in [11] assuming lepton universality, and include small contributions from leptonically decaying taus.

obtained in a signal enriched sample after background subtraction. The main background contributions are determined using data-driven methods, since the theoretical uncertainties on the normalisation of these backgrounds are relatively large. For both single-lepton and dilepton channels, alternative methods of signal extraction and/or background estimation are explored. In particular, two template shape fitting methods, which use additional signal regions to exploit the kinematic information in the events, are developed for the single-lepton mode. In this paper these two fitting methods serve as cross-checks of the counting method. The methods also provide alternative data-driven estimates of backgrounds and are expected to become more precise when more data become available.

2 Detector and data sample

The ATLAS detector [12] at the LHC covers nearly the entire solid angle[3] around the collision point. It consists of an inner tracking detector surrounded by a thin superconducting solenoid, electromagnetic and hadronic calorimeters, and an external muon spectrometer incorporating three large superconducting toroid magnet assemblies.

The inner-detector system is immersed in a $2\,T$ axial magnetic field and provides charged particle tracking in the range $|\eta| < 2.5$. The high-granularity silicon pixel detector covers the vertex region and provides typically three measurements per track, followed by the silicon microstrip tracker (SCT) which provides four measurements from eight strip layers. These silicon detectors are complemented by the transition radiation tracker (TRT), which enables extended track reconstruction up to $|\eta| = 2.0$. In giving typically more than 30 straw-tube measurements per track, the TRT is essential to the inner detector momentum resolution, and also provides electron identification information.

The calorimeter system covers the pseudorapidity range $|\eta| < 4.9$. Within the region $|\eta| < 3.2$, electromagnetic calorimetry is provided by barrel and endcap lead-liquid argon (LAr) electromagnetic calorimeters, with an additional thin LAr presampler covering $|\eta| < 1.8$ to correct for energy loss in material upstream of the calorimeters. Hadronic calorimetry is provided by the steel/scintillating-tile calorimeter, segmented into three barrel structures within $|\eta| < 1.7$, and two copper/LAr hadronic endcap calorimeters. The solid angle coverage is completed with forward copper/LAr and tungsten/LAr calorimeter modules optimised for electromagnetic and hadronic measurements respectively.

The muon spectrometer comprises separate trigger and high-precision tracking chambers measuring the deflection of muons in a magnetic field with a bending integral from 2 to 8 Tm in the central region, generated by three superconducting air-core toroids. The precision chamber system covers the region $|\eta| < 2.7$ with three layers of monitored drift tubes, complemented by cathode strip chambers in the forward region, where the background is highest. The muon trigger system covers the range $|\eta| < 2.4$ with resistive plate chambers in the barrel, and thin gap chambers in the endcap regions.

A three-level trigger system is used to select interesting events. The level-1 trigger is implemented in hardware and uses a subset of detector information to reduce the event rate to a design value of at most 75 kHz. This is followed by two software-based trigger levels, level-2 and the event filter, which together reduce the event rate to about 200 Hz.

Only data where all subsystems described above are fully operational are used. Applying these requirements to $\sqrt{s} = 7$ TeV pp collision data taken in stable beam conditions and recorded until 30$^{\text{th}}$ August 2010 results in a data sample of 2.9 pb^{-1}. This luminosity value has a relative uncertainty of 11% [13].

3 Simulated event samples

Monte-Carlo simulation samples are used to develop and validate the analysis procedures, to calculate the acceptance for $t\bar{t}$ events and to evaluate the contributions from some background processes. For the $t\bar{t}$ signal the next-to-leading order (NLO) generator MC@NLO v3.41 [14–16], is used with an assumed top-quark mass of 172.5 GeV and with the NLO parton density function (PDF) set CTEQ66 [17].

For the main backgrounds, consisting of QCD multi-jet events and W/Z boson production in association with multiple jets, ALPGEN v2.13 [18] is used, which implements the exact LO matrix elements for final states with up to 6 partons.[4] Using the LO PDF set CTEQ6L1 [19], the following backgrounds are generated: $W +$ jets events with up to 5 partons, $Z/\gamma^* +$ jets events with up to 5 partons and with the dilepton invariant mass $m_{\ell\ell} > 40$ GeV; QCD multi-jet events with up to 6 partons, and diboson $WW +$ jets, $WZ +$ jets and $ZZ +$ jets events. A separate sample of Z boson production generated with PYTHIA is used to cover the region 10 GeV $< m_{\ell\ell} < 40$ GeV. For all but the diboson processes, separate samples are generated that include

---

[3]In the right-handed ATLAS coordinate system, the pseudorapidity η is defined as $\eta = -\ln[\tan(\theta/2)]$, where the polar angle θ is measured with respect to the LHC beamline. The azimuthal angle ϕ is measured with respect to the x-axis, which points towards the centre of the LHC ring. The z-axis is parallel to the anti-clockwise beam viewed from above. Transverse momentum and energy are defined as $p_{\text{T}} = p \sin\theta$ and $E_{\text{T}} = E \sin\theta$, respectively.

---

[4]The 'MLM' matching scheme of the ALPGEN generator is used to remove overlaps between the n and $n+1$ parton samples with parameters RCLUS = 0.7 and ETCLUS = 20 GeV.

$b\bar{b}$ and $c\bar{c}$ quark pair production at the matrix element level. In addition, for the $W +$ jets process, a separate sample containing $W + c +$ jets events is produced. For the small background of single-top production MC@NLO is used, invoking the 'diagram removal scheme' [20] to remove overlaps between the single-top and the $t\bar{t}$ final states.

In simulation, the cross-section of $t\bar{t}$ production is normalised to 164.6 pb obtained from approximate NNLO calculations [4, 5]. The cross-sections for $W/Z +$ jets and diboson with jets have been rescaled by a factor 1.22 to match NNLO calculations of their inclusive cross-sections, as is done in [21]. The QCD multi-jet sample has not been rescaled as it is only used for validation studies.

Unless otherwise noted, all events are hadronised with HERWIG [22, 23], using JIMMY [24] for the underlying event model. Details on generator and underlying event tunes used for these samples are given in [25]. After event generation, all samples are processed by the standard AT-LAS detector and trigger simulation [26] and subject to the same reconstruction algorithms as the data.

3.1 Systematic uncertainties on the simulated samples

The use of simulated $t\bar{t}$ samples to calculate the signal acceptance gives rise to systematic uncertainties from the choice of generator, the amount of initial and final state radiation (ISR/FSR) and uncertainties on the PDF. The uncertainty due to the choice of generator is evaluated by comparing the predictions of MC@NLO with those of POWHEG [27] interfaced to both HERWIG or PYTHIA. The uncertainty due to ISR/FSR is evaluated by studies using the ACERMC generator [28] interfaced to PYTHIA, and by varying the parameters controlling ISR and FSR. For the ISR the variation ranges are similar to the ranges used in Perugia Soft and Perugia Hard tunes [29]. For the FSR the parameter variation ranges are larger those recommended in [30]. Finally, the uncertainty in the PDFs used to generate $t\bar{t}$ and single-top events is evaluated using a range of current PDF sets with the procedure described in [21]. In addition, the impact of the assumed top-quark mass is tested with a set of samples generated with different masses.

Simulation-based predictions of $W/Z +$ jets background events have uncertainties on their total cross-section, on the contribution of events with jets from heavy-flavour (b, c) quarks, and on the shape of kinematic distributions. The predictions of the total cross-section have uncertainties of up to $O(50\%)$ [31] increasing with jet multiplicity. Total W/Z cross-section predictions are not used in the cross-section analysis, but are used in simulation predictions shown in selected Figures. The heavy-flavor fractions in the $W/Z +$ jets samples are always taken from simulation, as the present data sample is too small to measure them. Here a fully correlated 100% uncertainty on the predicted fractions of $b\bar{b}$

and $c\bar{c}$ quark pairs is assumed, as well as a separate 100% uncertainty on the fraction of events with a single c quark. The uncertainty on the shape of $W +$ jets kinematic distributions, used in fit-based cross-checks of the single-lepton analysis, is assessed by changing the choice of factorisation scale from $m(W)^2 + \sum p_T^2$ (jet) to $m(W)^2$, and by comparing ALPGEN with SHERPA [32]. No systematic uncertainties are evaluated for the QCD multi-jet samples, as these are only used in validation studies.

For the small backgrounds from single-top and diboson production, only overall normalisation uncertainties are considered and these are taken to be 10%, determined from a comparison of MCFM and MC@NLO predictions, and 5%, determined from MCFM studies on scale and PDF uncertainties.

4 Object and event selection

For both the single lepton and the dilepton analysis, events are triggered by a single lepton trigger (electron or muon) [33]. The detailed trigger requirements vary through the data-taking period due to the rapidly increasing LHC luminosity and the commissioning of the trigger system, but the thresholds are always low enough to ensure that leptons with $p_T > 20$ GeV lie in the efficiency plateau.

The electron selection requires a level-1 electromagnetic cluster with $p_T > 10$ GeV. A more refined electromagnetic cluster selection is required in the level-2 trigger. Subsequently, a match between the selected calorimeter electromagnetic cluster and an inner detector track is required in the event filter. Muons are selected requiring a $p_T > 10$ GeV momentum threshold muon trigger chamber track at level-1, matched by a muon reconstructed in the precision chambers at the event filter.

After the trigger selections, events must have at least one offline-reconstructed primary vertex with at least five tracks, and are discarded if any jet with $p_T > 10$ GeV at the EM scale is identified as out-of-time activity or calorimeter noise [34].

The reconstruction of $t\bar{t}$ events makes use of electrons, muons and jets, and of missing transverse energy E_T^{miss} which is a measure of the energy imbalance in the transverse plane and is used as an indicator of undetected neutrinos.

Electron candidates are required to pass the electron selection as defined in Ref. [33], with $p_T > 20$ GeV and $|\eta_{\text{cluster}}| < 2.47$, where η_{cluster} is the pseudorapidity of the calorimeter cluster associated to the candidate. Candidates in the calorimeter transition region at $1.37 < |\eta_{\text{cluster}}| < 1.52$ are excluded. In addition, the ratio E/p of electron cluster energy measured in the calorimeter to momentum in the tracker must be consistent with that expected for an electron. Also, in order to suppress the background from photon

conversions, the track must have an associated hit in the innermost pixel layer, except when the track passes through one of the 2% of pixel modules known to be dead. Muon candidates are reconstructed from track segments in the different layers of the muon chambers [35]. These segments are then combined starting from the outermost layer, with a procedure that takes material effects into account, and matched with tracks found in the inner detector. The final candidates are refitted using the complete track information from both detector systems, and required to satisfy $p_T > 20$ GeV and $|\eta| < 2.5$.

To reduce the background due to leptons from decays of hadrons (including heavy flavours) produced in jets, the leptons in each event are required to be isolated. For electrons, the E_T deposited in the calorimeter towers in a cone in η–ϕ space of radius $\Delta R = 0.2$ around the electron position[5] is summed, and the E_T due to the electron (E_T^e) is subtracted. The remaining E_T is required to be less than $4\,\text{GeV} + 0.023 \cdot E_T^e$. For muons, the corresponding calorimeter isolation energy in a cone of $\Delta R = 0.3$ is required to be less than 4 GeV, and the scalar sum of track transverse momenta in a cone of $\Delta R = 0.3$ is also required to be less than 4 GeV after subtraction of the muon p_T. Additionally, muons are required to have a separation $\Delta R > 0.4$ from any jet with $p_T > 20$ GeV, to further suppress muons from heavy flavour decays inside jets.

Jets are reconstructed with the anti-k_t algorithm [36] ($\Delta R = 0.4$) from topological clusters [37] of energy deposits in the calorimeters, calibrated at the electromagnetic (EM) scale appropriate for the energy deposited by electrons or photons. These jets are then calibrated to the hadronic energy scale, using a correction factor obtained from simulation [37] which depends upon p_T and η. If the closest object to an electron candidate is a jet with a separation $\Delta R < 0.2$ the jet is removed in order to avoid double-counting of electrons as jets.

Jets originating from b-quarks are selected by exploiting the long lifetime of b-hadrons (about 1.5 ps) which leads to typical flight paths of a few millimetres which are observable in the detector. The SV0 b-tagging algorithm [38] used in this analysis explicitly reconstructs a displaced vertex from the decay products of the long-lived b-hadron. As input, the SV0 tagging algorithm is given a list of tracks associated to the calorimeter jet. Only tracks fulfilling certain quality criteria are used in the secondary vertex fit. Secondary vertices are reconstructed in an inclusive way starting from two-track vertices which are merged into a common vertex. Tracks giving large χ^2 contributions are then iteratively removed until the reconstructed vertex fulfils certain quality criteria. Two-track vertices at a radius consistent with the radius of one of the three pixel detector layers

---

[5]The radius ΔR between the object axis and the edge of the object cone is defined as $\Delta R = \sqrt{\Delta\phi^2 + \Delta\eta^2}$.

are removed, as these vertices likely originate from material interactions. A jet is considered b-tagged if it contains a secondary vertex, reconstructed with the SV0 tagging algorithm, with $L/\sigma(L) > 5.72$, where L is the decay length and $\sigma(L)$ its uncertainty. This operating point yields a 50% b-tagging efficiency in simulated $t\bar{t}$ events The sign of $L/\sigma(L)$ is given by the sign of the projection of the decay length vector on the jet axis. The typical probability for a light jet to be mis-identified as a b-jet ranges from 0.002 to 0.01 for jets with p_T ranging 20 and 200 GeV [38].

The missing transverse energy is constructed from the vector sum of all calorimeter cells contained in topological clusters. Calorimeter cells are associated with a parent physics object in a chosen order: electrons, jets and muons, such that a cell is uniquely associated to a single physics object [39]. Cells belonging to electrons are calibrated at the electron energy scale, but omitting the out-of-cluster correction to avoid double cell-energy counting, while cells belonging to jets are taken at the corrected energy scale used for jets. Finally, the contributions from muons passing selection requirements are included, and the contributions from any calorimeter cells associated to the muons are subtracted. The remaining clustered energies not associated to electrons or jets are included at the EM scale.

The modelled acceptances and efficiencies are verified by comparing Monte-Carlo simulations with data in control regions which are depleted of $t\bar{t}$ events. Lepton efficiencies are derived from data in the Z boson mass window. The acceptances for the jet multiplicity and E_T^{miss} cuts are validated using a number of control regions surrounding the $t\bar{t}$ signal region in phase-space.

4.1 Systematic uncertainties for reconstructed objects

The uncertainties due to Monte-Carlo simulation modelling of the lepton trigger, reconstruction and selection efficiencies are assessed using leptons from $Z \rightarrow ee$ and $Z \rightarrow \mu\mu$ events selected from the same data sample used for the $t\bar{t}$ analyses. Scale factors are applied to Monte-Carlo samples when calculating acceptances. The statistical and systematic uncertainties on the scale factors are included in the uncertainties on the acceptance values. The modelling of the lepton energy scale and resolution are studied using reconstructed Z boson mass distributions, and used to adjust the simulation accordingly.

The jet energy scale (JES) and its uncertainty are derived by combining information from test-beam data, LHC collision data and simulation [37]. The JES uncertainty varies in the range 6–10% as a function of jet p_T and η. The jet energy resolution (JER) and jet finding efficiency measured in data and in simulation are in agreement. The limited statistical precision of the comparisons for the energy resolution (14%) and the efficiency (1%) are taken as the systematic uncertainties in each case.

The b-tagging efficiency and mistag fraction of the SV0 b-tagging algorithm have been measured on data [38]. The efficiency measurement is based on a sample of jets containing muons and makes use of the transverse momentum of a muon relative to the jet axis. The measurement of the mistag fraction is performed on an inclusive jet sample and includes two methods, one which uses the invariant mass spectrum of tracks associated to reconstructed secondary vertices to separate light- and heavy-flavour jets and one which is based on the rate at which secondary vertices with negative decay-length significance are present in the data. Both the b-tagging efficiency and mistag fraction measured in data depend strongly on the jet kinematics. In the range $25 < p_T(\text{jet}) < 85$ GeV, the b-tagging efficiency rises from 40% to 60%, while the mistag fraction increases from 0.2% to 1% between 20 and 150 GeV. The measurements of the b-tagging efficiencies and mistag fractions are provided in the form of p_T-dependent scale factors correcting the b-tagging performance in simulation to that observed in data. The relative statistical (systematic) uncertainties for the b-tagging efficiency range from 3% to 10% (10% to 12%). For the b-tagging efficiency, the scale factor is close to one for all values of jet p_T. For light-flavour jets we correct the tagging efficiencies by factors of 1.27 ± 0.26 for jets with $p_T < 40$ GeV and 1.07 ± 0.25 for jets with $p_T > 40$ GeV.

The LHC instantaneous luminosity varied by several orders of magnitude during the data-taking period considered for this measurement, reaching a peak of about 1×10^{31} cm^{-2} s^{-1}. At this luminosity, an average of about two extra pp interactions were superimposed on each hard proton-proton interaction. This 'pileup' background produces additional activity in the detector, affecting variables like jet reconstruction and isolation energy. No attempts to correct the event reconstruction for these effects are made, since the data-driven determination of object identification and trigger efficiencies and backgrounds naturally include them. The residual effects on the $t\bar{t}$ event acceptance are assessed by using $t\bar{t}$ simulation samples with additional pileup interactions, simulated with PYTHIA, that were overlayed during event digitisation and reconstruction. In a scenario where on average two pileup interactions are added to each event, corresponding to conditions that exceed those observed during the data taking period, the largest relative change of acceptance observed in any of the channels is 3.6%. As the effect of pileup is small even in this pessimistic scenario, it is neglected in the acceptance systematics evaluation.

5 Single lepton analysis

5.1 Event selection

The single lepton $t\bar{t}$ final state is characterised by an isolated lepton with relatively high p_T and missing transverse energy

corresponding to the neutrino from the leptonic W decay, two b quark jets and two light jets from the hadronic W decay.

The selection of events for the single-lepton analysis consists of a series of requirements on the reconstructed objects defined in Sect. 4, designed to select events with the above topology. For each lepton flavour, the following event selections are first applied:

– The appropriate single-electron or single-muon trigger has fired.
– The event contains one and only one reconstructed lepton (electron or muon) with $p_T > 20$ GeV. Electrons are required to match the corresponding high-level trigger object.
– $E_T^{\text{miss}} > 20$ GeV and $E_T^{\text{miss}} + m_T(W) > 60$ GeV.[6] The cut on E_T^{miss} rejects a significant fraction of the QCD multi-jet background. Further rejection can be achieved by applying a cut in the (E_T^{miss}, $m_T(W)$) plane; true $W \to \ell\nu$ decays with large E_T^{miss} have also large $m_T(W)$, while mismeasured jets in QCD multi-jet events may result in large E_T^{miss} but small $m_T(W)$. The requirement on the sum of E_T^{miss} and $m_T(W)$ discriminates between the two cases.
– Finally, the event is required to have ≥ 1 jet with $p_T > 25$ GeV and $|\eta| < 2.5$. The requirement on the p_T and the pseudorapidity of the jets is a compromise between the efficiency of the $t\bar{t}$ events selection, and the rejection of $W + $ jets and QCD multi-jet background.

Events are then classified by the number of jets with $p_T > 25$ GeV and $|\eta| < 2.5$, being either 1, 2, 3 or at least 4. These samples are labelled '1-jet pre-tag' through '$\geq$4-jet pre-tag', where the number corresponds to the jet multiplicity as defined above and pre-tag refers to the fact that no b-tagging information has been used. Subsets of these samples are then defined with the additional requirement that at least one of the jets with $p_T > 25$ GeV is tagged as a b-jet. They are referred to as the '1-jet tagged' through '$\geq$4-jet tagged' samples.

Figure 1 shows the observed jet multiplicity for events in the pre-tag and tagged samples, together with the sum of all expected contributions as expected from simulation, except for QCD multi-jet, which is taken from a data-driven technique discussed in Sect. 5.2. The largest fraction of $t\bar{t}$ events is concentrated in $\geq$4-jets bin of the tagged sample, which is defined as the signal region and used for the $t\bar{t}$ signal extraction in the primary method described in Sect. 5.5.1. One of the cross-check methods, discussed in Sect. 5.5.2, uses in addition the 3-jet tagged sample for signal extraction. Other

---

[6] Here $m_T(W)$ is the W-boson transverse mass, defined as $\sqrt{2p_T^\ell p_T^\nu (1 - \cos(\phi^\ell - \phi^\nu))}$ where the measured missing E_T vector provides the neutrino information.
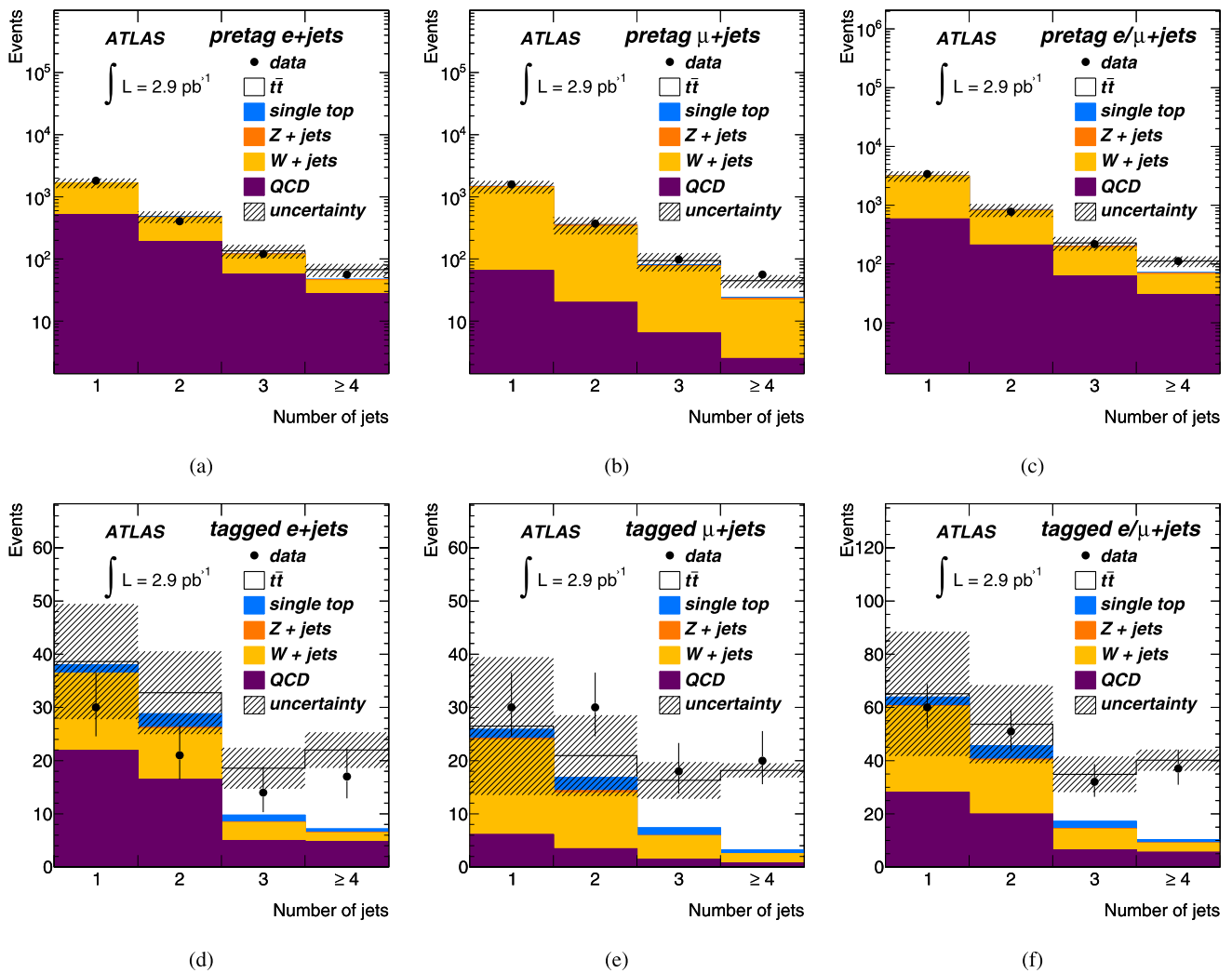
Fig. 1 Jet multiplicity distributions (i.e. number of jets with $p_T > 25$ GeV). *Top row*—pre-tag samples: **a** electron channel, **b** muon channel and **c** electron/muon combined. *Bottom row*—tagged samples: **d** electron channel, **e** muon channel and **f** electron/muon combined. The data are compared to the sum of all expected contributions. For the totals shown, simulation estimates are used for all contributions except QCD multi-jet, where a data-driven technique is used. The background uncertainty on the total expectation is represented by the *hatched area*. The $\geq$4-jet bin in the tagged sample represents the signal region

regions are used as control samples for the determination of backgrounds.

Table 1 lists the numbers of events in the four tagged samples, as well as the number of events in the 3-jet and $\geq$4-jet zero-tag samples, which comprise the events not containing b-tagged jets. These events are used for background normalisation in the second cross-check method described in Sect. 5.5.2. For all samples, Table 1 also lists the contributions estimated from Monte Carlo simulation for $t\bar{t}$, W + jets, Z + jets and single-top events. The quoted uncertainties are from object reconstruction and identification. For the data-driven estimates of W + jets and QCD multi-jet, the results of the procedures that will be detailed in Sects. 5.3 and 5.4 are quoted. The uncertainty on the background pre-

diction is mostly systematic and largely correlated between bins, and is also different in the electron and muon channels due to different sample composition in terms of QCD multi-jet and W + jets fractions. QCD multi-jet is larger than W + jets in the electron channel, while it is smaller for muons.

The estimated product of acceptance and branching fraction for $t\bar{t}$ events in the $\geq$4-jet tagged signal region, measured from Monte-Carlo samples, are $(3.1 \pm 0.7)\%$ and $(3.2 \pm 0.7)\%$ for e + jets and μ + jets, respectively. About 90% of the selected $t\bar{t}$ events come from the corresponding $t \to W \to e$ or μ decay including leptonic τ decays, and the acceptance for those events is $15 \pm 3\%$. The remaining 10% comes from dilepton events where one of the leptons was not reconstructed as electron or muon. The con-

Table 1 Number of tagged and zero-tag events with different jet multiplicities in (a) the $e +$ jets and (b) the $\mu +$ jets channel. The observed number of events are shown, together with the Monte-Carlo simulation estimates (MC) for $t\bar{t}$, $W +$ jets, $Z +$ jets and single-top events, normalised to the data integrated luminosity of 2.9 pb^{-1}. The data-driven estimates (DD) for QCD multi-jet (see Sect. 5.3) and $W +$ jets (see Sect. 5.4) backgrounds are also shown. The 'Total (non $t\bar{t}$)' row uses the simulation estimate for $W +$ jets for all samples. The uncertainties on all data-driven background estimates include the statistical uncertainty and all systematic uncertainties. The numbers in the 'Total expected' rows are rounded to a precision commensurate with the uncertainty

(a)

$e +$ jets channel						
	1-jet tagged	2-jet tagged	3-jet tagged	$\geq$4-jet tagged	3-jet zero-tag	$\geq$4-jet zero-tag
QCD (DD)	21.9 ± 3.4	16.4 ± 4.0	4.9 ± 2.7	4.8 ± 3.1	52.0 ± 19	23.0 ± 11
$W +$ jets (MC)	14.5 ± 10	9.5 ± 6.6	3.4 ± 2.7	1.5 ± 1.4	55.1 ± 26	15.1 ± 10
$W +$ jets (DD)	–	–	–	1.9 ± 1.1	–	9.3 ± 4.0
$Z +$ jets (MC)	0.1 ± 0.1	0.3 ± 0.1	0.1 ± 0.1	0.2 ± 0.1	4.6 ± 2.2	1.7 ± 1.3
Single top (MC)	1.6 ± 0.3	2.6 ± 0.6	1.3 ± 0.3	0.7 ± 0.2	0.9 ± 0.2	0.4 ± 0.1
Total (non $t\bar{t}$)	38.1 ± 11	28.8 ± 7.7	9.7 ± 3.8	7.2 ± 3.4	112.6 ± 32	40.2 ± 15
$t\bar{t}$ (MC)	0.6 ± 0.2	4.0 ± 1.0	8.8 ± 1.8	14.9 ± 3.5	4.5 ± 0.8	5.4 ± 1.2
Total expected	39 ± 11	33 ± 8	19 ± 4	22 ± 5	117 ± 32	46 ± 15
Observed	30	21	14	17	106	39

(b)

$\mu +$ jets channel						
	1-jet tagged	2-jet tagged	3-jet tagged	$\geq$4-jet tagged	3-jet zero-tag	$\geq$4-jet zero-tag
QCD (DD)	6.1 ± 2.9	3.4 ± 1.8	1.5 ± 0.8	0.8 ± 0.5	4.9 ± 2.3	1.7 ± 1.1
$W +$ jets (MC)	17.8 ± 12	10.5 ± 7.4	4.3 ± 3.3	1.7 ± 1.6	63.6 ± 28	17.6 ± 12
$W +$ jets (DD)	–	–	–	3.2 ± 1.7	–	15.7 ± 4.5
$Z +$ jets (MC)	0.3 ± 0.1	0.4 ± 0.2	0.1 ± 0.1	0.1 ± 0.1	3.3 ± 1.6	1.3 ± 0.8
Single top (MC)	1.7 ± 0.4	2.5 ± 0.5	1.5 ± 0.3	0.7 ± 0.2	1.1 ± 0.2	0.3 ± 0.1
Total (non $t\bar{t}$)	25.9 ± 13	16.8 ± 7.6	7.4 ± 3.4	3.3 ± 1.7	72.9 ± 29	20.9 ± 13
$t\bar{t}$ (MC)	0.7 ± 0.2	4.1 ± 1.1	9.0 ± 1.8	15.0 ± 3.4	4.6 ± 0.7	5.5 ± 1.2
Total expected	27 ± 13	21 ± 8	16 ± 4	18 ± 4	78 ± 29	26 ± 13
Observed	30	30	18	20	80	36

tribution from fully hadronic $t\bar{t}$ events is negligible. The uncertainties on the acceptance originate from physics process modelling and object selection uncertainties detailed in Sects. 3.1 and 4.1.

5.2 Background determination strategy

The expected dominant backgrounds in the single-lepton channel are $W +$ jet events, which can give rise to the same final state as $t\bar{t}$ signal, and QCD multi-jet events. QCD multi-jet events only contribute to the signal selection if the reconstructed $E_{\mathrm{T}}^{\mathrm{miss}}$ is sufficiently large and a fake lepton is reconstructed. Fake leptons originate in misidentified jets or are non-prompt leptons, e.g. from semileptonic decays of heavy quarks.

In the pre-tag samples both $W +$ jets and QCD multi-jet are dominated by events with light quarks and gluons. In the b-tagged samples, light-quark and gluon final states are strongly suppressed and their contributions become comparable to those with $b\bar{b}$ pairs, $c\bar{c}$ pairs and single c quarks, which are all of a similar magnitude.

The contribution of $W +$ jet events and QCD multi-jet events to the $\geq$4-jet bin are both measured with data-driven methods, as detector simulation and/or theoretical predictions are insufficiently precise. The remaining smaller backgrounds, notably single-top production and $Z +$ jets production, are estimated from simulation.

5.3 Background with fake and non-prompt leptons

5.3.1 Background estimate in the μ + jets channel

In the μ + jets channel, the background to 'real' (prompt) muons coming from 'fake' muons in QCD multi-jet events, is predominantly due to final states with a non-prompt muon. As all other processes ($t\bar{t}$, W + jets, Z + jets and single-top) in this channel feature a prompt muon from a W or Z boson decay, it is sufficient to estimate the number of events with a non-prompt muon to quantify the QCD multi-jet background.

The number of events in the sample with a non-prompt muon can be extracted from the data by considering the event count in the signal region with two sets of muon identification criteria. The 'standard' and 'loose' criteria comprise the standard muon definition described in Sect. 4, with and without, respectively, the requirements on the lepton isolation.

The procedure followed at this point is a so-called 'matrix method': the number of events selected by the loose and by the standard cuts, N^{loose} and N^{std} respectively, can be expressed as linear combinations of the number of events with a 'real' (prompt) or a 'fake' muon:

$$N^{\text{loose}} = N^{\text{loose}}_{\text{real}} + N^{\text{loose}}_{\text{fake}},$$
$$N^{\text{std}} = r N^{\text{loose}}_{\text{real}} + f N^{\text{loose}}_{\text{fake}}, \tag{1}$$

where r is the fraction of 'real' (prompt) muons in the loose selection that also pass the standard selection and f is the fraction of 'fake' (non-prompt) muons in the loose selection that also pass the standard selection. If r and f are known, the number of events with non-prompt muons can be calculated from (1) given a measured N^{loose} and N^{std}. The relative efficiencies r and f are measured in data in control samples enriched in either prompt or non-prompt muons. The key issue in selecting these control regions is that they should be kinematically representative of the signal region so that the measured control-region efficiency can be applied in the signal region.

An inclusive $Z \to \mu^+\mu^-$ control sample is used to measure the prompt muon efficiency $r = 0.990 \pm 0.003$. No statistically significant dependence on the jet multiplicity is observed. For the measurement of the non-prompt muon efficiency two control regions are used: a Sample A with low missing transverse energy ($E_T^{\text{miss}} < 10$ GeV) and at least one jet with $p_T > 25$ GeV, and a Sample B with the nominal missing transverse energy requirement ($E_T^{\text{miss}} > 20$ GeV), at least one jet with $p_T > 25$ GeV, and a high muon impact parameter significance. Sample A is dominated by QCD multi-jet events as most QCD multi-jet events have little real E_T^{miss} and the cross-section is comparatively large. The contribution from events with prompt muons from W/Z + jets which

remains in the $E_T^{\text{miss}} < 10$ GeV region has to be subtracted. Since the contribution of these processes is not accurately known, it is evaluated in an iterative procedure: the initial value obtained for f is used to predict the number of leptons in the full E_T^{miss} range. The excess of candidate lepton events in data is attributed to prompt muons from W/Z + jets, whose contribution to the $E_T^{\text{miss}} < 10$ GeV region is then subtracted, obtaining a new value for f. The procedure converges in few iterations and it results in $f^A = 0.382 \pm 0.007$, where the quoted uncertainty is statistical only. Sample B is kinematically close to the signal region, but the large impact parameter significance requirement selects muons that are incompatible with originating from the primary vertex and the sample is thus enriched in non-prompt muons. Here a value $f^B = 0.295 \pm 0.025$ is measured, where the uncertainty is again statistical only.

Since both samples A and B are reasonable, but imperfect, approximations of the signal region in terms of event kinematics, the unweighted average $f = 0.339 \pm 0.013 \, (\text{stat.}) \pm 0.061 \, (\text{syst.})$ is taken as the central value. The systematic uncertainty is determined by half the difference between the control regions, multiplied by $\sqrt{2}$ to obtain an unbiased estimate of the underlying uncertainty, assuming that the two control regions have similar kinematics as the signal region. A single value of f is used to estimate the background in each of the four pre-tag μ + jets samples using (1). The validity of this approach has been verified on samples of simulated events.

For the tagged samples, the estimated background in each pre-tag sample is multiplied by the measured probability for a similar QCD multi-jet event to have at least one b-tagged jet. This results in a more precise measurement of the tagged event rate than a measurement of f in a tagged control sample, which has a large statistical uncertainty due to the relatively small number of tagged events. The b-tagging probabilities for QCD multi-jet events are 0.09 ± 0.02, 0.17 ± 0.03, 0.23 ± 0.06 and 0.31 ± 0.10 for 1 through ≥ 4-jet, respectively. These per-event b-tag probabilities have been measured in a sample defined by the pre-tag criteria, but without the E_T^{miss} cut, and by relaxing the muon selection to the loose criteria. The systematic uncertainty on this per-event tagging probability is evaluated by varying the selection criteria of the sample used for the measurement.

The estimated yields of QCD multi-jet events in the tagged μ + (1, 2, 3 and ≥ 4-jet), zero-tag μ + (3 and ≥ 4-jet) and the pre-tag μ + (1 and 2-jet) are summarised in Table 1(b) and also shown in Table 2. Figure 2(a) shows the distribution of $m_T(W)$ for the 1-jet pre-tag sample without the $E_T^{\text{miss}} + m_T(W)$ requirement, while Figs. 2(b) and (c) show $m_T(W)$ for the 2-jet pre-tag and for the 2-jet tagged samples respectively after the $E_T^{\text{miss}} + m_T(W)$ requirement.

Table 2 Observed event yields in the pre-tag 1-jet and 2-jet samples and estimated contributions from non-W processes and $W \to \tau \nu$. The estimation for QCD multi-jet events is data-driven (DD), all other es-timates are based on simulation (MC). The last row gives the number of $W(l\nu)$ + jet events, estimated as the observed event count minus all other contributions

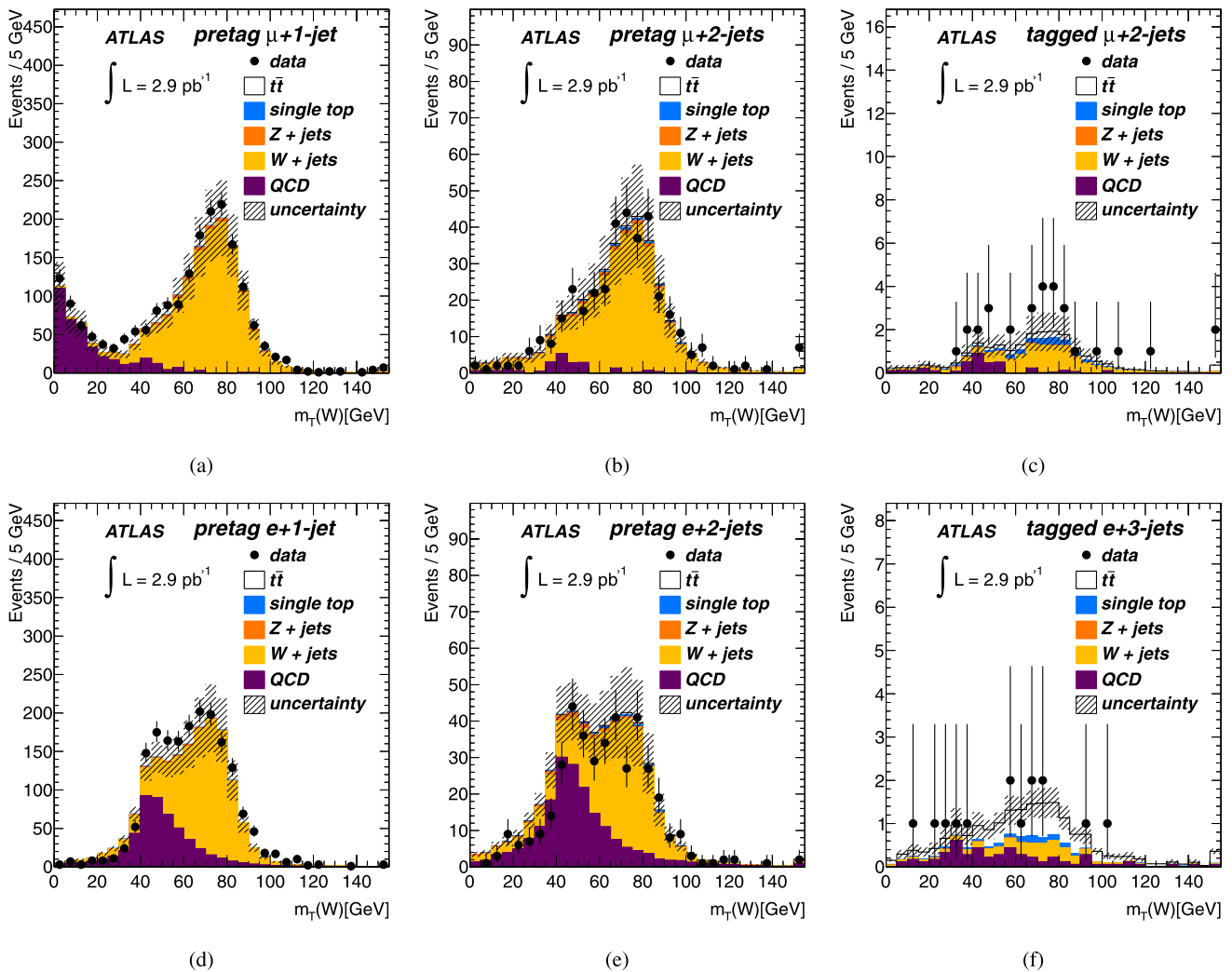|	1-jet pre-tag e	1-jet pre-tag μ	2-jet pre-tag e	2-jet pre-tag μ
Observed	1815	1593	404	370
QCD multijet (DD)	517 ± 89	65 ± 28	190 ± 43	20.0 ± 9.7
$W(\tau\nu)$ + jets (MC)	39 ± 10	43 ± 11	11.7 ± 4.4	13.6 ± 5.1
Z + jets (MC)	19.0 ± 9.1	48 ± 12	11.6 ± 5.2	14.0 ± 4.8
$t\bar{t}$ (MC)	1.7 ± 0.8	1.7 ± 0.8	7.0 ± 3.0	7.7 ± 3.3
single-t (MC)	4.4 ± 0.7	5.0 ± 0.8	5.2 ± 0.8	5.1 ± 0.8
diboson (MC)	4.8 ± 4.8	5.7 ± 5.7	3.8 ± 3.8	4.4 ± 4.4
Total (non $W(l\nu)$ + jets)	585 ± 90	168 ± 33	229 ± 44	65 ± 13
Estimated $W(l\nu)$ + jets	1230 ± 100	1425 ± 52	175 ± 49	305 ± 23

Fig. 2 Distributions of $m_T(W)$. *Top row—μ + jets channel:* **a** the 1-jet pre-tag sample (where the $E_T^{miss} + m_T(W)$ requirement is not ap-plied), **b** the 2-jet pre-tag sample and **c** the 2-jet tagged sample. *Bottom row—e + jets channel:* **d** the 1-jet pre-tag sample, **e** the 2-jet pre-tag sample and **f** the 3-jet tagged sample. In each plot data are compared to the sum of the data-driven QCD estimate plus the contributions from W/Z + jets and top from simulation. The background uncertainty on the total expectation is represented by the *hatched area*

Good agreement is observed comparing the data to the estimated rate of QCD multi-jet events summed with the other (non-QCD) simulation predictions.

The full QCD multi-jet background estimation procedure has been validated by applying the procedure on a sample of simulated events and comparing the result with the known amount of QCD multi-jet background in the sample. The systematic uncertainty on the $\mu +$ jets multi-jet background estimate is due to the control region uncertainty described above, and up to a relative 30% uncertainty originating from the method validation studies on the simulation and, for the tagged samples, the uncertainty originating from the per-event b-tagging probabilities.

5.3.2 *Background estimate in the* $e +$ jets *channel*

In the $e +$ jets channel, the background consists of both non-prompt electrons and fake electrons where the latter include both electrons from photon conversion and misidentified jets with high EM fractions. The relative magnitude of the non-prompt and fake components is not well known, as it depends on the details of electron misreconstruction effects that are not perfectly modelled in the simulation as well as on the fraction of QCD multi-jet events with non-prompt electrons in the final state. As the ratio also varies with the event kinematics, the method of (1), which relies on a representative control region to measure the input values of f, is not well suited for the electron channel.

A method, based on a binned likelihood template fit of the E_T^{miss} distribution, is used for the background estimate. For each previously defined pre-tag and tagged sample, the data are fitted to a sum of four templates describing the E_T^{miss} distribution of the QCD multi-jet, $t\bar{t}$, $W +$ jets and $Z +$ jets components respectively. The fit is performed in the region with $E_T^{\text{miss}} < 20$ GeV which is complementary to the signal region. To improve the statistical precision the requirement on $E_T^{\text{miss}} + m_T(W)$ is not applied. The templates for the $t\bar{t}$, $W +$ jets and $Z +$ jets components are taken from Monte-Carlo simulation, while the templates for the QCD multi-jet E_T^{miss} distributions are obtained from two data control samples. In the first sample called 'jet-electrons', events are selected which have, instead of the standard electron, an additional jet which passes the standard electron kinematic cuts and has at least 4 tracks and an EM fraction of 80–95%. In the second sample called 'non-electrons', the standard event selection is applied, except that the electron candidate must fail the track quality cut in the innermost layers of the tracking detector.

The fraction of QCD multi-jet events in the signal region is calculated by extrapolating the expected fraction of events for each component to the signal region using the template shape and accounting for the efficiency of the $E_T^{\text{miss}} + m_T(W)$ cut for each template. The output of the fit is

ρ_{QCD}, the predicted fraction of QCD multi-jet events in the signal region, which is then multiplied by the observed event count. Since both control samples are approximations of the signal region in terms of event kinematics, the unweighted average of ρ_{QCD} predicted by the template fits using the jet-electron and non-electron templates, respectively, is taken for the QCD multi-jet component. The uncertainty on ρ_{QCD} has a component from the template fit uncertainty, a component that quantifies the uncertainty related to the choice of control sample, evaluated as the difference in ρ_{QCD} from the two samples divided by $\sqrt{2}$, and a component related to the method calibration performed on simulation samples. The latter varies between 2% and 36% depending on the sample.

The results for the QCD multi-jet background contribution to the $e +$ jets channel are summarised in Table 1(a), and are also shown in Table 2. The estimates for the tagged $e +$ jets samples are performed directly in tagged control samples which have a sufficiently large number of events, and no per-event b-tagging probabilities are used.

Figure 2 (bottom row) shows the distributions of $m_T(W)$ for (d) the $e + 1$-jet pre-tag, (e) the $e + 2$-jet pre-tag, and (f) the $e + 3$-jet tagged samples. Acceptable agreement is observed between data and the sum of the QCD multi-jet background estimated with the fitting method and the other backgrounds estimated from simulation.

5.4 $W +$ jets background

The data-driven estimate for the $W +$ jets background in both electron and muon channels is constructed by multiplying the corresponding background contribution in the pre-tag sample by the per-event b-tagging probability:

$$W_{\text{tagged}}^{\geq 4\text{-jet}} = W_{\text{pre-tag}}^{\geq 4\text{-jet}} \cdot f_{\text{tagged}}^{\geq 4\text{-jet}}. \tag{2}$$

Here $W_{\text{pre-tag}}^{\geq 4\text{-jet}}$ is an estimate of the $W +$ jets event count in the pre-tag ≥ 4 jet sample and $f_{\text{tagged}}^{\geq 4\text{-jet}}$ is the fraction of these events that are tagged, calculated as

$$f_{\text{tagged}}^{\geq 4\text{-jet}} = f_{\text{tagged}}^{2\text{-jet}} \cdot f_{2 \rightarrow \geq 4}^{\text{corr}}, \tag{3}$$

where $f_{\text{tagged}}^{2-\text{jet}}$ is a measurement of the $W +$ jets tag fraction in the 2-jet sample and $f_{2 \rightarrow \geq 4}^{\text{corr}}$ accounts for the difference in flavour composition between the 2-jet and ≥ 4-jet samples as well as differences in the per-flavour event tagging probabilities, which may lead to different event rates after b-tagging.

For the first ingredient, $W_{\text{pre-tag}}^{\geq 4\text{-jet}}$, the fact that the ratio of $W + n + 1$ jets to $W + n$ jets is expected to be approximately constant as a function of n is exploited [40–42]. This is supported by the good agreement with the Standard Model ex-

pectation as shown in Fig. 1. The number of W events in the ≥ 4-jet pre-tag sample can thus be estimated as

$$W_{\text{pre-tag}}^{\geq 4\text{-jet}} = W_{\text{pre-tag}}^{2\text{-jet}} \cdot \sum_{n=2}^{\infty} (W_{\text{pre-tag}}^{2\text{-jet}} / W_{\text{pre-tag}}^{1\text{-jet}})^n, \tag{4}$$

where the sum is used to extrapolate to a sample with four or more jets. These rates are obtained by subtracting the estimated non-W boson contributions from the event count in the pre-tag 1-jet and 2-jet bins. The QCD multi-jet contribution is estimated from data as described in Sect. 5.3 and simulation-based estimates are used for the other backgrounds. The scaling behaviour of (4) does not apply to $W \to \tau \nu$ events as their selection efficiency depends significantly on the jet multiplicity. This contribution is subtracted from the observed event count in the $W_{\text{pre-tag}}^{1\text{-jet}}$ and $W_{\text{pre-tag}}^{2\text{-jet}}$ control samples and is estimated separately in the electron and the muon channel using the simulation to predict the ratio of $(W \to \tau \nu / W \to \ell \nu)$. The data-driven technique is used for the estimation of the $W \to e \nu$ background in the electron channel and the $W \to \mu \nu$ background in the muon channel. Table 2 compares the observed event yields in both the 1-jet and 2-jet samples with the estimated pre-tag backgrounds for both the electron and muon channels. Figures 2(b) and (e) show the $m_{\text{T}}(W)$ distribution for the 2-jet pre-tag samples in the muon and electron channels, respectively.

The ratio between the 2-jet and 1-jet rates is measured with significantly poorer precision in the electron channel, because of the larger QCD multi-jet contamination. Since the ratio between the 2-jet and 1-jet rates is expected to be independent of the W boson decay mode, the muon channel estimation is used also for the electron channel, giving

$$W_{\text{pre-tag}}^{\geq 4\text{-jet}} = 11.2 \pm 2.2(\text{stat.}) \pm 4.0(\text{syst.}), \quad e \text{ channel},$$

$$W_{\text{pre-tag}}^{\geq 4\text{-jet}} = 18.9 \pm 4.1(\text{stat.}) \pm 5.0(\text{syst.}), \quad \mu \text{ channel}.$$

The leading systematic uncertainties are the uncertainty on the purity of the low jet multiplicity control samples and the uncertainty associated with the assumption that the $(W + n + 1 \text{ jets})/(W + n \text{ jets})$ ratio is constant. The latter relative uncertainty has been evaluated to be 24% from the results reported in [43].

For the second ingredient, $f_{\text{tagged}}^{2\text{-jet}}$, the pre-tag yield is taken from Table 2 and the pre-tag non-W boson backgrounds (also from Table 2) are subtracted from this yield. This gives an estimate of the $W +$ jets contribution in the 2-jet pre-tag sample. The same is done in the tagged sample: the estimated non-W boson backgrounds, as shown in Table 1, are subtracted from the measured yield after applying the tagging criteria resulting in an estimate of the $W +$ jets contribution in the 2-jet sample after tagging. The ratio of

the tagged to the pre-tag contributions represents the estimate of the fraction of tagged events in the 2-jet sample

$$f_{\text{tagged}}^{2\text{-jet}} = 0.060 \pm 0.018(\text{stat.}) \pm 0.007(\text{syst.}).$$

This quantity is computed from the muon channel only, due to the large uncertainty originating from the QCD multi-jet contamination in the electron channel. Figures 2(b) and (c) show the distribution of the transverse mass $m_{\text{T}}(W)$ for the $\mu +$ jets 2-jet pre-tag and tagged samples respectively. Clear W signals are evident in both samples.

The final ingredient, the correction factor $f_{2 \to \geq 4}^{\text{corr}}$, is defined as $f_{2 \to \geq 4}^{\text{corr}} = f_{\text{tagged}}^{\geq 4\text{-jet}} / f_{\text{tagged}}^{2\text{-jet}}$. It is obtained from simulation studies on ALPGEN $W +$ jets events and is determined to be:

$$f_{2 \to \geq 4}^{\text{corr}} = 2.8 \pm 0.8(\text{syst.}). \tag{5}$$

The quoted uncertainty on $f_{2 \to \geq 4}^{\text{corr}}$ reflects uncertainties on the assumed flavour composition of the pre-tag 2-jet sample, the uncertainty on the scaling factors for the b-tagging efficiency for b, c and light-quark jets, and the uncertainty on the ratio of fractions in the 2-jet bin and the ≥ 4-jet bin for $W + b\bar{b} +$ jets, $W + c\bar{c} +$ jets and $W + c +$ jets. The leading uncertainty on $f_{2 \to \geq 4}^{\text{corr}}$ is due to the uncertainty on the predicted ratios of flavour fractions in the 2-jet and ≥ 4-jet bin. This is estimated by the variation of several ALPGEN generator parameters that are known to influence these ratios [18], and adds up to a relative 40%–60% per ratio. The uncertainty on the flavour composition in the 2-jet bin, while large in itself, has a small effect on $f_{2 \to \geq 4}^{\text{corr}}$ due to effective cancellations in the ratio.

Applying (2) and (3) the estimated yields for $W +$ jets in the ≥ 4-jet tagged samples are

$$W_{\text{tagged}}^{\geq 4\text{-jet}} = 1.9 \pm 0.7(\text{stat.}) \pm 0.9(\text{syst.}), \quad e \text{ channel},$$

$$W_{\text{tagged}}^{\geq 4\text{-jet}} = 3.2 \pm 1.2(\text{stat.}) \pm 1.2(\text{syst.}), \quad \mu \text{ channel}.$$

as reported in Table 1.

5.5 Cross-section measurement

5.5.1 Counting-based measurement of the cross-section in the ≥ 4-jet bin

In the ≥ 4-jet tagged sample the $t\bar{t}$ signal yield is obtained by subtracting the estimated rate of all backgrounds from the observed event yield. This method depends crucially on the understanding of the background, but makes minimal assumptions on $t\bar{t}$ signal properties for the yield calculation. For the QCD multi-jet and $W +$ jets backgrounds, the data-driven estimates described in detail in Sects. 5.3 and 5.4 are used, while for the expected background from $Z +$ jets and

single-top production, simulation estimates are used. Table 1 shows the complete overview of background contributions that are used in this calculation. The observed yields, the total expected background yields and the resulting $t\bar{t}$ signal yields for the $e +$ jets, $\mu +$ jets and combined channels are shown in Table 3.

The product of acceptance and branching fraction of $t\bar{t}$ events in the $\geq$4-jet tagged signal region, measured from Monte-Carlo samples and quoted in Sect. 5.1, is used together with the value of the integrated luminosity to extract the cross-section ($\sigma_{t\bar{t}}$) from the observed event yield. The resulting cross-sections are shown in Sect. 5.5.3.

Table 3 Observed event yield, estimated total background and $t\bar{t}$ signal using the counting method in the b-tagged $\geq$4-jet bin, for electrons and muons separately and combined. The total background consists of the sum of individual backgrounds listed in Table 1, choosing the data-driven estimate for $W +$ jets (instead of the simulation-based $W +$ jets estimate used in the 'total (non-$t\bar{t}$)' row of Table 1). The uncertainty on the total background includes statistical uncertainties in control regions and systematic uncertainties. The first quoted uncertainty on the $t\bar{t}$ signal yield is statistical, while the second is from the systematics on the background estimation

	$e +$ jets	$\mu +$ jets	combined
Observed	17	20	37
Estimated background	7.5 ± 3.1	4.7 ± 1.7	12.2 ± 3.9
$t\bar{t}$	$9.5 \pm 4.1 \pm 3.1$	$15.3 \pm 4.4 \pm 1.7$	$24.8 \pm 6.1 \pm 3.9$

Table 4 provides a detailed breakdown of the total systematic uncertainties on the cross-section for this method. The components listed under 'Object selection' relate to sources discussed in Sect. 4.1. The components listed under 'Background rates' relate to the uncertainties on background estimates detailed in Sects. 5.3 and 5.4. The components listed under 'Signal simulation' relate to sources discussed in Sect. 3.1. The largest systematic uncertainty is due to the normalisation of the QCD multi-jet background in the $e +$ jets channel, followed by the uncertainties which affect mainly the $t\bar{t}$ acceptance, like jet energy reconstruction, b-tagging and ISR/FSR. The dependence of the measured cross-section on the assumed top-quark mass is small. A change of ± 1 GeV in the assumed top-quark mass results in a change of $\mp 1\%$ in the cross-section.

While not used in the counting method, further information can be gained from the use of kinematic event properties: in the $t\bar{t}$ candidate events, three of the reconstructed jets are expected to come from a top quark which has decayed into hadrons. Following [21], the hadronic top quark candidate is empirically defined as the combination of three jets (with $p_T > 20$ GeV) having the highest vector sum p_T. This algorithm does not make use of the b-tagging information and selects the correct combination of the reconstructed jets in about 25% of cases. The observed distributions of the invariant mass (m_{jjj}) of the hadronic top quark candidates in the various $\geq$4-jet samples, shown in Figs. 3(a)–(c), demonstrate good agreement between the data and the

Table 4 Summary of individual systematic uncertainty contributions to the single-lepton cross-section determination using the counting method. The combined uncertainties listed in the bottom two rows include the luminosity uncertainty

	Relative cross-section uncertainty [%]	
Source	$e +$ jets	$\mu +$ jets
Statistical uncertainty	± 43	± 29
Object selection		
Lepton reconstruction, identification, trigger	± 3	± 2
Jet energy reconstruction	± 13	± 11
b-tagging	$-10/+15$	$-10/+14$
Background rates		
QCD normalisation	± 30	± 2
$W +$ jets normalisation	± 11	± 11
Other backgrounds normalisation	± 1	± 1
Signal simulation		
Initial/final state radiation	$-6/+13$	± 8
Parton distribution functions	± 2	± 2
Parton shower and hadronisation	± 1	± 3
Next-to-leading-order generator	± 4	± 6
Integrated luminosity	$-11/+14$	$-10/+13$
Total systematic uncertainty	$-38/+43$	$-23/+27$
Statistical + systematic uncertainty	$-58/+61$	$-37/+40$

Fig. 3 Distributions of the invariant mass of the 3-jet combination having the highest p_T for **a** the $\geq$4-jet tagged e + jets sample, **b** the $\geq$4-jet tagged μ + jets sample, **c** the $\geq$4-jet tagged samples combined and **d** the combined 3-jet tagged sample. The data is compared to the sum of all expected contributions. For the totals shown, simulation estimates are used for all contributions except QCD multi-jet, where a data-driven technique is used. The background uncertainty on the total expectation is represented by the *hatched area*
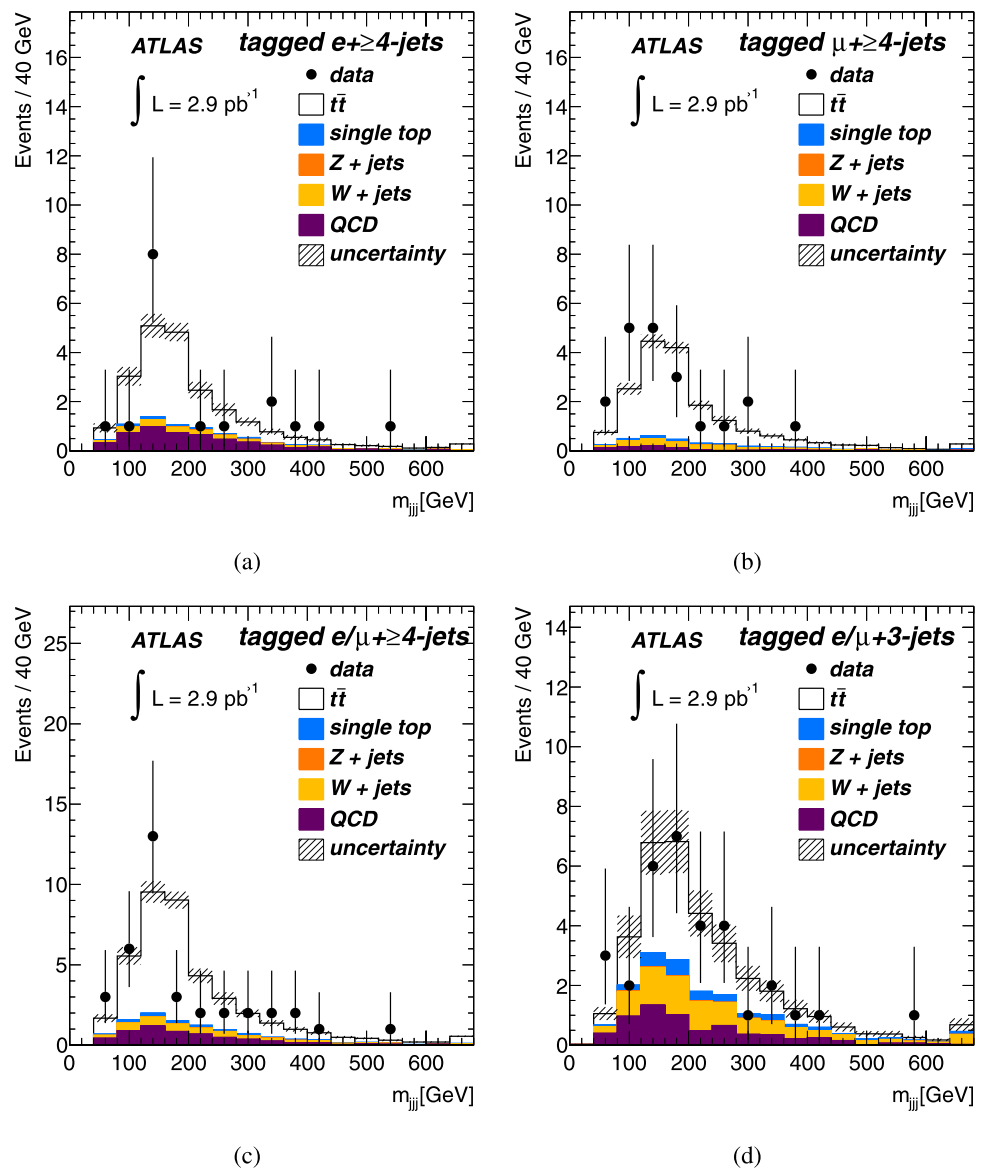
signal + background expectation. Figure 3(d) highlights a substantial contribution of $t\bar{t}$ signal events in the 3-jet tagged sample and demonstrates further information which is also not exploited by the baseline counting method.

5.5.2 Fit based cross-section measurement in the 3-jet and $\geq$4-jet samples

A complementary approach to measuring the cross-section exploits the data in both the 3-jet and $\geq$4-jet samples. With the current data sample, it provides an important cross-check of the counting method, as it makes different physics assumptions for the signal and background modelling. This technique is expected to become more precise once more data has been collected.

In the first approach (A), the tagged 3-jet and $\geq$4-jet samples are used. The m_{jjj} distribution for each sample is described by the sum of four templates for $t\bar{t}$, W + jets, QCD multi-jet and other backgrounds respectively. This method fits simultaneously the $t\bar{t}$ and W + jets components, relying mostly on shape information. The shapes of the templates for $t\bar{t}$, W + jets and smaller backgrounds are taken from simulation. The template for the QCD multi-jet background is taken from a data sample using a modified lepton definition, which requires at least one of the selection criteria listed in Sect. 4 to fail. A constraint is introduced on the ratio of the W + jets yields in the 3-jet and $\geq$4-jet samples, based on the simulation expectation of this ratio and accounting for its systematic uncertainty. This ratio and its uncertainty is similar to the $f_{2\rightarrow\geq4}^{corr}$ correction factor discussed in Sect. 5.4, and is calculated with the same procedure. Additionally, the

W + jets yields in the e + jets and μ + jets channels are related by their respective acceptances.

In the second approach (B), the tagged and zero-tag ≥ 4-jet samples are used to extract the cross section, with a template describing the sum of all backgrounds in each of these two samples. The 3-jet zero-tag and tagged samples, which have more background and less signal, are used to perform an auxiliary measurement of the fraction of the background that is tagged. This fraction is applied as a constraint on the relative rate of background events in the ≥ 4-jet zero-tag and ≥ 4-jet tagged samples. A simulation-based correction is applied to the 3-jet tagged background fraction to obtain the 4-jet tagged background fraction that accounts for expected differences in the background composition. The assumed rate of $t\bar{t}$ events in the 3-jet bin, used in the determination of the background yield in that bin, is iteratively adjusted to the measured cross-section. The template for $t\bar{t}$ and the relative contributions to the different samples are taken from simulation. As the shape of the W + jets background is compatible with the shape of the QCD background within the statistical uncertainty, the template for the sum of all backgrounds, is taken from a QCD multi-jet enhanced sample in data.

5.5.3 Results

The cross-sections obtained with the baseline counting method in the e + jets and μ + jets channels are shown in Table 5. The fit methods make different assumptions about the signal and background and therefore serve as good cross-checks; their cross-sections are also shown in Table 5 and are in good agreement with those obtained from the baseline counting method. Additionally, the estimate for the W + jets background in ≥ 4-jet tagged sample as measured in fit A is in agreement with the estimate quoted in Sect. 5.4. Table 5 also shows the cross-section obtained with the counting method for the e + jets and μ + jets channels, combined using the procedure described in Sect. 7. For the fit methods, the combined cross-sections are obtained from a simultaneous fit to the electron and muon samples.

Table 5 Inclusive $t\bar{t}$ cross-section measured in the single-lepton channel using the counting method and the template shape fitting techniques (A and B). The uncertainties represent respectively the statistical and systematic uncertainty including luminosity. The top row shows the counting-method results that are used for the combination presented in Sect. 7

Method	e + jets	μ + jets	e/μ + jets combined
Counting $\sigma_{t\bar{t}}$ [pb]	$105 \pm 46 \, ^{+45}_{-40}$	$168 \pm 49 \, ^{+46}_{-38}$	$142 \pm 34 \, ^{+50}_{-31}$
Fitted $\sigma_{t\bar{t}}$(A) [pb]	$98 \pm 58 \, ^{+34}_{-28}$	$167 \pm 68 \, ^{+46}_{-39}$	$130 \pm 44 \, ^{+38}_{-30}$
Fitted $\sigma_{t\bar{t}}$(B) [pb]	$110 \pm 50 \pm 39$	$134 \pm 52 \pm 39$	$118 \pm 34 \pm 34$

The systematic uncertainties of both fit-based methods are dominated by acceptance-related systematic uncertainties. Compared to the counting method, both fit-based techniques have a reduced sensitivity to the QCD multi-jet background rate but have method specific systematics: the ratio of tagged W + jets in the 3-jet and ≥ 4-jet bins and shape-modelling uncertainties for fit A, and the modelling of the b-tagged fraction for fit B. This trade-off results in a comparable total uncertainty for both methods compared to the counting method.

6 Dilepton analysis

6.1 Event selection

The dilepton $t\bar{t}$ final state is characterised by two isolated leptons with relatively high p_T, missing transverse energy corresponding to the neutrinos from the W leptonic decays, and two b quark jets. The selection of events in the signal region for the dilepton analysis consists of a series of kinematic requirements on the reconstructed objects defined in Sect. 4 and designed to select an orthogonal sample to the one described in Sect. 5.1:

- Exactly two oppositely-charged leptons (ee, $\mu\mu$ or $e\mu$) each satisfying $p_T > 20$ GeV, where at least one must be associated to a leptonic high-level trigger object.
- At least two jets with $p_T > 20$ GeV and with $|\eta| < 2.5$ are required, but no b-tagging requirements are imposed.
- To suppress backgrounds from Z + jets and QCD multi-jet events in the ee channel, the missing transverse energy must satisfy $E_T^{\mathrm{miss}} > 40$ GeV, and the invariant mass of the two leptons must differ by at least 5 GeV from the Z boson mass, i.e. $|m_{ee} - m_Z| > 5$ GeV. For the muon channel, the corresponding requirements are $E_T^{\mathrm{miss}} > 30$ GeV and $|m_{\mu\mu} - m_Z| > 10$ GeV.
- For the $e\mu$ channel, no E_T^{miss} or Z boson mass veto cuts are applied. However, the event H_T, defined as the scalar sum of the transverse energies of the two leptons and all selected jets, must satisfy $H_T > 150$ GeV to suppress backgrounds from Z + jets production.
- To remove events with cosmic-ray muons, events with two identified muons with large, oppositely signed transverse impact parameters ($d_0 > 500$ μm) and consistent with being back-to-back in the $r - \phi$ plane are discarded.

The E_T^{miss}, Z boson mass window, and H_T cuts are derived from a grid scan significance optimisation on simulated events which includes systematic uncertainties. The estimated $t\bar{t}$ acceptance, given a dilepton event, in each of the dilepton channels are $14.8 \pm 1.6\%$ (ee), $23.3 \pm 1.8\%$ ($\mu\mu$) and $24.8 \pm 1.2\%$ ($e\mu$). The corresponding acceptances including the $t\bar{t}$ branching ratios are 0.24% (ee), 0.38%
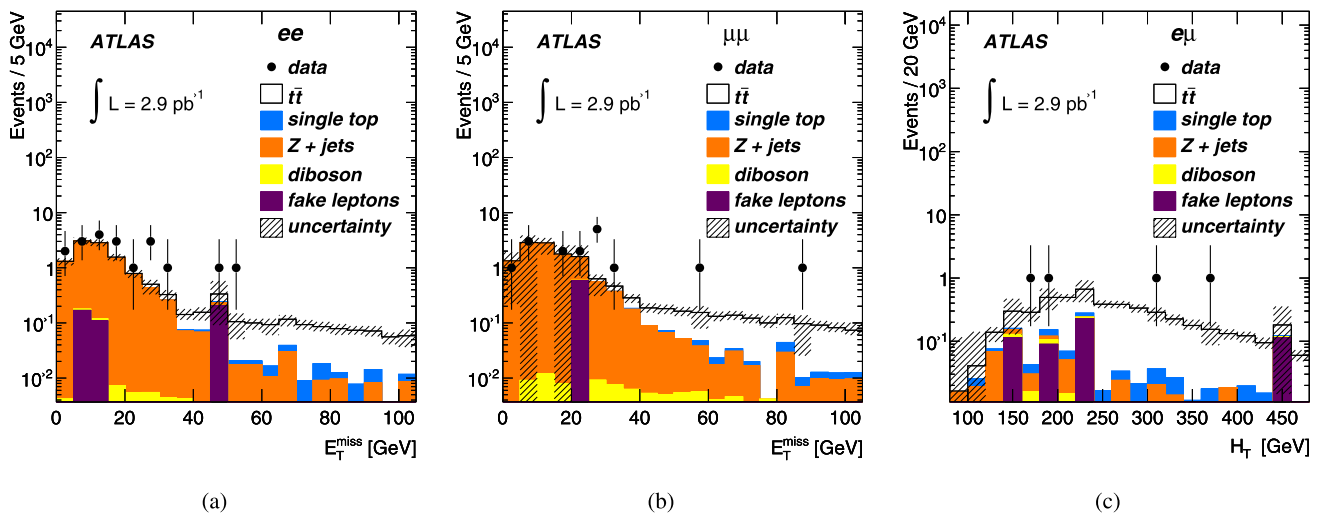
Fig. 4 The E_T^{miss} distribution in the signal region for **a** the *ee* channel without the $E_T^{miss} > 40$ GeV requirement, **b** the $\mu\mu$ channel without the $E_T^{miss} > 30$ GeV requirement, and **c** the distribution of the H_T, defined as the scalar sum of the transverse energies of the two leptons and all selected jets, in the signal region without the $H_T > 150$ GeV requirement
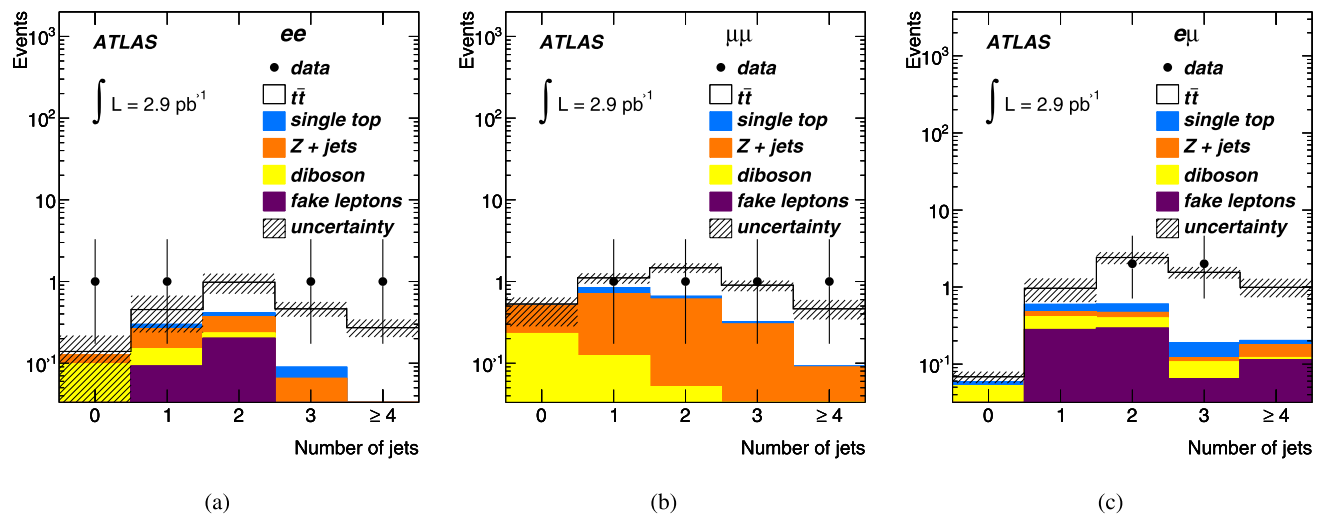

Fig. 5 Jet multiplicities for the signal region omitting the $N_{jets} \geq 2$ requirement in **a** the *ee* channel, **b** the $\mu\mu$ channel and **c** the *eμ* channel

($\mu\mu$) and 0.81% (*eμ*). The final numbers of expected and measured events in the signal region are shown in Table 6. Figure 4 shows the predicted and observed distributions of E_T^{miss} for the *ee* and $\mu\mu$ channels and of H_T for the *eμ* channel. The predicted and observed multiplicities of all jets and *b*-tagged jets are compared in Figs. 5 and 6 for each channel individually, and in Fig. 7 for all channels combined. Figure 7(b) shows that a majority of the selected events have at least one *b*-tagged jet, consistent with the hypothesis that the excess of events over the estimated background originates from $t\bar{t}$ decay. In each of these plots the selection has been relaxed to omit the cut on the observable shown.

6.2 Background determination strategy

The expected dominant backgrounds in the dilepton channel are Z boson production in association with jets, which can give rise to the same final state as $t\bar{t}$ signal, and W + jets. The latter can only contribute to the signal selection if the event contains at least one fake lepton.

Both Z + jets background and backgrounds with fake leptons are estimated from the data. The contributions from remaining electroweak background processes, such as single-top, WW, ZZ and WZ boson production are estimated from Monte-Carlo simulations.
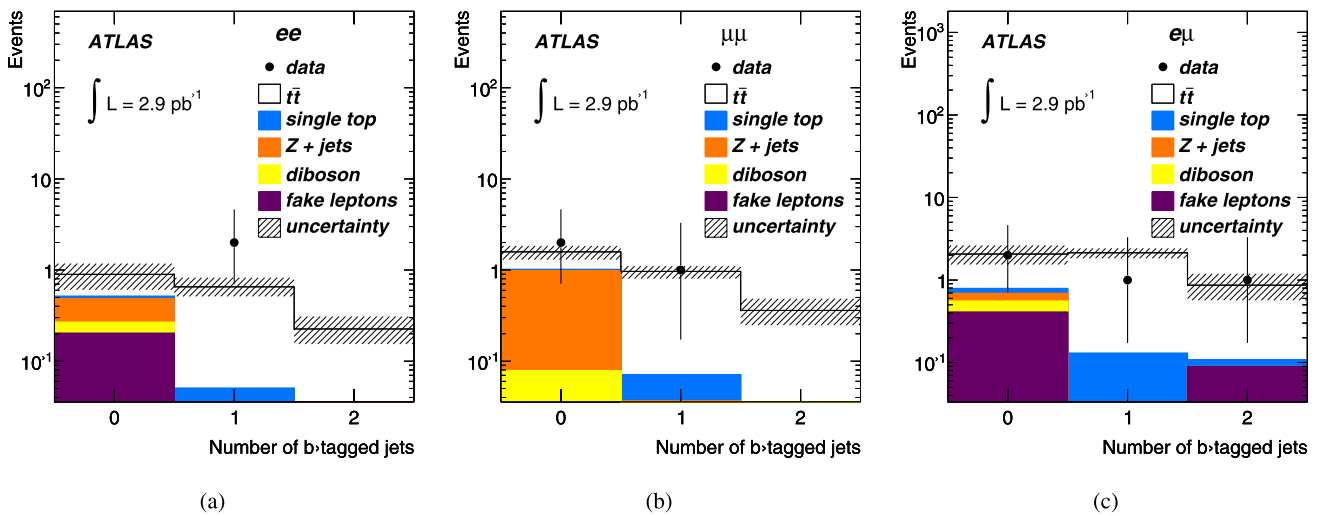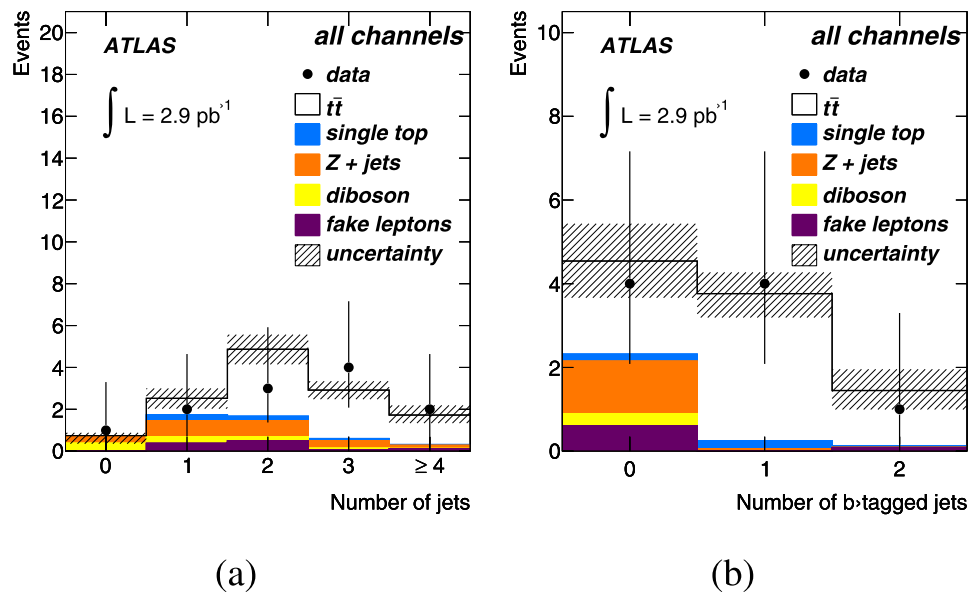
Fig. 6 The b-tagged jet multiplicities in the signal region for **a** the ee channel, **b** the $\mu\mu$ channel and **c** the $e\mu$ channel

Fig. 7 a Jet multiplicity in the signal region without the $N_{jets} \geq 2$ requirement and **b** the b-tagged jet multiplicity in the signal region, both for the combined dilepton channels

6.3 Non-Z lepton backgrounds

True $t\bar{t}$ dilepton events contain two leptons from W boson decays; the background comes predominantly from $W + $ jets events and single-lepton $t\bar{t}$ production with a fake lepton and a real lepton, though there is a smaller contribution with two fake leptons coming from QCD multi-jet production. As in the single-lepton analysis, in the case of muons, the dominant fake-lepton mechanism is a semi-leptonic decay of a heavy-flavour hadron, in which a muon survives the isolation requirement. In the case of electrons, the three mechanisms are heavy flavour decay, light flavour jets with a leading π^0 overlapping with a charged particle, and conversion of photons. Here 'fake' is used to mean both non-prompt

leptons and π^0s, conversions etc misidentified as leptons taken together.

The 'matrix method' introduced in Sect. 5.3.1 is extended here to measure the fraction of the dilepton sample that comes from fake leptons. A looser lepton selection is defined, and then it is used to count the number of observed dilepton events with zero, one or two tight ('T') leptons together with two, one or zero loose ('L') leptons, respectively (N_{LL}, N_{TL} and N_{LT}, N_{TT}, respectively). Then two probabilities are defined, $r(f)$, to be the probability that real (fake) leptons that pass the loose identification criteria, will also pass the tight criteria. Using r and f, linear expressions are then obtained for the observed yields as a function of the number or events with zero, one and two real leptons

together with two, one and zero fake leptons, respectively (N_{FF}, N_{FR} and N_{RF}, N_{RR}, respectively).

The method explicitly accounts for the presence of events with two fake leptons. These linear expressions form a matrix that is inverted in order to extract the real and fake content of the observed dilepton event sample:

$$\begin{bmatrix} N_{TT} \\ N_{TL} \\ N_{LT} \\ N_{LL} \end{bmatrix} = \begin{bmatrix} r^2 & rf & fr & f^2 \\ r(1-r) & r(1-f) & f(1-r) & f(1-f) \\ (1-r)r & (1-r)f & (1-f)r & (1-f)f \\ (1-r)^2 & (1-r)(1-f) & (1-f)(1-r) & (1-f)^2 \end{bmatrix}$$
$$\times \begin{bmatrix} N_{RR} \\ N_{RF} \\ N_{FR} \\ N_{FF} \end{bmatrix}. \qquad (6)$$

For muons, the loose selection is identical to the one described in Sect. 5.3.1. For loose electrons, the E/p cut and isolation requirements are dropped, and the 'medium' electron identification criteria as defined in Ref. [33] is replaced with the corresponding loose definition, with looser calorimeter and tracking cuts.

The efficiency for a real loose lepton to pass the full tight criteria, r, is measured in data in a sample of $Z \rightarrow \ell\ell$ events as a function of jet multiplicity. The corresponding efficiency for fake leptons, f, is measured in data in events with a single loose lepton, which are dominated by QCD di-jet production. Contributions from real leptons due to $W + $jets in the fake lepton control region are subtracted using simulated data.

The dominant systematic uncertainty on the $W + $jets background, as determined by the matrix method, comes from the possible difference in the mixture of processes where the efficiency for fake leptons f is measured, di-jet events and, where it is applied, the signal region. For electrons, a larger contribution is expected from heavy flavour events in the signal region due to $t\bar{t} \rightarrow \ell\nu bjjb$ events. This effect is accounted for by measuring the dependence of the efficiency for fake leptons on the heavy-flavour fraction and calculating a corrected efficiency for fake leptons based on the expected heavy-flavour fraction in the signal region in simulation studies. The fake estimate in the data includes contributions from events with tight and loose leptons, whose contributions have opposite signs. This can lead to some negative background estimates in the case of small statistics, but always consistent with zero. The results of the matrix method for the non-Z background are shown in Table 7 for 0, 1 and ≥ 2 jet bins. The results for the signal region (≥ 2 jets) is also reported in Table 6.

The most important cross-check comes from comparing the matrix method with two additional methods. The first (the 'weighting method') uses fake candidates in the single lepton sample and a fake rate to build an event weight for the fake lepton event. It uses a less restrictive loose definition and so probes the extrapolation of the fake rate f to the signal region. The method gives results consistent with the matrix method, as shown in Table 7. The second (the 'fitting method') makes no assumptions about the relative mixture of fake-lepton mechanisms, but uses data-derived templates in variables which can discriminate between real and fake leptons to fit for the fake-lepton fraction in the signal region. These variables are the expected lepton isolation and the number of high-threshold hits in the transition radiation tracker, allowing to distinguish electrons from heavy flavour decays or conversions. For the signal region the fitting method predicts $0.01^{+0.97}_{-0}\pm 0.01$ non-W boson events for the ee channel, $0.01^{+0.29}_{-0}\pm 0.01$ for the $\mu\mu$ channel, and $0.13^{+0.42}_{-0.13}\pm 0.14$ for the $e\mu$ channel. The estimate from the

Table 6 The full breakdown of the expected $t\bar{t}$-signal and background in the signal region compared to the observed event yields, for each of the dilepton channels (MC is simulation based, DD is data driven). All systematic uncertainties are included

	ee	$\mu\mu$	$e\mu$
$Z + $jets (DD)	0.25 ± 0.18	0.67 ± 0.38	–
$Z(\rightarrow \tau\tau) + $jets (MC)	0.07 ± 0.04	0.14 ± 0.07	0.13 ± 0.06
Non-Z leptons (DD)	0.16 ± 0.18	-0.08 ± 0.07	0.47 ± 0.28
Single top (MC)	0.08 ± 0.02	0.07 ± 0.03	0.22 ± 0.04
Dibosons (MC)	0.04 ± 0.02	0.07 ± 0.03	0.15 ± 0.05
Total (non $t\bar{t}$)	0.60 ± 0.27	0.88 ± 0.40	0.97 ± 0.30
$t\bar{t}$ (MC)	1.19 ± 0.19	1.87 ± 0.26	3.85 ± 0.51
Total expected	1.79 ± 0.38	2.75 ± 0.55	4.82 ± 0.65
Observed	2	3	4

Table 7 Overview of the estimated non-Z background yields in the signal region using two different data-driven methods with their statistical and systematic uncertainties respectively. The matrix method is the baseline method, the weighting method is used as a cross-check

Method	N_{jets}	ee	$\mu\mu$	$e\mu$
Matrix	0	$-0.07 \pm 0.05 \pm 0.05$	$-0.09 \pm 0.05 \pm 0.07$	$0.00 \pm 0.01 \pm 0.01$
	1	$0.09 \pm 0.14 \pm 0.07$	$-0.03 \pm 0.03 \pm 0.04$	$0.28 \pm 0.20 \pm 0.09$
	≥ 2	$0.16 \pm 0.17 \pm 0.06$	$-0.08 \pm 0.04 \pm 0.06$	$0.47 \pm 0.26 \pm 0.11$
Weighting	0	$0.03 \pm 0.03 \pm 0.02$	$0.34 \pm 0.14 \pm 0.32$	$0.00 \pm 0.04 \pm 0.04$
	1	$0.06 \pm 0.04 \pm 0.06$	$0.10 \pm 0.07 \pm 0.11$	$0.08 \pm 0.06 \pm 0.06$
	≥ 2	$0.10 \pm 0.06 \pm 0.08$	$0.00 \pm 0.04 \pm 0.04$	$0.10 \pm 0.05 \pm 0.09$

Table 8 Yields and uncertainties for the estimates of the $Z+$jets background. The uncertainties are statistical and systematic, respectively

	ee	$\mu\mu$
$Z+$jets (Monte-Carlo)	$0.14 \pm 0.03 \pm 0.16$	$0.56 \pm 0.06 \pm 0.39$
$Z+$jets (data-driven)	$0.25 \pm 0.09 \pm 0.16$	$0.67 \pm 0.22 \pm 0.31$

Table 9 Measured cross-sections in each individual dilepton channel and in the combined fit. The uncertainties represent the statistical and combined systematic uncertainty, respectively

Channel	$\sigma_{t\bar{t}}$ [pb]
ee	$193^{+243}_{-152}{}^{+84}_{-48}$
$\mu\mu$	$185^{+184}_{-124}{}^{+56}_{-47}$
$e\mu$	$129^{+100}_{-72}{}^{+32}_{-18}$
Combined	$151^{+78}_{-62}{}^{+37}_{-24}$

fitting method is based on data in the signal region, whereas the other methods provide estimates for the signal region based on measurement in control regions.

6.4 $Z+$jets background

Although the $t\bar{t}$ event selection is designed to reject $Z+$jets events, a small fraction of events which populate the E_T^{miss} tails and dilepton invariant mass more than 5 GeV (for ee) or 10 GeV (for $\mu\mu$) away from the Z boson mass will enter the signal sample. These events are difficult to model in simulations due to large uncertainties on the non-Gaussian missing energy tails, the Z boson cross-section for higher jet multiplicities, and the lepton energy resolution. The $Z+$jets events are expected to have significant E_T^{miss} tails, primarily originating from mis-measurements of the jet energies.

The $Z+$jets background is estimated by extrapolating from a control region orthogonal to the top quark signal region. This control region is defined using the cuts for the signal region, but with an inverted Z boson mass window (requiring $|m_{\ell\ell} - m_Z| < 5$ GeV for ee and $|m_{\ell\ell} - m_Z| < 10$ GeV for $\mu\mu$) and lowering the E_T^{miss} requirement to $E_T^{\mathrm{miss}} > 20$ GeV. For E_T^{miss} below the signal region the Z boson mass window is extended to $|m_{\ell\ell} - M_Z| < 15$ GeV to reduce systematic uncertainties from the lepton energy scale and resolution. A scale factor from $Z+$jets simulation is used to extrapolate from the observed yield in the control region to the expected yield in the signal region. The small non-Z boson background in the control region is corrected using the Monte-Carlo expectation.

The yield estimates obtained with this procedure are shown in Table 8, along with estimates of $Z+$jets background based on simulation only. The comparison demonstrates that data-driven normalisation using the control regions helps to reduce the effect of the systematic uncertainties. The estimated yields from data are higher than those from the Monte-Carlo prediction. This trend is also observed in the control regions involving E_T^{miss} where jets are used in the selection.

Due to the very limited data statistics, simulation is used for the $Z \to \tau\tau$ contribution instead of the data-driven method used to estimate $Z \to ee$ and $Z \to \mu\mu$ contributions. The modelling of the $Z \to \tau\tau$ is cross-checked in the $e\mu$ channel in the 0-jet bin, where five events are observed in data versus a total expectation of 3.1 events, with an expected $Z \to \tau\tau$ contribution of 2.4 events. The largest sys-

tematic uncertainty comes from that on the integrated luminosity. The estimated $Z+$jets backgrounds are summarised in Table 6.

Data-driven backgrounds and simulated acceptances and efficiencies are validated in control regions which are depleted of $t\bar{t}$ events: inside the Z boson peak for the same-flavour channels; the 0- and 1-jet bin for the $e\mu$ channel.

Figure 8(a) and (b) show the jet multiplicity for events where the dilepton mass lies inside the Z boson peak and tests the initial state radiation (ISR) modelling of jets for $Z+$jets processes. The dilepton mass plots, Figs. 8(c) and (d), probe the lepton energy scale and resolution.

The understanding of $\gamma \to e^+e^-$ conversions can be tested by using same-sign events. Five same-sign events are observed inside the Z boson peak in the inclusive ee channel and they are compatible, within the limited statistics, with the conversions modelled by the simulations. No same-sign events have been observed in the $\mu\mu$ or $e\mu$ channels.

6.5 Cross-section determination in the dilepton channels

The cross-section is measured in each dilepton channel and translated into an inclusive $t\bar{t}$ cross-section using the $W \to \ell\nu$ and $\tau \to \ell\nu\nu_\tau$ branching ratios. The cross-sections and uncertainties in the individual channels are estimated using the likelihood method as will be described in Sect. 7. The cross-sections are summarised in Table 9, and the breakdown of the individual sources of cross-section uncertainties are listed in Table 10. The dependence of the measured cross-section on the assumed top-quark mass is small. A change of ± 1 GeV in the assumed mass results in a change of $\mp 0.5\%$ in the cross-section.

7 Combination of the single lepton and the dilepton channels

The combined measurement of the $t\bar{t}$ production cross-section is based on a likelihood fit in which the number of

Fig. 8 *Top row*: Number of jets in events with the measured dilepton mass inside the Z boson mass window with inverted requirement on E_T^{miss} for **a** the ee channel and **b** the $\mu\mu$ channel. *Bottom row*: Invariant mass of opposite-signed lepton pairs in events with ≥ 2 jets with inverted requirement on E_T^{miss} for **c** the ee channel and **d** the $\mu\mu$ channel

(a)

(b)

(c)

(d)
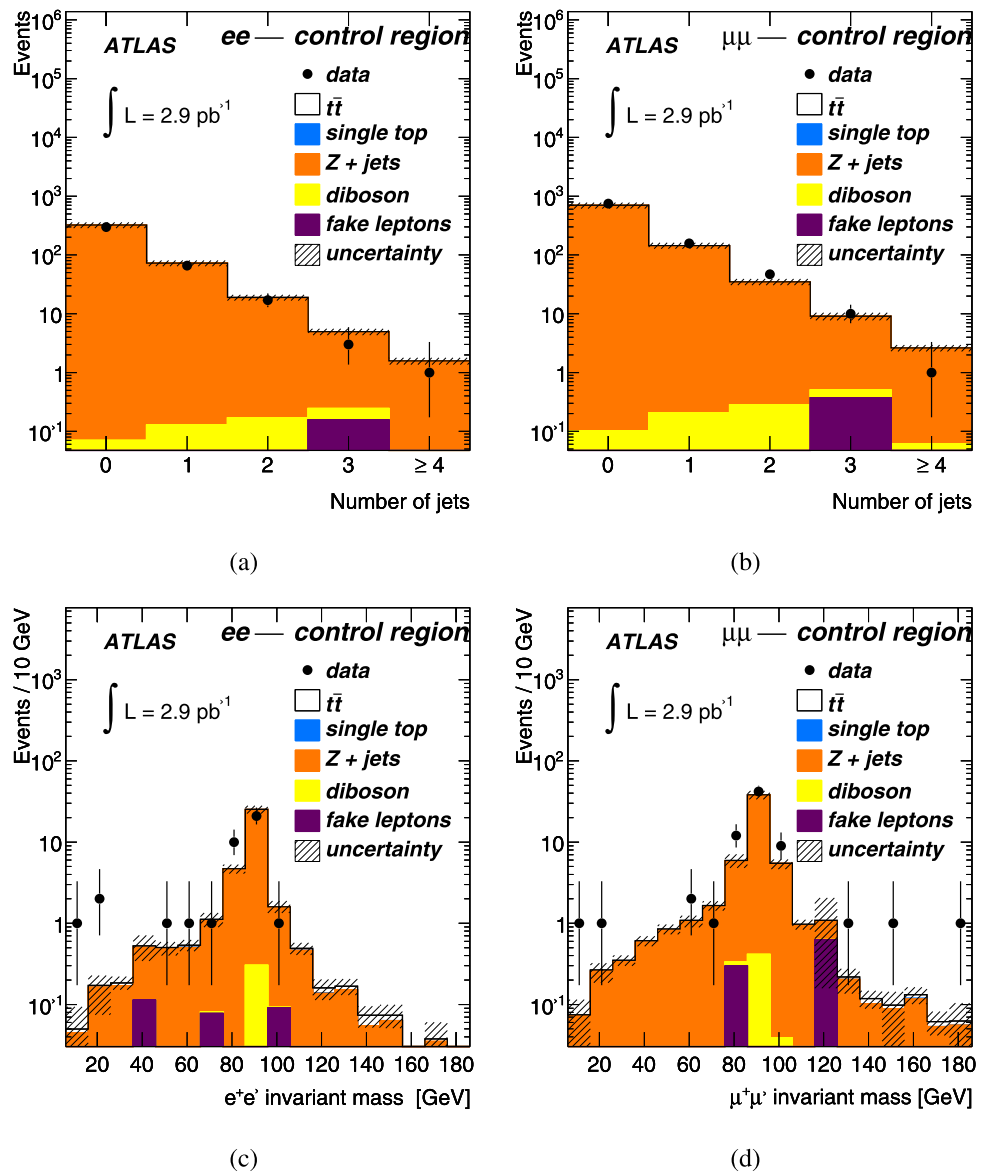
expected events is modelled as

$$N^{\mathrm{exp}}(\sigma_{t\bar{t}}, \alpha_j) = L \cdot \epsilon_{t\bar{t}}(\alpha_j) \cdot \sigma_{t\bar{t}}$$

$$+ \sum_{bkg} L \cdot \epsilon_{bkg}(\alpha_j) \cdot \sigma_{bkg}(\alpha_j)$$

$$+ N_{DD}(\alpha_j), \qquad (7)$$

where L is the integrated luminosity, $\epsilon_{t\bar{t}}$ is the signal acceptance, ϵ_{bkg}, σ_{bkg} are the efficiency and cross-section for backgrounds as obtained from MC simulation respectively, and N_{DD} is the number of expected events from data-driven estimates. The acceptance and background estimates depend on sources of systematic uncertainty labelled as α_j. The

likelihood for a single channel is defined as

$$\mathcal{L}(\sigma_{t\bar{t}}, L, \alpha_j) = \mathrm{Poisson}\big(N^{\mathrm{obs}} \mid N^{\mathrm{exp}}(\sigma_{t\bar{t}}, \alpha_j)\big)$$

$$\times \mathrm{Gauss}(L_0 \mid L, \delta_L) \times \prod_{j \in \mathrm{syst}} \Gamma_j(\alpha_j), \qquad (8)$$

where L_0 is the integrated luminosity of the data sample and $\delta_L = 11\% \cdot L_0$. Sources of systematic uncertainties are grouped into subsets that are uncorrelated to each other. However each group can have correlated effects on multiple signal and background estimates. The relationship between the channels is enforced by identifying the α_j common to different channels in the construction of the combined likelihood function. Ensembles of pseudo-data were generated and the resulting estimate of the cross-section was confirmed to be unbiased. The method is the same as the

Table 10 Individual systematic uncertainties on the $t\bar{t}$ cross-section in the dilepton channels. The combined uncertainties listed in the bottom two rows include the luminosity uncertainty

	Relative cross-section uncertainty [%]		
Source	ee	$\mu\mu$	$e\mu$
Statistical uncertainty	−79/+126	−67/+100	−56/+77
Object selection			
Lepton reconstruction, identification, trigger	−2/+11	−4/+3	−1/+3
Jet energy reconstruction	−7/+13	−14/+9	−3/+5
Background rates			
Fake leptons	−31/+24	−4/+1	−15/+8
Z + jets	−12/+4	−19/+5	−2/+1
Monte-Carlo simulation statistics	−5/+3	−3/+4	±2
Theoretical cross-sections	± 3	−5/+4	±3
Signal simulation			
Initial/final state radiation	−4/+5	−2/+3	−2/+3
Parton distribution functions	−2/+1	−2/+3	−2/+3
Parton shower and hadronisation	−9/+14	−6/+9	±3
Next-to-leading order generator	−8/+11	−11/+13	−3/+4
Integrated luminosity	−11/+16	−11/+16	−12/+14
Total systematic uncertainty	−25/+44	−25/+30	−14/+25
Statistical + systematic uncertainty	−83/+134	−72/+104	−57/+81

Table 11 Summary of $t\bar{t}$ cross-section and signal significance calculated by combining the single lepton and dilepton channels individually and for all channels combined

	Cross-section [pb]	Signal significance [σ]
Single lepton channels	$142 \pm 34 ^{+50}_{-31}$	4.0
Dilepton channels	$151 ^{+78}_{-62} ^{+37}_{-24}$	2.8
All channels	$145 \pm 31 ^{+42}_{-27}$	4.8

one used in [44] and described in [45]; however, in this case systematic uncertainties are modelled with gamma distributions, which are more suitable priors for large systematics than truncated Gaussians [46]. In the small systematic uncertainty limit, the gamma distribution coincides with the conventional choice of a Gaussian.

Table 11 lists the cross-sections and signal significance for the single-lepton, dilepton and the combined channels with the corresponding statistical and systematic uncertainties extracted from the likelihood fit. By combining all five channels, the background-only hypothesis is excluded at a significance of 4.8σ obtained with the approximate method of [45]. If Gaussian distributions are assumed for all systematic uncertainties, a significance of 5.1σ is obtained. The absence of bias in the fit is validated by pseudo-experiments. Similarly, the traditional hybrid Bayesian-frequentist approach in which the α_j are randomised in an ensemble of pseudo-experiments finds a signal significance consistent with the results from the likelihood method within 0.1σ. The

results also agree with those obtained from an alternative method based on a purely Bayesian methodology.

8 Summary

Measurements of the $t\bar{t}$ production cross-section in the single-lepton and dilepton channels using the ATLAS detector are reported. In a sample of 2.9 pb^{-1}, 37 $t\bar{t}$ candidate events are observed in the single-lepton topology, as well as 9 candidate events in the dilepton topology, resulting in a measurement of the inclusive $t\bar{t}$ cross-section of

$$\sigma_{t\bar{t}} = 145 \pm 31 ^{+42}_{-27} \text{ pb}.$$

This is the first ATLAS Collaboration measurement making simultaneous use of reconstructed electrons, muons, jets, b-tagged jets and missing transverse energy, therefore exploiting the full capacity of the detector. The combined measurement, consisting of the first measurement of the $t\bar{t}$ cross-section in the single-lepton channel at the LHC and a measurement in the dilepton channel, is the most precise measurement to date of the $t\bar{t}$ cross-section at $\sqrt{s} = 7$ TeV.

The cross-sections measured in each of the five sub-channels are consistent with each other and kinematic properties of the selected events are consistent with SM $t\bar{t}$ production. The measured $t\bar{t}$ cross-section is in good agreement with the measurement in the dilepton channel by CMS [10],
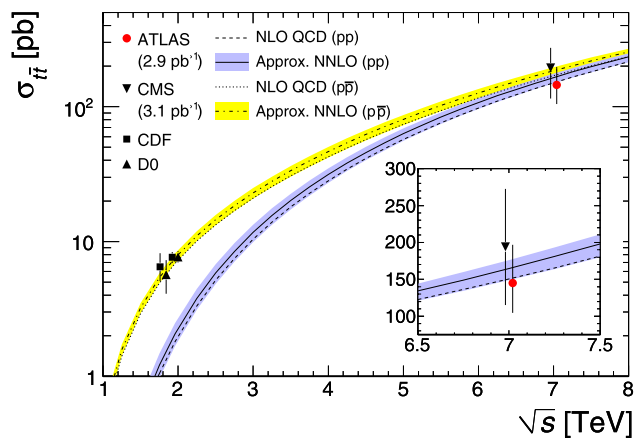
Fig. 9 Top quark pair-production cross-section at hadron colliders as measured by CDF and D0 at Tevatron, CMS and ATLAS (this measurement). The theoretical predictions for pp and $p\bar{p}$ collisions include the scale and PDF uncertainties, obtained using the HATHOR tool with the CTEQ6.6 PDFs and assume a top-quark mass of 172.5 GeV

as well as with NLO QCD predictions [47–51] and the approximate NNLO top quark cross-section calculation [52]. Figure 9 shows the ATLAS and CMS measurements together with previous Tevatron measurements [6–9].

With the prospect of accumulation of larger data samples, the statistical and systematic uncertainty on the $t\bar{t}$ cross-section will decrease and a precise measurement can challenge the SM prediction based on QCD calculations and constrain the parton distribution functions. Larger samples of $t\bar{t}$ events will also be instrumental in precision studies of the production, mass and decay properties of top quarks, and be vital in new physics searches in which SM $t\bar{t}$ production is an important background.

References

1. S.L. Glashow, Partial symmetries of weak interactions. Nucl. Phys. **22**, 579 (1961)
2. S. Weinberg, A model of leptons. Phys. Rev. Lett. **19**, 1264 (1967)
3. A. Salam, Weak and electromagnetic interactions, in *Elementary Particle Theory*, ed. by N. Svartholm (Almqvist and Wiksell, Stockholm, 1968), p. 367
4. S. Moch, P. Uwer, Theoretical status and prospects for top-quark pair production at hadron colliders. Phys. Rev. D **78**, 034003 (2008)
5. U. Langenfeld, S. Moch, P. Uwer, New results for $t\bar{t}$ production at hadron colliders, in *Proc. XVII Int. Workshop on Deep-Inelastic Scattering and Related Topics* (2009). 10.3360/dis.2009.131. arXiv:0907.2527 [hep-ph]
6. T. Affolder et al. (CDF Run I), Measurement of the $t\bar{t}$ production cross-section in $p\bar{p}$ collisions at $\sqrt{s} = 1.8$ TeV. Phys. Rev. D **64**, 032002 (2001). erratum-ibid. D **67**, 119901 (2003)
7. T. Affolder et al. (CDF Run I), CDF public note 10137 (2010) (Run II)
8. V.M. Abazov et al. (D0 Run I), $t\bar{t}$ production cross section in $p\bar{p}$ collisions at $\sqrt{s} = 1.8$ TeV. Phys. Rev. D **67**, 012004 (2003)
9. V.M. Abazov et al. (D0 Run I), D0 note 6037-CONF (2010) (Run II)
10. The CMS Collaboration, First measurement of the cross section for top-quark pair production in proton-proton collisions at $\sqrt{s} = 7$ TeV. Phys. Lett. B **695**, 424 (2011). arXiv:1010.5994 [hep-ex]
11. K. Nakamura et al. (Particle Data Group), The review of particle physics. J. Phys. G **37**, 075021 (2010)
12. ATLAS Collaboration, The ATLAS experiment at the CERN Large Hadron Collider. J. Instrum. **3**, S08003 (2008)
13. ATLAS Collaboration, Luminosity determination using the ATLAS detector. ATLAS-CONF-2010-060. cdsweb.cern.ch/record/1281333
14. S. Frixione, B.R. Webber, Matching NLO QCD computations and parton shower simulations. J. High Energy Phys. **06**, 029 (2002)
15. S. Frixione, P. Nason, B.R. Webber, Matching NLO QCD and parton showers in heavy flavour production. J. High Energy Phys. **08**, 007 (2003)
16. S. Frixione, E. Laenen, P. Motylinski, Single-top production in MC@NLO. J. High Energy Phys. **03**, 092 (2006)
17. P.M. Nadolsky et al., Implications of CTEQ global analysis for collider observables. Phys. Rev. D **78**, 013004 (2008)
18. M.L. Mangano, M. Moretti, F. Piccinini, R. Pittau, A.D. Polosa, ALPGEN, a generator for hard multiparton processes in hadronic collisions. J. High Energy Phys. **07**, 001 (2003)
19. J. Pumplin et al., New generation of parton distributions with uncertainties from global QCD analysis. J. High Energy Phys. **07**, 012 (2002)
20. S. Frixione, E. Laenen, P. Motylinski, B.R. Webber, C.D. White, Single-top hadroproduction in association with a W boson. J. High Energy Phys. **07**, 029 (2008)
21. ATLAS Collaboration, Expected performance of the ATLAS experiment—detector, trigger and physics. CERN-OPEN-2008-020, pp. 874–881. arXiv:0901.0512 [hep-ex]

22. G. Corcella et al., HERWIG 6.5: an event generator for hadron emission reactions with interfering gluons (including supersymmetric processes). J. High Energy Phys. **01**, 010 (2001)

23. G. Corcella et al., HERWIG 6.5 release notes. arXiv:hep-ph/0210213

24. J.M. Butterworth et al., Multiparton interactions in photoproduction at HERA. Z. Phys. C **72**, 637 (1996)

25. ATLAS Collaboration, ATLAS Monte Carlo tunes for MC09, ATLAS-PHYS-PUB-2010-002

26. ATLAS Collaboration, The ATLAS Simulation Infrastructure. Eur. Phys. J. C (2010). doi:10.1140/epjc/s10052-010-1429-9. arXiv:1005.4568

27. P. Nason, A new method for combining NLO QCD with shower Monte Carlo algorithms. J. High Energy Phys. **11546**, 040 (2004)

28. B.P. Kersevan, E. Richter-Was, The Monte Carlo event generator AcerMC version 2.0 with interfaces to PYTHIA 6.2 and HERWIG 6.5. arXiv:hep-ph/0405247

29. P. Skands, Tuning Monte Carlo generators: The Perugia tunes. Phys. Rev. D **82**, 074018 (2010)

30. A. Buckley et al., Systematic event generator tuning for the LHC. Eur. Phys. J. C **65**, 331–357 (2010)

31. M. Mangano, Understanding the Standard Model, as a bridge to the discovery of new phenomena at the LHC, CERN-PH-TH-2008-019. arXiv:0802.0026 [hep-ph]

32. T. Gleisberg et al., Event generation with SHERPA 1.1. J. High Energy Phys. **02**, 007 (2009)

33. ATLAS Collaboration, Measurement of the $W \to \ell\nu$ and $Z/\gamma^* \to \ell\ell$ production cross-sections in proton-proton collisions at $\sqrt{s} = 7$ TeV with the ATLAS detector. J. High Energy Phys. **12**, 060 (2010). arXiv:1010.2130 [hep-ex]

34. ATLAS Collaboration, Data-quality requirements and event cleaning for jets and missing transverse energy reconstruction with the ATLAS detector in proton-proton collisions at a center-of-mass energy of $\sqrt{s} = 7$ TeV. ATLAS-CONF-2010-038. cdsweb.cern.ch/record/1277678

35. ATLAS Collaboration, Muon performance in minimum bias pp collision data at $\sqrt{s} = 7$ TeV with ATLAS. ATLAS-CONF-2010-036. cdsweb.cern.ch/record/1277675

36. M. Cacciari, G.P. Salam, G. Soyez, The anti-kt jet clustering algorithm. J. High Energy Phys. **0804**, 063 (2008)

37. ATLAS Collaboration, Measurement of inclusive jet and dijet cross-sections in proton-proton collisions at 7 TeV centre-of-mass energy with the ATLAS detector. Eur. Phys. J. C **71**, 1512 (2011). arXiv:1009.5908

38. ATLAS Collaboration, Calibrating the b-tag and mistag efficiencies of the SV0 b-tagging algorithm in 3 pb^{-1} of data with the ATLAS detector. ATLAS-CONF-2010-099. cdsweb.cern.ch/record/1312145

39. ATLAS Collaboration, Performance of the missing transverse energy reconstruction and calibration in proton-proton collisions at a center-of-mass energy of $\sqrt{s} = 7$ TeV with the ATLAS detector. ATLAS-CONF-2010-057. cdsweb.cern.ch/record/1281330

40. F.A. Berends, W.T. Giele, H. Kuijf, R. Kleiss, W.J. Stirling, Nucl. Phys. B **357**, 1 (1991)

41. C.F. Berger et al., Precise predictions for $W + 4$ jet production at the Large Hadron Collider., September 2010. 5pp. Temporary entry e-Print: arXiv:1009.2338 [hep-ph]

42. S.D. Ellis, R. Kleiss, W.J. Stirling, W's, Z's and jets. Phys. Lett. B **154**, 435 (1985)

43. J. Alwall et al., Comparative study of various algorithms for the merging of parton showers and matrix elements in hadronic collisions. Eur. J. Phys. C **53**, 473 (2008)

44. ATLAS Collaboration, Prospects for measuring top pair production in the dilepton channel with early ATLAS data at $\sqrt{s} = 10$ TeV. ATL-PHYS-PUB-2009-086. cdsweb.cern.ch/record/1200287

45. G. Cowan, K. Cranmer, E. Gross, O. Vitelles, Asymptotic formulae for likelihood-based test of new physics. Eur. Phys. J. (submitted). arXiv:1007.1727 [hep-ex]

46. R.D. Cousins, J. Linnemann, J. Tucker, Evaluation of three methods for calculating statistical significance when incorporating a systematic uncertainty into a test of the background-only hypothesis for a Poisson process. Nucl. Instrum. Methods Phys. Res., Sect. A, Accel. Spectrom. Detect. Assoc. Equip. **595**, 480–501 (2008)

47. P. Nason, S. Dawson, R.K. Ellis, The total cross-section for the production of heavy quarks in hadronic collisions. Nucl. Phys. B **303**, 607 (1988)

48. W. Beenakker, H. Kuijf, W.L. van Neerven, J. Smith, QCD corrections to heavy quark production in $p\bar{p}$ collisions. Phys. Rev. D **40**, 54–82 (1989)

49. M. Czakon, A. Mitov, Inclusive heavy flavor hadroproduction in NLO QCD: the exact analytic result. Nucl. Phys. B **824**, 111–135 (2010)

50. S. Moch, P. Uwer, Theoretical status and prospects for top-quark pair production at hadron colliders. Phys. Rev. D **78**, 034003 (2008)

51. M. Beneke, M. Czakon, P. Falgari, A. Mitov, C. Schwinn, Threshold expansion of the $gg(q\bar{q}) \to Q\bar{Q} + X$ cross section at $O(\alpha_s^4)$. Phys. Lett. B **690**, 483–490 (2010)

52. M. Aliev et al., HATHOR—HAdronic Top and Heavy quarks crOss section calculatoR. arXiv:1007.1327 [hep-ph]

The ATLAS Collaboration

G. Aad[48], B. Abbott[111], J. Abdallah[11], A.A. Abdelalim[49], A. Abdesselam[118], O. Abdinov[10], B. Abi[112], M. Abolins[88], H. Abramowicz[153], H. Abreu[115], E. Acerbi[89a,89b], B.S. Acharya[164a,164b], M. Ackers[20], D.L. Adams[24], T.N. Addy[56], J. Adelman[175], M. Aderholz[99], S. Adomeit[98], P. Adragna[75], T. Adye[129], S. Aefsky[22], J.A. Aguilar-Saavedra[124b,a], M. Aharrouche[81], S.P. Ahlen[21], F. Ahles[48], A. Ahmad[148], H. Ahmed[2], M. Ahsan[40], G. Aielli[133a,133b], T. Akdogan[18a], T.P.A. Åkesson[79], G. Akimoto[155], A.V. Akimov [94], M.S. Alam[1], M.A. Alam[76], S. Albrand[55], M. Aleksa[29],

I.N. Aleksandrov[65], M. Aleppo[89a,89b], F. Alessandria[89a], C. Alexa[25a], G. Alexander[153], G. Alexandre[49], T. Alexopoulos[9], M. Alhroob[20], M. Aliev[15], G. Alimonti[89a], J. Alison[120], M. Aliyev[10], P.P. Allport[73], S.E. Allwood-Spiers[53], J. Almond[82], A. Aloisio[102a,102b], R. Alon[171], A. Alonso[79], J. Alonso[14], M.G. Alviggi[102a,102b], K. Amako[66], P. Amaral[29], C. Amelung[22], V.V. Ammosov[128], A. Amorim[124a,b], G. Amorós[167], N. Amram[153], C. Anastopoulos[139], T. Andeen[34], C.F. Anders[20], K.J. Anderson[30], A. Andreazza[89a,89b], V. Andrei[58a], M.-L. Andrieux[55], X.S. Anduaga[70], A. Angerami[34], F. Anghinolfi[29], N. Anjos[124a], A. Annovi[47], A. Antonaki[8], M. Antonelli[47], S. Antonelli[19a,19b], J. Antos[144b], B. Antunovic[41], F. Anulli[132a], S. Aoun[83], L. Aperio Bella[4], R. Apolle[118], G. Arabidze[88], I. Aracena[143], Y. Arai[66], A.T.H. Arce[44], J.P. Archambault[28], S. Arfaoui[29,c], J.-F. Arguin[14], E. Arik[18a,*], M. Arik[18a], A.J. Armbruster[87], K.E. Arms[109], S.R. Armstrong[24], O. Arnaez[81], C. Arnault[115], A. Artamonov[95], G. Artoni[132a,132b], D. Arutinov[20], S. Asai[155], R. Asfandiyarov[172], S. Ask[27], B. Åsman[146a,146b], L. Asquith[5], K. Assamagan[24], A. Astbury[169], A. Astvatsatourov[52], G. Atoian[175], B. Aubert[4], B. Auerbach[175], E. Auge[115], K. Augsten[127], M. Aurousseau[4], N. Austin[73], R. Avramidou[9], D. Axen[168], C. Ay[54], G. Azuelos[93,d], Y. Azuma[155], M.A. Baak[29], G. Baccaglioni[89a], C. Bacci[134a,134b], A.M. Bach[14], H. Bachacou[136], K. Bachas[29], G. Bachy[29], M. Backes[49], E. Badescu[25a], P. Bagnaia[132a,132b], S. Bahinipati[2], Y. Bai[32a], D.C. Bailey[158], T. Bain[158], J.T. Baines[129], O.K. Baker[175], S. Baker[77], F. Baltasar Dos Santos Pedrosa[29], E. Banas[38], P. Banerjee[93], Sw. Banerjee[169], D. Banfi[89a,89b], A. Bangert[137], V. Bansal[169], H.S. Bansil[17], L. Barak[171], S.P. Baranov[94], A. Barashkou[65], A. Barbaro Galtieri[14], T. Barber[27], E.L. Barberio[86], D. Barberis[50a,50b], M. Barbero[20], D.Y. Bardin[65], T. Barillari[99], M. Barisonzi[174], T. Barklow[143], N. Barlow[27], B.M. Barnett[129], R.M. Barnett[14], A. Baroncelli[134a], A.J. Barr[118], F. Barreiro[80], J. Barreiro Guimar aes da Costa[57], P. Barrillon[115], R. Bartoldus[143], A.E. Barton[71], D. Bartsch[20], R.L. Bates[53], L. Batkova[144a], J.R. Batley[27], A. Battaglia[16], M. Battistin[29], G. Battistoni[89a], F. Bauer[136], H.S. Bawa[143], B. Beare[158], T. Beau[78], P.H. Beauchemin[118], R. Beccherle[50a], P. Bechtle[41], H.P. Beck[16], M. Beckingham[48], K.H. Becks[174], A.J. Beddall[18c], A. Beddall[18c], V.A. Bednyakov[65], C. Bee[83], M. Begel[24], S. Behar Harpaz[152], P.K. Behera[63], M. Beimforde[99], C. Belanger-Champagne[166], B. Belhorma[55], P.J. Bell[49], W.H. Bell[49], G. Bella[153], L. Bellagamba[19a], F. Bellina[29], G. Bellomo[89a,89b], M. Bellomo[119a], A. Belloni[57], K. Belotskiy[96], O. Beltramello[29], S. Ben Ami[152], O. Benary[153], D. Benchekroun[135a], C. Benchouk[83], M. Bendel[81], B.H. Benedict[163], N. Benekos[165], Y. Benhammou[153], D.P. Benjamin[44], M. Benoit[115], J.R. Bensinger[22], K. Benslama[130], S. Bentvelsen[105], D. Berge[29], E. Bergeaas Kuutmann[41], N. Berger[4], F. Berghaus[169], E. Berglund[49], J. Beringer[14], K. Bernardet[83], P. Bernat[115], R. Bernhard[48], C. Bernius[24], T. Berry[76], A. Bertin[19a,19b], F. Bertinelli[29], F. Bertolucci[122a,122b], M.I. Besana[89a,89b], N. Besson[136], S. Bethke[99], W. Bhimji[45], R.M. Bianchi[48], M. Bianco[72a,72b], O. Biebel[98], J. Biesiada[14], M. Biglietti[132a,132b], H. Bilokon[47], M. Bindi[19a,19b], A. Bingul[18c], C. Bini[132a,132b], C. Biscarat[177], R. Bischof[62], U. Bitenc[48], K.M. Black[21], R.E. Blair[5], J.-B. Blanchard[115], G. Blanchot[29], C. Blocker[22], J. Blocki[38], A. Blondel[49], W. Blum[81], U. Blumenschein[54], C. Boaretto[132a,132b], G.J. Bobbink[105], V.B. Bobrovnikov[107], A. Bocci[44], R. Bock[29], C.R. Boddy[118], M. Boehler[41], J. Boek[174], N. Boelaert[35], S. Böser[77], J.A. Bogaerts[29], A. Bogdanchikov[107], A. Bogouch[90,*], C. Bohm[146a], V. Boisvert[76], T. Bold[163,e], V. Boldea[25a], M. Boonekamp[136], G. Boorman[76], C.N. Booth[139], P. Booth[139], J.R.A. Booth[17], S. Bordoni[78], C. Borer[16], A. Borisov[128], G. Borissov[71], I. Borjanovic[12a], S. Borroni[132a,132b], K. Bos[105], D. Boscherini[19a], M. Bosman[11], H. Boterenbrood[105], D. Botterill[129], J. Bouchami[93], J. Boudreau[123], E.V. Bouhova-Thacker[71], C. Boulahouache[123], C. Bourdarios[115], N. Bousson[83], A. Boveia[30], J. Boyd[29], I.R. Boyko[65], N.I. Bozhko[128], I. Bozovic-Jelisavcic[12b], S. Braccini[47], J. Bracinik[17], A. Braem[29], E. Brambilla[72a,72b], P. Branchini[134a], G.W. Brandenburg[57], A. Brandt[7], G. Brandt[41], O. Brandt[54], U. Bratzler[156], B. Brau[84], J.E. Brau[114], H.M. Braun[174], B. Brelier[158], J. Bremer[29], R. Brenner[166], S. Bressler[152], D. Breton[115], N.D. Brett[118], P.G. Bright-Thomas[17], D. Britton[53], F.M. Brochu[27], I. Brock[20], R. Brock[88], T.J. Brodbeck[71], E. Brodet[153], F. Broggi[89a], C. Bromberg[88], G. Brooijmans[34], W.K. Brooks[31b], G. Brown[82], E. Brubaker[30], P.A. Bruckman de Renstrom[38], D. Bruncko[144b], R. Bruneliere[48], S. Brunet[61], A. Bruni[19a], G. Bruni[19a], M. Bruschi[19a], T. Buanes[13], F. Bucci[49], J. Buchanan[118], N.J. Buchanan[2], P. Buchholz[141], R.M. Buckingham[118], A.G. Buckley[45], S.I. Buda[25a], I.A. Budagov[65], B. Budick[108], V. Büscher[81], L. Bugge[117], D. Buira-Clark[118], E.J. Buis[105], O. Bulekov[96], M. Bunse[42], T. Buran[117], H. Burckhart[29], S. Burdin[73], T. Burgess[13], S. Burke[129], E. Busato[33], P. Bussey[53], C.P. Buszello[166], F. Butin[29], B. Butler[143], J.M. Butler[21], C.M. Buttar[53], J.M. Butterworth[77], W. Buttinger[27], T. Byatt[77], S. Cabrera Urbán[167], M. Caccia[89a,89b], D. Caforio[19a,19b], O. Cakir[3a], P. Calafiura[14], G. Calderini[78], P. Calfayan[98], R. Calkins[106], L.P. Caloba[23a], R. Caloi[132a,132b], D. Calvet[33], S. Calvet[33], A. Camard[78], P. Camarri[133a,133b], M. Cambiaghi[119a,119b], D. Cameron[117], J. Cammin[20], S. Campana[29], M. Campanelli[77], V. Canale[102a,102b], F. Canelli[30], A. Canepa[159a], J. Cantero[80], L. Capasso[102a,102b], M.D.M. Capeans Garrido[29], I. Caprini[25a], M. Caprini[25a], M. Caprio[102a,102b], D. Capriotti[99], M. Capua[36a,36b], R. Caputo[148], C. Caramarcu[25a], R. Cardarelli[133a], T. Carli[29], G. Carlino[102a], L. Carminati[89a,89b], B. Caron[159a], S. Caron[48], C. Carpentieri[48], G.D. Carrillo Montoya[172], S. Carron Montero[158], A.A. Carter[75], J.R. Carter[27], J. Carvalho[124a,f], D. Casadei[108], M.P. Casado[11], M. Cascella[122a,122b], C. Caso[50a,50b,*], A.M. Castaneda Hernandez[172], E. Castaneda-Miranda[172], V. Castillo Gimenez[167], N.F. Castro[124b,a], G. Cataldi[72a], F. Cataneo[29], A. Catinaccio[29], J.R. Catmore[71], A. Cattai[29], G. Cattani[133a,133b], S. Caughron[34], A. Cavallari[132a,132b], P. Cavalleri[78], D. Cavalli[89a], M. Cavalli-Sforza[11], V. Cavasinni[122a,122b], A. Cazzato[72a,72b], F. Ceradini[134a,134b], C. Cerna[83], A.S. Cerqueira[23a], A. Cerri[29], L. Cerrito[75], F. Cerutti[47], M. Cervetto[50a,50b],

S.A. Cetin[18b], F. Cevenini[102a,102b], A. Chafaq[135a], D. Chakraborty[106], K. Chan[2], B. Chapleau[85], J.D. Chapman[27], J.W. Chapman[87], E. Chareyre[78], D.G. Charlton[17], V. Chavda[82], S. Cheatham[71], S. Chekanov[5], S.V. Chekulaev[159a], G.A. Chelkov[65], H. Chen[24], L. Chen[2], S. Chen[32c], T. Chen[32c], X. Chen[172], S. Cheng[32a], A. Cheplakov[65], V.F. Chepurnov[65], R. Cherkaoui El Moursli[135d], V. Chernyatin[24], E. Cheu[6], S.L. Cheung[158], L. Chevalier[136], F. Chevallier[136], G. Chiefari[102a,102b], L. Chikovani[51], J.T. Childers[58a], A. Chilingarov[71], G. Chiodini[72a], M.V. Chizhov[65], G. Choudalakis[30], S. Chouridou[137], I.A. Christidi[77], A. Christov[48], D. Chromek-Burckhart[29], M.L. Chu[151], J. Chudoba[125], G. Ciapetti[132a,132b], A.K. Ciftci[3a], R. Ciftci[3a], D. Cinca[33], V. Cindro[74], M.D. Ciobotaru[163], C. Ciocca[19a,19b], A. Ciocio[14], M. Cirilli[87], M. Cirilli[87], A. Clark[49], P.J. Clark[45], W. Cleland[123], J.C. Clemens[83], B. Clement[55], C. Clement[146a,146b], R.W. Clifft[129], Y. Coadou[83], M. Cobal[164a,164c], A. Coccaro[50a,50b], J. Cochran[64], P. Coe[118], J.G. Cogan[143], J. Coggeshall[165], E. Cogneras[177], C.D. Cojocaru[28], J. Colas[4], A.P. Colijn[105], C. Collard[115], N.J. Collins[17], C. Collins-Tooth[53], J. Collot[55], G. Colon[84], R. Coluccia[72a,72b], G. Comune[88], P. Conde Mui no[124a], E. Coniavitis[118], M.C. Conidi[11], M. Consonni[104], S. Constantinescu[25a], C. Conta[119a,119b], F. Conventi[102a,g], J. Cook[29], M. Cooke[14], B.D. Cooper[75], A.M. Cooper-Sarkar[118], N.J. Cooper-Smith[76], K. Copic[34], T. Cornelissen[50a,50b], M. Corradi[19a], S. Correard[83], F. Corriveau[85,h], A. Cortes-Gonzalez[165], G. Cortiana[99], G. Costa[89a], M.J. Costa[167], D. Costanzo[139], T. Costin[30], D. Côté[29], R. Coura Torres[23a], L. Courneyea[169], G. Cowan[76], C. Cowden[27], B.E. Cox[82], K. Cranmer[108], M. Cristinziani[20], G. Crosetti[36a,36b], R. Crupi[72a,72b], S. Crépé-Renaudin[55], C. Cuenca Almenar[175], T. Cuhadar Donszelmann[139], S. Cuneo[50a,50b], M. Curatolo[47], C.J. Curtis[17], P. Cwetanski[61], H. Czirr[141], Z. Czyczula[175], S. D'Auria[53], M. D'Onofrio[73], A. D'Orazio[132a,132b], A. Da Rocha Gesualdi Mello[23a], P.V.M. Da Silva[23a], C. Da Via[82], W. Dabrowski[37], A. Dahlhoff[48], T. Dai[87], C. Dallapiccola[84], S.J. Dallison[129,*], M. Dam[35], M. Dameri[50a,50b], D.S. Damiani[137], H.O. Danielsson[29], R. Dankers[105], D. Dannheim[99], V. Dao[49], G. Darbo[50a], G.L. Darlea[25b], C. Daum[105], J.P. Dauvergne[29], W. Davey[86], T. Davidek[126], N. Davidson[86], R. Davidson[71], M. Davies[93], A.R. Davison[77], E. Dawe[142], I. Dawson[139], J.W. Dawson[5,*], R.K. Daya[39], K. De[7], R. de Asmundis[102a], S. De Castro[19a,19b], S. De Cecco[78], J. de Graat[98], N. De Groot[104], P. de Jong[105], E. De La Cruz-Burelo[87], C. De La Taille[115], B. De Lotto[164a,164c], L. De Mora[71], L. De Nooij[105], M. De Oliveira Branco[29], D. De Pedis[132a], P. de Saintignon[55], A. De Salvo[132a], U. De Sanctis[164a,164c], A. De Santo[149], J.B. De Vivie De Regie[115], S. Dean[77], G. Dedes[99], D.V. Dedovich[65], J. Degenhardt[120], M. Dehchar[118], M. Deile[98], C. Del Papa[164a,164c], J. Del Peso[80], T. Del Prete[122a,122b], A. Dell'Acqua[29], L. Dell'Asta[89a,89b], M. Della Pietra[102a,g], D. della Volpe[102a,102b], M. Delmastro[29], P. Delpierre[83], N. Delruelle[29], P.A. Delsart[55], C. Deluca[148], S. Demers[175], M. Demichev[65], B. Demirkoz[11], J. Deng[163], S.P. Denisov[128], C. Dennis[118], D. Derendarz[38], J.E. Derkaoui[135c], F. Derue[78], P. Dervan[73], K. Desch[20], E. Devetak[148], P.O. Deviveiros[158], A. Dewhurst[129], B. DeWilde[148], S. Dhaliwal[158], R. Dhullipudi[24,i], A. Di Ciaccio[133a,133b], L. Di Ciaccio[4], A. Di Girolamo[29], B. Di Girolamo[29], S. Di Luise[134a,134b], A. Di Mattia[88], R. Di Nardo[133a,133b], A. Di Simone[133a,133b], R. Di Sipio[19a,19b], M.A. Diaz[31a], M.M. Diaz Gomez[49], F. Diblen[18c], E.B. Diehl[87], H. Dietl[99], J. Dietrich[48], T.A. Dietzsch[58a], S. Diglio[115], K. Dindar Yagci[39], J. Dingfelder[20], C. Dionisi[132a,132b], P. Dita[25a], S. Dita[25a], F. Dittus[29], F. Djama[83], R. Djilkibaev[108], T. Djobava[51], M.A.B. do Vale[23a], A. Do Valle Wemans[124a], T.K.O. Doan[4], M. Dobbs[85], R. Dobinson[29,*], D. Dobos[42], E. Dobson[29], M. Dobson[163], J. Dodd[34], O.B. Dogan[18a,*], C. Doglioni[118], T. Doherty[53], Y. Doi[66], J. Dolejsi[126], I. Dolenc[74], Z. Dolezal[126], B.A. Dolgoshein[96], T. Dohmae[155], M. Donadelli[23b], M. Donega[120], J. Donini[55], J. Dopke[174], A. Doria[102a], A. Dos Anjos[172], M. Dosil[11], A. Dotti[122a,122b], M.T. Dova[70], J.D. Dowell[17], A.D. Doxiadis[105], A.T. Doyle[53], Z. Drasal[126], J. Drees[174], N. Dressnandt[120], H. Drevermann[29], C. Driouichi[35], M. Dris[9], J.G. Drohan[77], J. Dubbert[99], T. Dubbs[137], S. Dube[14], E. Duchovni[171], G. Duckeck[98], A. Dudarev[29], F. Dudziak[115], M. Dührssen[29], I.P. Duerdoth[82], L. Duflot[115], M.-A. Dufour[85], M. Dunford[29], H. Duran Yildiz[3b], R. Duxfield[139], M. Dwuznik[37], F. Dydak[29], D. Dzahini[55], M. Düren[52], J. Ebke[98], S. Eckert[48], S. Eckweiler[81], K. Edmonds[81], C.A. Edwards[76], I. Efthymiopoulos[49], W. Ehrenfeld[41], T. Ehrich[99], T. Eifert[29], G. Eigen[13], K. Einsweiler[14], E. Eisenhandler[75], T. Ekelof[166], M. El Kacimi[4], M. Ellert[166], S. Elles[4], F. Ellinghaus[81], K. Ellis[75], N. Ellis[29], J. Elmsheuser[98], M. Elsing[29], R. Ely[14], D. Emeliyanov[129], R. Engelmann[148], A. Engl[98], B. Epp[62], A. Eppig[87], J. Erdmann[54], A. Ereditato[16], D. Eriksson[146a], J. Ernst[1], M. Ernst[24], J. Ernwein[136], D. Errede[165], S. Errede[165], E. Ertel[81], M. Escalier[115], C. Escobar[167], X. Espinal Curull[11], B. Esposito[47], F. Etienne[83], A.I. Etienvre[136], E. Etzion[153], D. Evangelakou[54], H. Evans[61], L. Fabbri[19a,19b], C. Fabre[29], K. Facius[35], R.M. Fakhrutdinov[128], S. Falciano[132a], A.C. Falou[115], Y. Fang[172], M. Fanti[89a,89b], A. Farbin[7], A. Farilla[134a], J. Farley[148], T. Farooque[158], S.M. Farrington[118], P. Farthouat[29], D. Fasching[172], P. Fassnacht[29], D. Fassouliotis[8], B. Fatholahzadeh[158], L. Fayard[115], S. Fazio[36a,36b], R. Febbraro[33], P. Federic[144a], O.L. Fedin[121], I. Fedorko[29], W. Fedorko[29], M. Fehling-Kaschek[48], L. Feligioni[83], D. Fellmann[5], C.U. Felzmann[86], C. Feng[32d], E.J. Feng[30], A.B. Fenyuk[128], J. Ferencei[144b], D. Ferguson[172], J. Ferland[93], B. Fernandes[124a,j], W. Fernando[109], S. Ferrag[53], J. Ferrando[118], V. Ferrara[41], A. Ferrari[166], P. Ferrari[105], R. Ferrari[119a], A. Ferrer[167], M.L. Ferrer[47], D. Ferrere[49], C. Ferretti[87], A. Ferretto Parodi[50a,50b], F. Ferro[50a,50b], M. Fiascaris[30], F. Fiedler[81], A. Filipčič[74], A. Filippas[9], F. Filthaut[104], M. Fincke-Keeler[169], M.C.N. Fiolhais[124a,f], L. Fiorini[11], A. Firan[39], G. Fischer[41], P. Fischer[20], M.J. Fisher[109], S.M. Fisher[129], J. Flammer[29], M. Flechl[48], I. Fleck[141], J. Fleckner[81], P. Fleischmann[173], S. Fleis-

chmann[20], T. Flick[174], L.R. Flores Castillo[172], M.J. Flowerdew[99], F. Föhlisch[58a], M. Fokitis[9], T. Fonseca Martin[16], D.A. Forbush[138], A. Formica[136], A. Forti[82], D. Fortin[159a], J.M. Foster[82], D. Fournier[115], A. Foussat[29], A.J. Fowler[44], K. Fowler[137], H. Fox[71], P. Francavilla[122a,122b], S. Franchino[119a,119b], D. Francis[29], T. Frank[171], M. Franklin[57], S. Franz[29], M. Fraternali[119a,119b], S. Fratina[120], S.T. French[27], R. Froeschl[29], D. Froidevaux[29], J.A. Frost[27], C. Fukunaga[156], E. Fullana Torregrosa[29], J. Fuster[167], C. Gabaldon[29], O. Gabizon[171], T. Gadfort[24], S. Gadomski[49], G. Gagliardi[50a,50b], P. Gagnon[61], C. Galea[98], E.J. Gallas[118], M.V. Gallas[29], V. Gallo[16], B.J. Gallop[129], P. Gallus[125], E. Galyaev[40], K.K. Gan[109], Y.S. Gao[143,k], V.A. Gapienko[128], A. Gaponenko[14], F. Garberson[175], M. Garcia-Sciveres[14], C. García[167], J.E. García Navarro[49], R.W. Gardner[30], N. Garelli[29], H. Garitaonandia[105], V. Garonne[29], J. Garvey[17], C. Gatti[47], G. Gaudio[119a], O. Gaumer[49], B. Gaur[141], L. Gauthier[136], I.L. Gavrilenko[94], C. Gay[168], G. Gaycken[20], J.-C. Gayde[29], E.N. Gazis[9], P. Ge[32d], C.N.P. Gee[129], Ch. Geich-Gimbel[20], K. Gellerstedt[146a,146b], C. Gemme[50a], A. Gemmell[53], M.H. Genest[98], S. Gentile[132a,132b], F. Georgatos[9], S. George[76], P. Gerlach[174], A. Gershon[153], C. Geweniger[58a], H. Ghazlane[135d], P. Ghez[4], N. Ghodbane[33], B. Giacobbe[19a], S. Giagu[132a,132b], V. Giakoumopoulou[8], V. Giangiobbe[122a,122b], F. Gianotti[29], B. Gibbard[24], A. Gibson[158], S.M. Gibson[29], G.F. Gieraltowski[5], L.M. Gilbert[118], M. Gilchriese[14], O. Gildemeister[29], V. Gilewsky[91], D. Gillberg[28], A.R. Gillman[129], D.M. Gingrich[2,d], J. Ginzburg[153], N. Giokaris[8], R. Giordano[102a,102b], F.M. Giorgi[15], P. Giovannini[99], P.F. Giraud[136], D. Giugni[89a], P. Giusti[19a], B.K. Gjelsten[117], L.K. Gladilin[97], C. Glasman[80], J. Glatzer[48], A. Glazov[41], K.W. Glitza[174], G.L. Glonti[65], J. Godfrey[142], J. Godlewski[29], M. Goebel[41], T. Göpfert[43], C. Goeringer[81], C. Gössling[42], T. Göttfert[99], S. Goldfarb[87], D. Goldin[39], T. Golling[175], N.P. Gollub[29], S.N. Golovnia[128], A. Gomes[124a,l], L.S. Gomez Fajardo[41], R. Gonçalo[76], L. Gonella[20], C. Gong[32b], A. Gonidec[29], S. Gonzalez[172], S. González de la Hoz[167], M.L. Gonzalez Silva[26], S. Gonzalez-Sevilla[49], J.J. Goodson[148], L. Goossens[29], P.A. Gorbounov[95], H.A. Gordon[24], I. Gorelov[103], G. Gorfine[174], B. Gorini[29], E. Gorini[72a,72b], A. Gorišek[74], E. Gornicki[38], S.A. Gorokhov[128], B.T. Gorski[29], V.N. Goryachev[128], B. Gosdzik[41], M. Gosselink[105], M.I. Gostkin[65], M. Gouanère[4], I. Gough Eschrich[163], M. Gouighri[135a], D. Goujdami[135a], M.P. Goulette[49], A.G. Goussiou[138], C. Goy[4], I. Grabowska-Bold[163,e], V. Grabski[176], P. Grafström[29], C. Grah[174], K.-J. Grahn[147], F. Grancagnolo[72a], S. Grancagnolo[15], V. Grassi[148], V. Gratchev[121], N. Grau[34], H.M. Gray[34,m], J.A. Gray[148], E. Graziani[134a], O.G. Grebenyuk[121], D. Greenfield[129], T. Greenshaw[73], Z.D. Greenwood[24,i], I.M. Gregor[41], P. Grenier[143], E. Griesmayer[46], J. Griffiths[138], N. Grigalashvili[65], A.A. Grillo[137], K. Grimm[148], S. Grinstein[11], Y.V. Grishkevich[97], J.-F. Grivaz[115], J. Grognuz[29], M. Groh[99], E. Gross[171], J. Grosse-Knetter[54], J. Groth-Jensen[79], M. Gruwe[29], K. Grybel[141], V.J. Guarino[5], C. Guicheney[33], A. Guida[72a,72b], T. Guillemin[4], S. Guindon[54], H. Guler[85,n], J. Gunther[125], B. Guo[158], J. Guo[34], A. Gupta[30], Y. Gusakov[65], V.N. Gushchin[128], A. Gutierrez[93], P. Gutierrez[111], N. Guttman[153], O. Gutzwiller[172], C. Guyot[136], C. Gwenlan[118], C.B. Gwilliam[73], A. Haas[143], S. Haas[29], C. Haber[14], R. Hackenburg[24], H.K. Hadavand[39], D.R. Hadley[17], P. Haefner[99], R. Härtel[99], F. Hahn[29], S. Haider[29], Z. Hajduk[38], H. Hakobyan[176], J. Haller[54], K. Hamacher[174], A. Hamilton[49], S. Hamilton[161], H. Han[32a], L. Han[32b], K. Hanagaki[116], M. Hance[120], C. Handel[81], P. Hanke[58a], C.J. Hansen[166], J.R. Hansen[35], J.B. Hansen[35], J.D. Hansen[35], P.H. Hansen[35], P. Hansson[143], K. Hara[160], G.A. Hare[137], T. Harenberg[174], D. Harper[87], R. Harper[139], R.D. Harrington[21], O.M. Harris[138], K. Harrison[17], J.C. Hart[129], J. Hartert[48], F. Hartjes[105], T. Haruyama[66], A. Harvey[56], S. Hasegawa[101], Y. Hasegawa[140], S. Hassani[136], M. Hatch[29], D. Hauff[99], S. Haug[16], M. Hauschild[29], R. Hauser[88], M. Havranek[125], B.M. Hawes[118], C.M. Hawkes[17], R.J. Hawkings[29], D. Hawkins[163], T. Hayakawa[67], D. Hayden[76], H.S. Hayward[73], S.J. Haywood[129], E. Hazen[21], M. He[32d], S.J. Head[17], V. Hedberg[79], L. Heelan[28], S. Heim[88], B. Heinemann[14], S. Heisterkamp[35], L. Helary[4], M. Heldmann[48], M. Heller[115], S. Hellman[146a,146b], C. Helsens[11], R.C.W. Henderson[71], P.J. Hendriks[105], M. Henke[58a], A. Henrichs[54], A.M. Henriques Correia[29], S. Henrot-Versille[115], F. Henry-Couannier[83], C. Hensel[54], T. Henß[174], Y. Hernández Jiménez[167], R. Herrberg[15], A.D. Hershenhorn[152], G. Herten[48], R. Hertenberger[98], L. Hervas[29], N.P. Hessey[105], A. Hidvegi[146a], E. Higón-Rodriguez[167], D. Hill[5,*], J.C. Hill[27], N. Hill[5], K.H. Hiller[41], S. Hillert[20], S.J. Hillier[17], I. Hinchliffe[14], D. Hindson[118], E. Hines[120], M. Hirose[116], F. Hirsch[42], D. Hirschbuehl[174], J. Hobbs[148], N. Hod[153], M.C. Hodgkinson[139], P. Hodgson[139], A. Hoecker[29], M.R. Hoeferkamp[103], J. Hoffman[39], D. Hoffmann[83], M. Hohlfeld[81], M. Holder[141], T.I. Hollins[17], A. Holmes[118], S.O. Holmgren[146a], T. Holy[127], J.L. Holzbauer[88], R.J. Homer[17], Y. Homma[67], T. Horazdovsky[127], C. Horn[143], S. Horner[48], K. Horton[118], J.-Y. Hostachy[55], T. Hott[99], S. Hou[151], M.A. Houlden[73], A. Hoummada[135a], J. Howarth[82], D.F. Howell[118], I. Hristova[41], J. Hrivnac[115], I. Hruska[125], T. Hryn'ova[4], P.J. Hsu[175], S.-C. Hsu[14], G.S. Huang[111], Z. Hubacek[127], F. Hubaut[83], F. Huegging[20], T.B. Huffman[118], E.W. Hughes[34], G. Hughes[71], R.E. Hughes-Jones[82], M. Huhtinen[29], P. Hurst[57], M. Hurwitz[14], U. Husemann[41], N. Huseynov[65,o], J. Huston[88], J. Huth[57], G. Iacobucci[102a], G. Iakovidis[9], M. Ibbotson[82], I. Ibragimov[141], R. Ichimiya[67], L. Iconomidou-Fayard[115], J. Idarraga[115], M. Idzik[37], P. Iengo[4], O. Igonkina[105], Y. Ikegami[66], M. Ikeno[66], Y. Ilchenko[39], D. Iliadis[154], D. Imbault[78], M. Imhaeuser[174], M. Imori[155], T. Ince[20], J. Inigo-Golfin[29], P. Ioannou[8], M. Iodice[134a], G. Ionescu[4], A. Irles Quiles[167], K. Ishii[66], A. Ishikawa[67], M. Ishino[66], R. Ishmukhametov[39], T. Isobe[155], C. Issever[118], S. Istin[18a], Y. Itoh[101], A.V. Ivashin[128], W. Iwanski[38], H. Iwasaki[66], J.M. Izen[40], V. Izzo[102a], B. Jackson[120], J.N. Jackson[73], P. Jackson[143], M.R. Jaekel[29], V. Jain[61], K. Jakobs[48], S. Jakobsen[35], J. Jakubek[127], D.K. Jana[111],

E. Jankowski[158], E. Jansen[77], A. Jantsch[99], M. Janus[20], G. Jarlskog[79], L. Jeanty[57], K. Jelen[37], I. Jen-La Plante[30], P. Jenni[29], A. Jeremie[4], P. Jež[35], S. Jézéquel[4], H. Ji[172], W. Ji[79], J. Jia[148], Y. Jiang[32b], M. Jimenez Belenguer[29], G. Jin[32b], S. Jin[32a], O. Jinnouchi[157], M.D. Joergensen[35], D. Joffe[39], L.G. Johansen[13], M. Johansen[146a,146b], K.E. Johansson[146a], P. Johansson[139], S. Johnert[41], K.A. Johns[6], K. Jon-And[146a,146b], G. Jones[82], M. Jones[118], R.W.L. Jones[71], T.W. Jones[77], T.J. Jones[73], O. Jonsson[29], K.K. Joo[158], C. Joram[29], P.M. Jorge[124a,b], S. Jorgensen[11], J. Joseph[14], X. Ju[130], V. Juranek[125], P. Jussel[62], V.V. Kabachenko[128], S. Kabana[16], M. Kaci[167], A. Kaczmarska[38], P. Kadlecik[35], M. Kado[115], H. Kagan[109], M. Kagan[57], S. Kaiser[99], E. Kajomovitz[152], S. Kalinin[174], L.V. Kalinovskaya[65], S. Kama[39], N. Kanaya[155], M. Kaneda[155], T. Kanno[157], V.A. Kantserov[96], J. Kanzaki[66], B. Kaplan[175], A. Kapliy[30], J. Kaplon[29], D. Kar[43], M. Karagoz[118], M. Karnevskiy[41], K. Karr[5], V. Kartvelishvili[71], A.N. Karyukhin[128], L. Kashif[57], A. Kasmi[39], R.D. Kass[109], A. Kastanas[13], M. Kataoka[4], Y. Kataoka[155], E. Katsoufis[9], J. Katzy[41], V. Kaushik[6], K. Kawagoe[67], T. Kawamoto[155], G. Kawamura[81], M.S. Kayl[105], V.A. Kazanin[107], M.Y. Kazarinov[65], S.I. Kazi[86], J.R. Keates[82], R. Keeler[169], R. Kehoe[39], M. Keil[54], G.D. Kekelidze[65], M. Kelly[82], J. Kennedy[98], C.J. Kenney[143], M. Kenyon[53], O. Kepka[125], N. Kerschen[29], B.P. Kerševan[74], S. Kersten[174], K. Kessoku[155], C. Ketterer[48], M. Khakzad[28], F. Khalil-zada[10], H. Khandanyan[165], A. Khanov[112], D. Kharchenko[65], A. Khodinov[148], A.G. Kholodenko[128], A. Khomich[58a], T.J. Khoo[27], G. Khoriauli[20], N. Khovanskiy[65], V. Khovanskiy[95], E. Khramov[65], J. Khubua[51], G. Kilvington[76], H. Kim[7], M.S. Kim[2], P.C. Kim[143], S.H. Kim[160], N. Kimura[170], O. Kind[15], B.T. King[73], M. King[67], R.S.B. King[118], J. Kirk[129], G.P. Kirsch[118], L.E. Kirsch[22], A.E. Kiryunin[99], D. Kisielewska[37], T. Kittelmann[123], A.M. Kiver[128], H. Kiyamura[67], E. Kladiva[144b], J. Klaiber-Lodewigs[42], M. Klein[73], U. Klein[73], K. Kleinknecht[81], M. Klemetti[85], A. Klier[171], A. Klimentov[24], R. Klingenberg[42], E.B. Klinkby[35], T. Klioutchnikova[29], P.F. Klok[104], S. Klous[105], E.-E. Kluge[58a], T. Kluge[73], P. Kluit[105], S. Kluth[99], E. Kneringer[62], J. Knobloch[29], A. Knue[54], B.R. Ko[44], T. Kobayashi[155], M. Kobel[43], B. Koblitz[29], M. Kocian[143], A. Kocnar[113], P. Kodys[126], K. Köneke[29], A.C. König[104], S. Koenig[81], S. König[48], L. Köpke[81], F. Koetsveld[104], P. Koevesarki[20], T. Koffas[29], E. Koffeman[105], F. Kohn[54], Z. Kohout[127], T. Kohriki[66], T. Koi[143], T. Kokott[20], G.M. Kolachev[107], H. Kolanoski[15], V. Kolesnikov[65], I. Koletsou[89a,89b], J. Koll[88], D. Kollar[29], M. Kollefrath[48], S.D. Kolya[82], A.A. Komar[94], J.R. Komaragiri[142], T. Kondo[66], T. Kono[41,p], A.I. Kononov[48], R. Konoplich[108,q], N. Konstantinidis[77], A. Kootz[174], S. Koperny[37], S.V. Kopikov[128], K. Korcyl[38], K. Kordas[154], V. Koreshev[128], A. Korn[14], A. Korol[107], I. Korolkov[11], E.V. Korolkova[139], V.A. Korotkov[128], O. Kortner[99], S. Kortner[99], V.V. Kostyukhin[20], M.J. Kotamäki[29], S. Kotov[99], V.M. Kotov[65], C. Kourkoumelis[8], A. Koutsman[105], R. Kowalewski[169], T.Z. Kowalski[37], W. Kozanecki[136], A.S. Kozhin[128], V. Kral[127], V.A. Kramarenko[97], G. Kramberger[74], O. Krasel[42], M.W. Krasny[78], A. Krasznahorkay[108], J. Kraus[88], A. Kreisel[153], S. Kreiss[108], F. Krejci[127], J. Kretzschmar[73], N. Krieger[54], P. Krieger[158], G. Krobath[98], K. Kroeninger[54], H. Kroha[99], J. Kroll[120], J. Kroseberg[20], J. Krstic[12a], U. Kruchonak[65], H. Krüger[20], Z.V. Krumshteyn[65], A. Kruth[20], T. Kubota[155], S. Kuehn[48], A. Kugel[58c], T. Kuhl[174], D. Kuhn[62], V. Kukhtin[65], Y. Kulchitsky[90], S. Kuleshov[31b], C. Kummer[98], M. Kuna[83], N. Kundu[118], J. Kunkle[120], A. Kupco[125], H. Kurashige[67], M. Kurata[160], Y.A. Kurochkin[90], V. Kus[125], W. Kuykendall[138], M. Kuze[157], P. Kuzhir[91], O. Kvasnicka[125], R. Kwee[15], A. La Rosa[29], L. La Rotonda[36a,36b], L. Labarga[80], J. Labbe[4], C. Lacasta[167], F. Lacava[132a,132b], H. Lacker[15], D. Lacour[78], V.R. Lacuesta[167], E. Ladygin[65], R. Lafaye[4], B. Laforge[78], T. Lagouri[80], S. Lai[48], E. Laisne[55], M. Lamanna[29], M. Lambacher[98], C.L. Lampen[6], W. Lampl[6], E. Lancon[136], U. Landgraf[48], M.P.J. Landon[75], H. Landsman[152], J.L. Lane[82], C. Lange[41], A.J. Lankford[163], F. Lanni[24], K. Lantzsch[29], V.V. Lapin[128,*], S. Laplace[4], C. Lapoire[20], J.F. Laporte[136], T. Lari[89a], A.V. Larionov[128], A. Larner[118], C. Lasseur[29], M. Lassnig[29], W. Lau[118], P. Laurelli[47], A. Lavorato[118], W. Lavrijsen[14], P. Laycock[73], A.B. Lazarev[65], A. Lazzaro[89a,89b], O. Le Dortz[78], E. Le Guirriec[83], C. Le Maner[158], E. Le Menedeu[136], M. Leahu[29], A. Lebedev[64], C. Lebel[93], M. Lechowski[115], T. LeCompte[5], F. Ledroit-Guillon[55], H. Lee[105], J.S.H. Lee[150], S.C. Lee[151], L. Lee[175], M. Lefebvre[169], M. Legendre[136], A. Leger[49], B.C. LeGeyt[120], F. Legger[98], C. Leggett[14], M. Lehmacher[20], G. Lehmann Miotto[29], M. Lehto[139], X. Lei[6], M.A.L. Leite[23b], R. Leitner[126], D. Lellouch[171], J. Lellouch[78], M. Leltchouk[34], V. Lendermann[58a], K.J.C. Leney[145b], T. Lenz[174], G. Lenzen[174], B. Lenzi[136], K. Leonhardt[43], S. Leontsinis[9], J. Lepidis[174], C. Leroy[93], J.-R. Lessard[169], J. Lesser[146a], C.G. Lester[27], A. Leung Fook Cheong[172], J. Levêque[83], D. Levin[87], L.J. Levinson[171], M.S. Levitski[128], M. Lewandowska[21], G.H. Lewis[108], M. Leyton[15], B. Li[83], H. Li[172], S. Li[32b], X. Li[87], Z. Liang[39], Z. Liang[118,r], B. Liberti[133a], P. Lichard[29], M. Lichtnecker[98], K. Lie[165], W. Liebig[13], R. Lifshitz[152], J.N. Lilley[17], H. Lim[5], A. Limosani[86], M. Limper[63], S.C. Lin[151,s], F. Linde[105], J.T. Linnemann[88], E. Lipeles[120], L. Lipinsky[125], A. Lipniacka[13], T.M. Liss[165], A. Lister[49], A.M. Litke[137], C. Liu[28], D. Liu[151,t], H. Liu[87], J.B. Liu[87], M. Liu[32b], S. Liu[2], Y. Liu[32b], M. Livan[119a,119b], S.S.A. Livermore[118], A. Lleres[55], S.L. Lloyd[75], E. Lobodzinska[41], P. Loch[6], W.S. Lockman[137], S. Lockwitz[175], T. Loddenkoetter[20], F.K. Loebinger[82], A. Loginov[175], C.W. Loh[168], T. Lohse[15], K. Lohwasser[48], M. Lokajicek[125], J. Loken[118], R.E. Long[71], L. Lopes[124a,b], D. Lopez Mateos[34,m], M. Losada[162], P. Loscutoff[14], M.J. Losty[159a], X. Lou[40], A. Lounis[115], K.F. Loureiro[162], J. Love[21], P.A. Love[71], A.J. Lowe[143], F. Lu[32a], J. Lu[2], L. Lu[39], H.J. Lubatti[138], C. Luci[132a,132b], A. Lucotte[55], A. Ludwig[43], D. Ludwig[41], I. Ludwig[48], J. Ludwig[48], F. Luehring[61], G. Luijckx[105], D. Lumb[48], L. Luminari[132a], E. Lund[117], B. Lund-Jensen[147], B. Lundberg[79],

J. Lundberg[29], J. Lundquist[35], M. Lungwitz[81], A. Lupi[122a,122b], G. Lutz[99], D. Lynn[24], J. Lynn[118], J. Lys[14], E. Lytken[79], H. Ma[24], L.L. Ma[172], M. Maaßen[48], J.A. Macana Goia[93], G. Maccarrone[47], A. Macchiolo[99], B. Maček[74], J. Machado Miguens[124a,b], D. Macina[49], R. Mackeprang[35], R.J. Madaras[14], W.F. Mader[43], R. Maenner[58c], T. Maeno[24], P. Mättig[174], S. Mättig[41], P.J. Magalhaes Martins[124a,f], L. Magnoni[29], E. Magradze[51], C.A. Magrath[104], Y. Mahalalel[153], K. Mahboubi[48], G. Mahout[17], C. Maiani[132a,132b], C. Maidantchik[23a], A. Maio[124a,l], S. Majewski[24], Y. Makida[66], N. Makovec[115], P. Mal[6], Pa. Malecki[38], P. Malecki[38], V.P. Maleev[121], F. Malek[55], U. Mallik[63], D. Malon[5], S. Maltezos[9], V. Malyshev[107], S. Malyukov[65], R. Mameghani[98], J. Mamuzic[12b], A. Manabe[66], L. Mandelli[89a], I. Mandić[74], R. Mandrysch[15], J. Maneira[124a], P.S. Mangeard[88], M. Mangin-Brinet[49], I.D. Manjavidze[65], A. Mann[54], W.A. Mann[161], P.M. Manning[137], A. Manousakis-Katsikakis[8], B. Mansoulie[136], A. Manz[99], A. Mapelli[29], L. Mapelli[29], L. March [80], J.F. Marchand[29], F. Marchese[133a,133b], M. Marchesotti[29], G. Marchiori[78], M. Marcisovsky[125], A. Marin[21,*], C.P. Marino[61], F. Marroquim[23a], R. Marshall[82], Z. Marshall[34,m], F.K. Martens[158], S. Marti-Garcia[167], A.J. Martin[175], B. Martin[29], B. Martin[88], F.F. Martin[120], J.P. Martin[93], Ph. Martin[55], T.A. Martin[17], B. Martin dit Latour[49], M. Martinez[11], V. Martinez Outschoorn[57], A.C. Martyniuk[82], M. Marx[82], F. Marzano[132a], A. Marzin[111], L. Masetti[81], T. Mashimo[155], R. Mashinistov[94], J. Masik[82], A.L. Maslennikov[107], M. Maß[42], I. Massa[19a,19b], G. Massaro[105], N. Massol[4], A. Mastroberardino[36a,36b], T. Masubuchi[155], M. Mathes[20], P. Matricon[115], H. Matsumoto[155], H. Matsunaga[155], T. Matsushita[67], C. Mattravers[118,u], J.M. Maugain[29], S.J. Maxfield[73], E.N. May[5], A. Mayne[139], R. Mazini[151], M. Mazur[20], M. Mazzanti[89a], E. Mazzoni[122a,122b], S.P. Mc Kee[87], A. McCarn[165], R.L. McCarthy[148], T.G. McCarthy[28], N.A. McCubbin[129], K.W. McFarlane[56], J.A. Mcfayden[139], S. McGarvie[76], H. McGlone[53], G. Mchedlidze[51], R.A. McLaren[29], T. Mclaughlan[17], S.J. McMahon[129], T.R. McMahon[76], T.J. McMahon[17], R.A. McPherson[169,h], A. Meade[84], J. Mechnich[105], M. Mechtel[174], M. Medinnis[41], R. Meera-Lebbai[111], T. Meguro[116], R. Mehdiyev[93], S. Mehlhase[41], A. Mehta[73], K. Meier[58a], J. Meinhardt[48], B. Meirose[79], C. Melachrinos[30], B.R. Mellado Garcia[172], L. Mendoza Navas[162], Z. Meng[151,t], A. Mengarelli[19a,19b], S. Menke[99], C. Menot[29], E. Meoni[11], D. Merkl[98], P. Mermod[118], L. Merola[102a,102b], C. Meroni[89a], F.S. Merritt[30], A. Messina[29], J. Metcalfe[103], A.S. Mete[64], S. Meuser[20], C. Meyer[81], J.-P. Meyer[136], J. Meyer[173], J. Meyer[54], T.C. Meyer[29], W.T. Meyer[64], J. Miao[32d], S. Michal[29], L. Micu[25a], R.P. Middleton[129], P. Miele[29], S. Migas[73], A. Migliaccio[102a,102b], L. Mijović[41], G. Mikenberg[171], M. Mikestikova[125], B. Mikulec[49], M. Mikuž[74], D.W. Miller[143], R.J. Miller[88], W.J. Mills[168], C. Mills[57], A. Milov[171], D.A. Milstead[146a,146b], D. Milstein[171], A.A. Minaenko[128], M. Miñano[167], I.A. Minashvili[65], A.I. Mincer[108], B. Mindur[37], M. Mineev[65], Y. Ming[130], L.M. Mir[11], G. Mirabelli[132a], L. Miralles Verge[11], S. Miscetti[47], A. Misiejuk[76], A. Mitra[118], J. Mitrevski[137], G.Y. Mitrofanov[128], V.A. Mitsou[167], S. Mitsui[66], P.S. Miyagawa[82], K. Miyazaki[67], J.U. Mjörnmark[79], T. Moa[146a,146b], P. Mockett[138], S. Moed[57], V. Moeller[27], K. Mönig[41], N. Möser[20], S. Mohapatra[148], B. Mohn[13], W. Mohr[48], S. Mohrdieck-Möck[99], A.M. Moisseev[128,*], R. Moles-Valls[167], J. Molina-Perez[29], L. Moneta[49], J. Monk[77], E. Monnier[83], S. Montesano[89a,89b], F. Monticelli[70], S. Monzani[19a,19b], R.W. Moore[2], G.F. Moorhead[86], C. Mora Herrera[49], A. Moraes[53], A. Morais[124a,b], N. Morange[136], J. Morel[54], G. Morello[36a,36b], D. Moreno[81], M. Moreno Llácer[167], P. Morettini[50a], M. Morii[57], J. Morin[75], Y. Morita[66], A.K. Morley[29], G. Mornacchi[29], M.-C. Morone[49], J.D. Morris[75], H.G. Moser[99], M. Mosidze[51], J. Moss[109], R. Mount[143], E. Mountricha[9], S.V. Mouraviev[94], T.H. Moye[17], E.J.W. Moyse[84], M. Mudrinic[12b], F. Mueller[58a], J. Mueller[123], K. Mueller[20], T.A. Müller[98], D. Muenstermann[42], A. Muijs[105], A. Muir[168], Y. Munwes[153], K. Murakami[66], W.J. Murray[129], I. Mussche[105], E. Musto[102a,102b], A.G. Myagkov[128], M. Myska[125], J. Nadal[11], K. Nagai[160], K. Nagano[66], Y. Nagasaka[60], A.M. Nairz[29], Y. Nakahama[115], K. Nakamura[155], I. Nakano[110], G. Nanava[20], A. Napier[161], M. Nash[77,u], I. Nasteva[82], N.R. Nation[21], T. Nattermann[20], T. Naumann[41], F. Nauyock[82], G. Navarro[162], H.A. Neal[87], E. Nebot[80], P.Yu. Nechaeva[94], A. Negri[119a,119b], G. Negri[29], S. Nektarijevic[49], A. Nelson[64], S. Nelson[143], T.K. Nelson[143], S. Nemecek[125], P. Nemethy[108], A.A. Nepomuceno[23a], M. Nessi[29], S.Y. Nesterov[121], M.S. Neubauer[165], L. Neukermans[4], A. Neusiedl[81], R.M. Neves[108], P. Nevski[24], P.R. Newman[17], C. Nicholson[53], R.B. Nickerson[118], R. Nicolaidou[136], L. Nicolas[139], B. Nicquevert[29], F. Niedercorn[115], J. Nielsen[137], T. Niinikoski[29], A. Nikiforov[15], V. Nikolaenko[128], K. Nikolaev[65], I. Nikolic-Audit[78], K. Nikolopoulos[24], H. Nilsen[48], P. Nilsson[7], Y. Ninomiya [155], A. Nisati[132a], T. Nishiyama[67], R. Nisius[99], L. Nodulman[5], M. Nomachi[116], I. Nomidis[154], H. Nomoto[155], M. Nordberg[29], B. Nordkvist[146a,146b], O. Norniella Francisco[11], P.R. Norton[129], J. Novakova[126], M. Nozaki[66], M. Nožička[41], I.M. Nugent[159a], A.-E. Nuncio-Quiroz[20], G. Nunes Hanninger[20], T. Nunnemann[98], E. Nurse[77], T. Nyman[29], B.J. O'Brien[45], S.W. O'Neale[17,*], D.C. O'Neil[142], V. O'Shea[53], F.G. Oakham[28,d], H. Oberlack[99], J. Ocariz[78], A. Ochi[67], S. Oda[155], S. Odaka[66], J. Odier[83], G.A. Odino[50a,50b], H. Ogren[61], A. Oh[82], S.H. Oh[44], C.C. Ohm[146a,146b], T. Ohshima[101], H. Ohshita[140], T.K. Ohska[66], T. Ohsugi[59], S. Okada[67], H. Okawa[163], Y. Okumura[101], T. Okuyama[155], M. Olcese[50a], A.G. Olchevski[65], M. Oliveira[124a,f], D. Oliveira Damazio[24], C. Oliver[80], E. Oliver Garcia[167], D. Olivito[120], A. Olszewski[38], J. Olszowska[38], C. Omachi[67], A. Onofre[124a,v], P.U.E. Onyisi[30], C.J. Oram[159a], G. Ordonez[104], M.J. Oreglia[30], F. Orellana[49], Y. Oren[153], D. Orestano[134a,134b], I. Orlov[107], C. Oropeza Barrera[53], R.S. Orr[158], E.O. Ortega[130], B. Osculati[50a,50b], R. Ospanov[120], C. Osuna[11], G. Otero y Garzon[26], J.P. Ottersbach[105], B. Ottewell[118], M. Ouchrif[135c], F. Ould-Saada[117], A. Ouraou[136], Q. Ouyang[32a], M. Owen[82], S. Owen[139],

A. Oyarzun[31b], O.K. Øye[13], V.E. Ozcan[77], N. Ozturk[7], A. Pacheco Pages[11], C. Padilla Aranda[11], E. Paganis[139], F. Paige[24], K. Pajchel[117], S. Palestini[29], D. Pallin[33], A. Palma[124a,b], J.D. Palmer[17], M.J. Palmer[27], Y.B. Pan[172], E. Panagiotopoulou[9], B. Panes[31a], N. Panikashvili[87], S. Panitkin[24], D. Pantea[25a], M. Panuskova[125], V. Paolone[123], A. Paoloni[133a,133b], A. Papadelis[146a,146b], Th.D. Papadopoulou[9], A. Paramonov[5], S.J. Park[54], W. Park[24,w], M.A. Parker[27], F. Parodi[50a,50b], J.A. Parsons[34], U. Parzefall[48], E. Pasqualucci[132a], A. Passeri[134a], F. Pastore[134a,134b], Fr. Pastore[29], G. Pásztor[49,x], S. Pataraia[172], N. Patel[150], J.R. Pater[82], S. Patricelli[102a,102b], T. Pauly[29], M. Pecsy[144a], M.I. Pedraza Morales[172], S.J.M. Peeters[105], S.V. Peleganchuk[107], H. Peng[172], R. Pengo[29], A. Penson[34], J. Penwell[61], M. Perantoni[23a], K. Perez[34,m], T. Perez Cavalcanti[41], E. Perez Codina[11], M.T. Pérez García-Estañ[167], V. Perez Reale[34], I. Peric[20], L. Perini[89a,89b], H. Pernegger[29], R. Perrino[72a], P. Perrodo[4], S. Persembe[3a], P. Perus[115], V.D. Peshekhonov[65], E. Petereit[5], O. Peters[105], B.A. Petersen[29], J. Petersen[29], T.C. Petersen[35], E. Petit[83], A. Petridis[154], C. Petridou[154], E. Petrolo[132a], F. Petrucci[134a,134b], D. Petschull[41], M. Petteni[142], R. Pezoa[31b], A. Phan[86], A.W. Phillips[27], P.W. Phillips[129], G. Piacquadio[29], E. Piccaro[75], M. Piccinini[19a,19b], A. Pickford[53], R. Piegaia[26], J.E. Pilcher[30], A.D. Pilkington[82], J. Pina[124a,l], M. Pinamonti[164a,164c], A. Pinder[118], J.L. Pinfold[2], J. Ping[32c], B. Pinto[124a,b], O. Pirotte[29], C. Pizio[89a,89b], R. Placakyte[41], M. Plamondon[169], W.G. Plano[82], M.-A. Pleier[24], A.V. Pleskach[128], A. Poblaguev[24], S. Poddar[58a], F. Podlyski[33], L. Poggioli[115], T. Poghosyan[20], M. Pohl[49], F. Polci[55], G. Polesello[119a], A. Policicchio[138], A. Polini[19a], J. Poll[75], V. Polychronakos[24], D.M. Pomarede[136], D. Pomeroy[22], K. Pommès[29], L. Pontecorvo[132a], B.G. Pope[88], G.A. Popeneciu[25a], D.S. Popovic[12a], A. Poppleton[29], X. Portell Bueso[48], R. Porter[163], C. Posch[21], G.E. Pospelov[99], S. Pospisil[127], I.N. Potrap[99], C.J. Potter[149], C.T. Potter[85], G. Poulard[29], J. Poveda[172], R. Prabhu[77], P. Pralavorio[83], S. Prasad[57], R. Pravahan[7], S. Prell[64], K. Pretzl[16], L. Pribyl[29], D. Price[61], L.E. Price[5], M.J. Price[29], P.M. Prichard[73], D. Prieur[123], M. Primavera[72a], K. Prokofiev[29], F. Prokoshin[31b], S. Protopopescu[24], J. Proudfoot[5], X. Prudent[43], H. Przysieznik[4], S. Psoroulas[20], E. Ptacek[114], J. Purdham[87], M. Purohit[24,w], P. Puzo[115], Y. Pylypchenko[117], J. Qian[87], Z. Qian[83], Z. Qin[41], A. Quadt[54], D.R. Quarrie[14], W.B. Quayle[172], F. Quinonez[31a], M. Raas[104], V. Radescu[58b], B. Radics[20], T. Rador[18a], F. Ragusa[89a,89b], G. Rahal[177], A.M. Rahimi[109], S. Rajagopalan[24], S. Rajek[42], M. Rammensee[48], M. Rammes[141], M. Ramstedt[146a,146b], K. Randrianarivony[28], P.N. Ratoff[71], F. Rauscher[98], E. Rauter[99], M. Raymond[29], A.L. Read[117], D.M. Rebuzzi[119a,119b], A. Redelbach[173], G. Redlinger[24], R. Reece[120], K. Reeves[40], A. Reichold[105], E. Reinherz-Aronis[153], A. Reinsch[114], I. Reisinger[42], D. Reljic[12a], C. Rembser[29], Z.L. Ren[151], A. Renaud[115], P. Renkel[39], B. Rensch[35], M. Rescigno[132a], S. Resconi[89a], B. Resende[136], P. Reznicek[98], R. Rezvani[158], A. Richards[77], R. Richter[99], E. Richter-Was[38,y], M. Ridel[78], S. Rieke[81], M. Rijpstra[105], M. Rijssenbeek[148], A. Rimoldi[119a,119b], L. Rinaldi[19a], R.R. Rios[39], I. Riu[11], G. Rivoltella[89a,89b], F. Rizatdinova[112], E. Rizvi[75], S.H. Robertson[85,h], A. Robichaud-Veronneau[49], D. Robinson[27], J.E.M. Robinson[77], M. Robinson[114], A. Robson[53], J.G. Rocha de Lima[106], C. Roda[122a,122b], D. Roda Dos Santos[29], S. Rodier[80], D. Rodriguez[162], Y. Rodriguez Garcia[15], A. Roe[54], S. Roe[29], O. Røhne[117], V. Rojo[1], S. Rolli[161], A. Romaniouk[96], V.M. Romanov[65], G. Romeo[26], D. Romero Maltrana[31a], L. Roos[78], E. Ros[167], S. Rosati[138], M. Rose[76], G.A. Rosenbaum[158], E.I. Rosenberg[64], P.L. Rosendahl[13], L. Rosselet[49], V. Rossetti[11], E. Rossi[102a,102b], L.P. Rossi[50a], L. Rossi[89a,89b], M. Rotaru[25a], I. Roth[171], J. Rothberg[138], I. Rottländer[20], D. Rousseau[115], C.R. Royon[136], A. Rozanov[83], Y. Rozen[152], X. Ruan[115], I. Rubinskiy[41], B. Ruckert[98], N. Ruckstuhl[105], V.I. Rud[97], G. Rudolph[62], F. Rühr[6], F. Ruggieri[134a], A. Ruiz-Martinez[64], E. Rulikowska-Zarebska[37], V. Rumiantsev[91,*], L. Rumyantsev[65], K. Runge[48], O. Runolfsson[20], Z. Rurikova[48], N.A. Rusakovich[65], D.R. Rust[61], J.P. Rutherfoord[6], C. Ruwiedel[14], P. Ruzicka[125], Y.F. Ryabov[121], V. Ryadovikov[128], P. Ryan[88], M. Rybar[126], G. Rybkin[115], N.C. Ryder[118], S. Rzaeva[10], A.F. Saavedra[150], I. Sadeh[153], H.F.-W. Sadrozinski[137], R. Sadykov[65], F. Safai Tehrani[132a,132b], H. Sakamoto[155], G. Salamanna[105], A. Salamon[133a], M. Saleem[111], D. Salihagic[99], A. Salnikov[143], J. Salt[167], B.M. Salvachua Ferrando[5], D. Salvatore[36a,36b], F. Salvatore[149], A. Salvucci[47], A. Salzburger[29], D. Sampsonidis[154], B.H. Samset[117], H. Sandaker[13], H.G. Sander[81], M.P. Sanders[98], M. Sandhoff[174], P. Sandhu[158], T. Sandoval[27], R. Sandstroem[105], S. Sandvoss[174], D.P.C. Sankey[129], A. Sansoni[47], C. Santamarina Rios[85], C. Santoni[33], R. Santonico[133a,133b], H. Santos[124a], J.G. Saraiva[124a,l], T. Sarangi[172], E. Sarkisyan-Grinbaum[7], F. Sarri[122a,122b], G. Sartisohn[174], O. Sasaki[66], T. Sasaki[66], N. Sasao[68], I. Satsounkevitch[90], G. Sauvage[4], J.B. Sauvan[115], P. Savard[158,d], V. Savinov[123], P. Savva[9], L. Sawyer[24,i], D.H. Saxon[53], L.P. Says[33], C. Sbarra[19a,19b], A. Sbrizzi[19a,19b], O. Scallon[93], D.A. Scannicchio[163], J. Schaarschmidt[43], P. Schacht[99], U. Schäfer[81], S. Schaetzel[58b], A.C. Schaffer[115], D. Schaile[98], R.D. Schamberger[148], A.G. Schamov[107], V. Scharf[58a], V.A. Schegelsky[121], D. Scheirich[87], M.I. Scherzer[14], C. Schiavi[50a,50b], J. Schieck[98], M. Schioppa[36a,36b], S. Schlenker[29], J.L. Schlereth[5], E. Schmidt[48], M.P. Schmidt[175,*], K. Schmieden[20], C. Schmitt[81], M. Schmitz[20], A. Schöning[58b], M. Schott[29], D. Schouten[142], J. Schovancova[125], M. Schram[85], A. Schreiner[63], C. Schroeder[81], N. Schroer[58c], S. Schuh[29], G. Schuler[29], J. Schultes[174], H.-C. Schultz-Coulon[58a], H. Schulz[15], J.W. Schumacher[43], M. Schumacher[48], B.A. Schumm[137], Ph. Schune[136], C. Schwanenberger[82], A. Schwartzman[143], D. Schweiger[29], Ph. Schwemling[78], R. Schwienhorst[88], R. Schwierz[43], J. Schwindling[136], W.G. Scott[129], J. Searcy[114], E. Sedykh[121], E. Segura[11], S.C. Seidel[103], A. Seiden[137], F. Seifert[43], J.M. Seixas[23a], G. Sekhniaidze[102a], D.M. Seliverstov[121], B. Sellden[146a], G. Sellers[73], M. Seman[144b], N. Semprini-Cesari[19a,19b], C. Serfon[98], L. Serin[115], R. Seuster[99], H. Severini[111], M.E. Se-

vior[86], A. Sfyrla[29], E. Shabalina[54], M. Shamim[114], L.Y. Shan[32a], J.T. Shank[21], Q.T. Shao[86], M. Shapiro[14], P.B. Shatalov[95], L. Shaver[6], C. Shaw[53], K. Shaw[164a,164c], D. Sherman[175], P. Sherwood[77], A. Shibata[108], S. Shimizu[29], M. Shimojima[100], T. Shin[56], A. Shmeleva[94], M.J. Shochet[30], D. Short[118], M.A. Shupe[6], P. Sicho[125], A. Sidoti[15], A. Siebel[174], F. Siegert[48], J. Siegrist[14], Dj. Sijacki[12a], O. Silbert[171], J. Silva[124a,z], Y. Silver[153], D. Silverstein[143], S.B. Silverstein[146a], V. Simak[127], Lj. Simic[12a], S. Simion[115], B. Simmons[77], M. Simonyan[35], P. Sinervo[158], N.B. Sinev[114], V. Sipica[141], G. Siragusa[81], A.N. Sisakyan[65], S.Yu. Sivoklokov[97], J. Sjölin[146a,146b], T.B. Sjursen[13], L.A. Skinnari[14], K. Skovpen[107], P. Skubic[111], N. Skvorodnev[22], M. Slater[17], T. Slavicek[127], K. Sliwa[161], T.J. Sloan[71], J. Sloper[29], V. Smakhtin[171], S.Yu. Smirnov[96], L.N. Smirnova[97], O. Smirnova[79], B.C. Smith[57], D. Smith[143], K.M. Smith[53], M. Smizanska[71], K. Smolek[127], A.A. Snesarev[94], S.W. Snow[82], J. Snow[111], J. Snuverink[105], S. Snyder[24], M. Soares[124a], R. Sobie[169,h], J. Sodomka[127], A. Soffer[153], C.A. Solans[167], M. Solar[127], J. Solc[127], U. Soldevila[167], E. Solfaroli Camillocci[132a,132b], A.A. Solodkov[128], O.V. Solovyanov[128], J. Sondericker[24], N. Soni[2], V. Sopko[127], B. Sopko[127], M. Sorbi[89a,89b], M. Sosebee[7], A. Soukharev[107], S. Spagnolo[72a,72b], F. Spanò[34], R. Spighi[19a], G. Spigo[29], F. Spila[132a,132b], E. Spiriti[134a], R. Spiwoks[29], M. Spousta[126], T. Spreitzer[158], B. Spurlock[7], R.D. St. Denis[53], T. Stahl[141], J. Stahlman[120], R. Stamen[58a], E. Stanecka[29], R.W. Stanek[5], C. Stanescu[134a], S. Stapnes[117], E.A. Starchenko[128], J. Stark[55], P. Staroba[125], P. Starovoitov[91], A. Staude[98], P. Stavina[144a], G. Stavropoulos[14], G. Steele[53], E. Stefanidis[77], P. Steinbach[43], P. Steinberg[24], I. Stekl[127], B. Stelzer[142], H.J. Stelzer[41], O. Stelzer-Chilton[159a], H. Stenzel[52], K. Stevenson[75], G.A. Stewart[53], T. Stockmanns[20], M.C. Stockton[29], M. Stodulski[38], K. Stoerig[48], G. Stoicea[25a], S. Stonjek[99], P. Strachota[126], A.R. Stradling[7], A. Straessner[43], J. Strandberg[87], S. Strandberg[146a,146b], A. Strandlie[117], M. Strang[109], E. Strauss[143], M. Strauss[111], P. Strizenec[144b], R. Ströhmer[173], D.M. Strom[114], J.A. Strong[76,*], R. Stroynowski[39], J. Strube[129], B. Stugu[13], I. Stumer[24,*], J. Stupak[148], P. Sturm[174], D.A. Soh[151,r], D. Su[143], S. Subramania[2], Y. Sugaya[116], T. Sugimoto[101], C. Suhr[106], K. Suita[67], M. Suk[126], V.V. Sulin[94], S. Sultansoy[3d], T. Sumida[29], X. Sun[55], J.E. Sundermann[48], K. Suruliz[164a,164b], S. Sushkov[11], G. Susinno[36a,36b], M.R. Sutton[139], Y. Suzuki[66], Yu.M. Sviridov[128], S. Swedish[168], I. Sykora[144a], T. Sykora[126], B. Szeless[29], J. Sánchez[167], D. Ta[105], K. Tackmann[29], A. Taffard[163], R. Tafirout[159a], A. Taga[117], N. Taiblum[153], Y. Takahashi[101], H. Takai[24], R. Takashima[69], H. Takeda[67], T. Takeshita[140], M. Talby[83], A. Talyshev[107], M.C. Tamsett[24], J. Tanaka[155], R. Tanaka[115], S. Tanaka[131], S. Tanaka[66], Y. Tanaka[100], K. Tani[67], N. Tannoury[83], G.P. Tappern[29], S. Tapprogge[81], D. Tardif[158], S. Tarem[152], F. Tarrade[24], G.F. Tartarelli[89a], P. Tas[126], M. Tasevsky[125], E. Tassi[36a,36b], M. Tatarkhanov[14], C. Taylor[77], F.E. Taylor[92], G. Taylor[137], G.N. Taylor[86], W. Taylor[159b], M. Teixeira Dias Castanheira[75], P. Teixeira-Dias[76], K.K. Temming[48], H. Ten Kate[29], P.K. Teng[151], Y.D. Tennenbaum-Katan[152], S. Terada[66], K. Terashi[155], J. Terron[80], M. Terwort[41,p], M. Testa[47], R.J. Teuscher[158,h], C.M. Tevlin[82], J. Thadome[174], J. Therhaag[20], T. Theveneaux-Pelzer[78], M. Thioye[175], S. Thoma[48], J.P. Thomas[17], E.N. Thompson[84], P.D. Thompson[17], P.D. Thompson[158], A.S. Thompson[53], E. Thomson[120], M. Thomson[27], R.P. Thun[87], T. Tic[125], V.O. Tikhomirov[94], Y.A. Tikhonov[107], C.J.W.P. Timmermans[104], P. Tipton[175], F.J. Tique Aires Viegas[29], S. Tisserant[83], J. Tobias[48], B. Toczek[37], T. Todorov[4], S. Todorova-Nova[161], B. Toggerson[163], J. Tojo[66], S. Tokár[144a], K. Tokunaga[67], K. Tokushuku[66], K. Tollefson[88], M. Tomoto[101], L. Tompkins[14], K. Toms[103], A. Tonazzo[134a,134b], G. Tong[32a], A. Tonoyan[13], C. Topfel[16], N.D. Topilin[65], I. Torchiani[29], E. Torrence[114], E. Torró Pastor[167], J. Toth[83,x], F. Touchard[83], D.R. Tovey[139], D. Traynor[75], T. Trefzger[173], J. Treis[20], L. Tremblet[29], A. Tricoli[29], I.M. Trigger[159a], S. Trincaz-Duvoid[78], T.N. Trinh[78], M.F. Tripiana[70], N. Triplett[64], W. Trischuk[158], A. Trivedi[24,w], B. Trocmé[55], C. Troncon[89a], M. Trottier-McDonald[142], A. Trzupek[38], C. Tsarouchas[29], J.C.-L. Tseng[118], M. Tsiakiris[105], P.V. Tsiareshka[90], D. Tsionou[4], G. Tsipolitis[9], V. Tsiskaridze[48], E.G. Tskhadadze[51], I.I. Tsukerman[95], V. Tsulaia[123], J.-W. Tsung[20], S. Tsuno[66], D. Tsybychev[148], A. Tua[139], J.M. Tuggle[30], M. Turala[38], D. Turecek[127], I. Turk Cakir[3e], E. Turlay[105], P.M. Tuts[34], A. Tykhonov[74], M. Tylmad[146a,146b], M. Tyndel[129], D. Typaldos[17], H. Tyrvainen[29], G. Tzanakos[8], K. Uchida[20], I. Ueda[155], R. Ueno[28], M. Ugland[13], M. Uhlenbrock[20], M. Uhrmacher[54], F. Ukegawa[160], G. Unal[29], D.G. Underwood[5], A. Undrus[24], G. Unel[163], Y. Unno[66], D. Urbaniec[34], E. Urkovsky[153], P. Urquijo[49], P. Urrejola[31a], G. Usai[7], M. Uslenghi[119a,119b], L. Vacavant[83], V. Vacek[127], B. Vachon[85], S. Vahsen[14], C. Valderanis[99], J. Valenta[125], P. Valente[132a], S. Valentinetti[19a,19b], S. Valkar[126], E. Valladolid Gallego[167], S. Vallecorsa[152], J.A. Valls Ferrer[167], H. van der Graaf[105], E. van der Kraaij[105], E. van der Poel[105], D. van der Ster[29], B. Van Eijk[105], N. van Eldik[84], P. van Gemmeren[5], Z. van Kesteren[105], I. van Vulpen[105], W. Vandelli[29], G. Vandoni[29], A. Vaniachine[5], P. Vankov[41], F. Vannucci[78], F. VarelaRodriguez[29], R. Vari[132a], E.W. Varnes[6], D. Varouchas[14], A. Vartapetian[7], K.E. Varvell[150], V.I. Vassilakopoulos[56], F. Vazeille[33], G. Vegni[89a,89b], J.J. Veillet[115], C. Vellidis[8], F. Veloso[124a], R. Veness[29], S. Veneziano[132a], A. Ventura[72a,72b], D. Ventura[138], S. Ventura[47], M. Venturi[48], N. Venturi[16], V. Vercesi[119a], M. Verducci[138], W. Verkerke[105], J.C. Vermeulen[105], L. Vertogardov[118], A. Vest[43], M.C. Vetterli[142,d], I. Vichou[165], T. Vickey[145b,aa], G.H.A. Viehhauser[118], S. Viel[168], M. Villa[19a,19b], M. Villaplana Perez[167], E. Vilucchi[47], M.G. Vincter[28], E. Vinek[29], V.B. Vinogradov[65], M. Virchaux[136,*], S. Viret[33], J. Virzi[14], A. Vitale[19a,19b], O. Vitells[171], I. Vivarelli[48], F. Vives Vaque[11], S. Vlachos[9], M. Vlasak[127], N. Vlasov[20], A. Vogel[20], P. Vokac[127], M. Volpi[11], G. Volpini[89a], H. von der Schmitt[99], J. von Loeben[99], H. von Radziewski[48], E. von Toerne[20], V. Vorobel[126], A.P. Vorobiev[128], V. Vorwerk[11], M. Vos[167], R. Voss[29],

T.T. Voss[174], J.H. Vossebeld[73], A.S. Vovenko[128], N. Vranjes[12a], M. Vranjes Milosavljevic[12a], V. Vrba[125], M. Vreeswijk[105], T. Vu Anh[81], R. Vuillermet[29], I. Vukotic[115], W. Wagner[174], P. Wagner[120], H. Wahlen[174], J. Wakabayashi[101], J. Walbersloh[42], S. Walch[87], J. Walder[71], R. Walker[98], W. Walkowiak[141], R. Wall[175], P. Waller[73], C. Wang[44], H. Wang[172], J. Wang[32d], J.C. Wang[138], S.M. Wang[151], A. Warburton[85], C.P. Ward[27], M. Warsinsky[48], P.M. Watkins[17], A.T. Watson[17], M.F. Watson[17], G. Watts[138], S. Watts[82], A.T. Waugh[150], B.M. Waugh[77], J. Weber[42], M. Weber[129], M.S. Weber[16], P. Weber[54], A.R. Weidberg[118], J. Weingarten[54], C. Weiser[48], H. Wellenstein[22], P.S. Wells[29], M. Wen[47], T. Wenaus[24], S. Wendler[123], Z. Weng[151,r], T. Wengler[29], S. Wenig[29], N. Wermes[20], M. Werner[48], P. Werner[29], M. Werth[163], M. Wessels[58a], K. Whalen[28], S.J. Wheeler-Ellis[163], S.P. Whitaker[21], A. White[7], M.J. White[86], S.R. Whitehead[118], D. Whiteson[163], D. Whittington[61], F. Wicek[115], D. Wicke[174], F.J. Wickens[129], W. Wiedenmann[172], M. Wielers[129], P. Wienemann[20], C. Wiglesworth[73], L.A.M. Wiik[48], A. Wildauer[167], M.A. Wildt[41,p], I. Wilhelm[126], H.G. Wilkens[29], J.Z. Will[98], E. Williams[34], H.H. Williams[120], W. Willis[34], S. Willocq[84], J.A. Wilson[17], M.G. Wilson[143], A. Wilson[87], I. Wingerter-Seez[4], S. Winkelmann[48], F. Winklmeier[29], M. Wittgen[143], M.W. Wolter[38], H. Wolters[124,a,f], G. Wooden[118], B.K. Wosiek[38], J. Wotschack[29], M.J. Woudstra[84], K. Wraight[53], C. Wright[53], B. Wrona[73], S.L. Wu[172], X. Wu[49], Y. Wu[32b], E. Wulf[34], R. Wunstorf[42], B.M. Wynne[45], L. Xaplanteris[9], S. Xella[35], S. Xie[48], Y. Xie[32a], C. Xu[32b], D. Xu[139], G. Xu[32a], B. Yabsley[150], M. Yamada[66], A. Yamamoto[66], K. Yamamoto[64], S. Yamamoto[155], T. Yamamura[155], J. Yamaoka[44], T. Yamazaki[155], Y. Yamazaki[67], Z. Yan[21], H. Yang[87], S. Yang[118], U.K. Yang[82], Y. Yang[61], Y. Yang[32a], Z. Yang[146a,146b], S. Yanush[91], W.-M. Yao[14], Y. Yao[14], Y. Yasu[66], J. Ye[39], S. Ye[24], M. Yilmaz[3c], R. Yoosoofmiya[123], K. Yorita[170], R. Yoshida[5], C. Young[143], S. Youssef[21], D. Yu[24], J. Yu[7], J. Yu[32c,ab], L. Yuan[32a,ac], A. Yurkewicz[148], V.G. Zaets[128], R. Zaidan[63], A.M. Zaitsev[128], Z. Zajacova[29], Yo.K. Zalite[121], L. Zanello[132a,132b], P. Zarzhitsky[39], A. Zaytsev[107], M. Zdrazil[14], C. Zeitnitz[174], M. Zeller[175], P.F. Zema[29], A. Zemla[38], C. Zendler[20], A.V. Zenin[128], O. Zenin[128], T. Ženiš[144a], Z. Zenonos[122a,122b], S. Zenz[14], D. Zerwas[115], G. Zevi della Porta[57], Z. Zhan[32d], D. Zhang[32b], H. Zhang[88], J. Zhang[5], X. Zhang[32d], Z. Zhang[115], L. Zhao[108], T. Zhao[138], Z. Zhao[32b], A. Zhemchugov[65], S. Zheng[32a], J. Zhong[151,ad], B. Zhou[87], N. Zhou[163], Y. Zhou[151], C.G. Zhu[32d], H. Zhu[41], Y. Zhu[172], X. Zhuang[98], V. Zhuravlov[99], D. Zieminska[61], B. Zilka[144a], R. Zimmermann[20], S. Zimmermann[20], S. Zimmermann[48], M. Ziolkowski[141], R. Zitoun[4], L. Živković[34], V.V. Zmouchko[128,*], G. Zobernig[172], A. Zoccoli[19a,19b], Y. Zolnierowski[4], A. Zsenei[29], M. zur Nedden[15], V. Zutshi[106], L. Zwalinski[29]

[1]University at Albany, 1400 Washington Ave, Albany, NY 12222, United States of America

[2]University of Alberta, Department of Physics, Centre for Particle Physics, Edmonton, AB T6G 2G7, Canada

[3]Ankara University[(a)], Faculty of Sciences, Department of Physics, TR 061000 Tandogan, Ankara; Dumlupinar University[(b)], Faculty of Arts and Sciences, Department of Physics, Kutahya; Gazi University[(c)], Faculty of Arts and Sciences, Department of Physics, 06500, Teknikokullar, Ankara; TOBB University of Economics and Technology[(d)], Faculty of Arts and Sciences, Division of Physics, 06560, Sogutozu, Ankara; Turkish Atomic Energy Authority[(e)], 06530, Lodumlu, Ankara, Turkey

[4]LAPP, Université de Savoie, CNRS/IN2P3, Annecy-le-Vieux, France

[5]Argonne National Laboratory, High Energy Physics Division, 9700 S. Cass Avenue, Argonne, IL 60439, United States of America

[6]University of Arizona, Department of Physics, Tucson, AZ 85721, United States of America

[7]The University of Texas at Arlington, Department of Physics, Box 19059, Arlington, TX 76019, United States of America

[8]University of Athens, Nuclear & Particle Physics, Department of Physics, Panepistimiopouli, Zografou, GR 15771 Athens, Greece

[9]National Technical University of Athens, Physics Department, 9-Iroon Polytechniou, GR 15780 Zografou, Greece

[10]Institute of Physics, Azerbaijan Academy of Sciences, H. Javid Avenue 33, AZ 143 Baku, Azerbaijan

[11]Institut de Física d'Altes Energies, IFAE, Edifici Cn, Universitat Autònoma de Barcelona, ES - 08193 Bellaterra (Barcelona), Spain

[12]University of Belgrade[(a)], Institute of Physics, P.O. Box 57, 11001 Belgrade; Vinca Institute of Nuclear Sciences[(b)], M. Petrovica Alasa 12-14, 11000 Belgrade, Serbia

[13]University of Bergen, Department for Physics and Technology, Allegaten 55, NO - 5007 Bergen, Norway

[14]Lawrence Berkeley National Laboratory and University of California, Physics Division, MS50B-6227, 1 Cyclotron Road, Berkeley, CA 94720, United States of America

[15]Humboldt University, Institute of Physics, Berlin, Newtonstr. 15, D-12489 Berlin, Germany

[16] University of Bern, Albert Einstein Center for Fundamental Physics, Laboratory for High Energy Physics, Sidlerstrasse 5, CH - 3012 Bern, Switzerland

[17] University of Birmingham, School of Physics and Astronomy, Edgbaston, Birmingham B15 2TT, United Kingdom

[18] Bogazici University[a], Faculty of Sciences, Department of Physics, TR - 80815 Bebek-Istanbul; Dogus University[b], Faculty of Arts and Sciences, Department of Physics, 34722, Kadikoy, Istanbul; [c]Gaziantep University, Faculty of Engineering, Department of Physics Engineering, 27310, Sehitkamil, Gaziantep; Istanbul Technical University[d], Faculty of Arts and Sciences, Department of Physics, 34469, Maslak, Istanbul, Turkey

[19] INFN Sezione di Bologna[a]; Università di Bologna, Dipartimento di Fisica[b], viale C. Berti Pichat, 6/2, IT - 40127 Bologna, Italy

[20] University of Bonn, Physikalisches Institut, Nussallee 12, D - 53115 Bonn, Germany

[21] Boston University, Department of Physics, 590 Commonwealth Avenue, Boston, MA 02215, United States of America

[22] Brandeis University, Department of Physics, MS057, 415 South Street, Waltham, MA 02454, United States of America

[23] Universidade Federal do Rio De Janeiro, COPPE/EE/IF[a], Caixa Postal 68528, Ilha do Fundao, BR - 21945-970 Rio de Janeiro; [b]Universidade de Sao Paulo, Instituto de Fisica, R.do Matao Trav. R.187, Sao Paulo - SP, 05508 - 900, Brazil

[24] Brookhaven National Laboratory, Physics Department, Bldg. 510A, Upton, NY 11973, United States of America

[25] National Institute of Physics and Nuclear Engineering[a], Str. Atomistilor 407, P.O. Box MG-6, R-077125, Bucharest-Magurele; University Politehnica Bucharest[b], Rectorat - AN 001, 313 Splaiul Independentei, sector 6, 060042 Bucuresti; West University of Timisoara[c], Bd. Vasile Parvan 4, Timisoara, Romania

[26] Universidad de Buenos Aires, FCEyN, Dto. Fisica, Pab I - C. Universitaria, 1428 Buenos Aires, Argentina

[27] University of Cambridge, Cavendish Laboratory, J J Thomson Avenue, Cambridge CB3 0HE, United Kingdom

[28] Carleton University, Department of Physics, 1125 Colonel By Drive, Ottawa ON K1S 5B6, Canada

[29] CERN, CH - 1211 Geneva 23, Switzerland

[30] University of Chicago, Enrico Fermi Institute, 5640 S. Ellis Avenue, Chicago, IL 60637, United States of America

[31] Pontificia Universidad Católica de Chile, Facultad de Fisica, Departamento de Fisica[a], Avda. Vicuna Mackenna 4860, San Joaquin, Santiago; Universidad Técnica Federico Santa María, Departamento de Física[b], Avda. España 1680, Casilla 110-V, Valparaíso, Chile

[32] Institute of High Energy Physics, Chinese Academy of Sciences[a], P.O. Box 918, 19 Yuquan Road, Shijing Shan District, CN - Beijing 100049; University of Science & Technology of China (USTC), Department of Modern Physics[b], Hefei, CN - Anhui 230026; Nanjing University, Department of Physics[c], Nanjing, CN - Jiangsu 210093; Shandong University, High Energy Physics Group[d], Jinan, CN - Shandong 250100, China

[33] Laboratoire de Physique Corpusculaire, Clermont Université, Université Blaise Pascal, CNRS/IN2P3, FR - 63177 Aubiere Cedex, France

[34] Columbia University, Nevis Laboratory, 136 So. Broadway, Irvington, NY 10533, United States of America

[35] University of Copenhagen, Niels Bohr Institute, Blegdamsvej 17, DK - 2100 Kobenhavn 0, Denmark

[36] INFN Gruppo Collegato di Cosenza[a]; Università della Calabria, Dipartimento di Fisica[b], IT-87036 Arcavacata di Rende, Italy

[37] Faculty of Physics and Applied Computer Science of the AGH-University of Science and Technology, (FPACS, AGH-UST), al. Mickiewicza 30, PL-30059 Cracow, Poland

[38] The Henryk Niewodniczanski Institute of Nuclear Physics, Polish Academy of Sciences, ul. Radzikowskiego 152, PL - 31342 Krakow, Poland

[39] Southern Methodist University, Physics Department, 106 Fondren Science Building, Dallas, TX 75275-0175, United States of America

[40] University of Texas at Dallas, 800 West Campbell Road, Richardson, TX 75080-3021, United States of America

[41] DESY, Notkestr. 85, D-22603 Hamburg and Platanenallee 6, D-15738 Zeuthen, Germany

[42] TU Dortmund, Experimentelle Physik IV, DE - 44221 Dortmund, Germany

[43] Technical University Dresden, Institut für Kern- und Teilchenphysik, Zellescher Weg 19, D-01069 Dresden, Germany

[44] Duke University, Department of Physics, Durham, NC 27708, United States of America

[45] University of Edinburgh, School of Physics & Astronomy, James Clerk Maxwell Building, The Kings Buildings, Mayfield Road, Edinburgh EH9 3JZ, United Kingdom

[46] Fachhochschule Wiener Neustadt; Johannes Gutenbergstrasse 3, AT - 2700 Wiener Neustadt, Austria

[47] INFN Laboratori Nazionali di Frascati, via Enrico Fermi 40, IT-00044 Frascati, Italy

[48] Albert-Ludwigs-Universität, Fakultät für Mathematik und Physik, Hermann-Herder Str. 3, D - 79104 Freiburg i.Br., Germany

[49]Université de Genève, Section de Physique, 24 rue Ernest Ansermet, CH - 1211 Geneve 4, Switzerland

[50]INFN Sezione di Genova[(a)]; Università di Genova, Dipartimento di Fisica[(b)], via Dodecaneso 33, IT - 16146 Genova, Italy

[51]Institute of Physics of the Georgian Academy of Sciences, 6 Tamarashvili St., GE - 380077 Tbilisi; Tbilisi State University, HEP Institute, University St. 9, GE - 380086 Tbilisi, Georgia

[52]Justus-Liebig-Universität Giessen, II Physikalisches Institut, Heinrich-Buff Ring 16, D-35392 Giessen, Germany

[53]University of Glasgow, Department of Physics and Astronomy, Glasgow G12 8QQ, United Kingdom

[54]Georg-August-Universität, II. Physikalisches Institut, Friedrich-Hund Platz 1, D-37077 Göttingen, Germany

[55]LPSC, CNRS/IN2P3 and Univ. Joseph Fourier Grenoble, 53 avenue des Martyrs, FR-38026 Grenoble Cedex, France

[56]Hampton University, Department of Physics, Hampton, VA 23668, United States of America

[57]Harvard University, Laboratory for Particle Physics and Cosmology, 18 Hammond Street, Cambridge, MA 02138, United States of America

[58]Ruprecht-Karls-Universität Heidelberg, Kirchhoff-Institut für Physik[(a)], Im Neuenheimer Feld 227, D-69120 Heidelberg; Physikalisches Institut[(b)], Philosophenweg 12, D-69120 Heidelberg; ZITI Ruprecht-Karls-University Heidelberg[(c)], Lehrstuhl für Informatik V, B6, 23-29, DE - 68131 Mannheim, Germany

[59]Hiroshima University, Faculty of Science, 1-3-1 Kagamiyama, Higashihiroshima-shi, JP - 739-8526 Hiroshima, Japan

[60]Hiroshima Institute of Technology, Faculty of Applied Information Science, 2-1-1 Miyake Saeki-ku, Hiroshima-shi, JP - 731-5193 Hiroshima, Japan

[61]Indiana University, Department of Physics, Swain Hall West 117, Bloomington, IN 47405-7105, United States of America

[62]Institut für Astro- und Teilchenphysik, Technikerstrasse 25, A - 6020 Innsbruck, Austria

[63]University of Iowa, 203 Van Allen Hall, Iowa City, IA 52242-1479, United States of America

[64]Iowa State University, Department of Physics and Astronomy, Ames High Energy Physics Group, Ames, IA 50011-3160, United States of America

[65]Joint Institute for Nuclear Research, JINR, Dubna, RU-141980 Moscow Region, Russia

[66]KEK, High Energy Accelerator Research Organization, 1-1 Oho, Tsukuba-shi, Ibaraki-ken 305-0801, Japan

[67]Kobe University, Graduate School of Science, 1-1 Rokkodai-cho, Nada-ku, JP 657-8501 Kobe, Japan

[68]Kyoto University, Faculty of Science, Oiwake-cho, Kitashirakawa, Sakyou-ku, Kyoto-shi, JP - 606-8502 Kyoto, Japan

[69]Kyoto University of Education, 1 Fukakusa, Fujimori, fushimi-ku, Kyoto-shi, JP - 612-8522 Kyoto, Japan

[70]Universidad Nacional de La Plata, FCE, Departamento de Física, IFLP (CONICET-UNLP), C.C. 67, 1900 La Plata, Argentina

[71]Lancaster University, Physics Department, Lancaster LA1 4YB, United Kingdom

[72]INFN Sezione di Lecce[(a)]; Università del Salento, Dipartimento di Fisica[(b)] Via Arnesano, IT - 73100 Lecce, Italy

[73]University of Liverpool, Oliver Lodge Laboratory, P.O. Box 147, Oxford Street, Liverpool L69 3BX, United Kingdom

[74]Jožef Stefan Institute and University of Ljubljana, Department of Physics, SI-1000 Ljubljana, Slovenia

[75]Queen Mary University of London, Department of Physics, Mile End Road, London E1 4NS, United Kingdom

[76]Royal Holloway, University of London, Department of Physics, Egham Hill, Egham, Surrey TW20 0EX, United Kingdom

[77]University College London, Department of Physics and Astronomy, Gower Street, London WC1E 6BT, United Kingdom

[78]Laboratoire de Physique Nucléaire et de Hautes Energies, Université Pierre et Marie Curie (Paris 6), Université Denis Diderot (Paris-7), CNRS/IN2P3, Tour 33, 4 place Jussieu, FR - 75252 Paris Cedex 05, France

[79]Fysiska institutionen, Lunds universitet, Box 118, SE - 221 00 Lund, Sweden

[80]Universidad Autonoma de Madrid, Facultad de Ciencias, Departamento de Fisica Teorica, ES - 28049 Madrid, Spain

[81]Universität Mainz, Institut für Physik, Staudinger Weg 7, DE - 55099 Mainz, Germany

[82]University of Manchester, School of Physics and Astronomy, Manchester M13 9PL, United Kingdom

[83]CPPM, Aix-Marseille Université, CNRS/IN2P3, Marseille, France

[84]University of Massachusetts, Department of Physics, 710 North Pleasant Street, Amherst, MA 01003, United States of America

[85]McGill University, High Energy Physics Group, 3600 University Street, Montreal, Quebec H3A 2T8, Canada

[86]University of Melbourne, School of Physics, Parkville, Victoria AU - 3010, Australia

[87]The University of Michigan, Department of Physics, 2477 Randall Laboratory, 500 East University, Ann Arbor, MI 48109-1120, United States of America

[88]Michigan State University, Department of Physics and Astronomy, High Energy Physics Group, East Lansing, MI 48824-2320, United States of America

[89]INFN Sezione di Milano[(a)]; Università di Milano, Dipartimento di Fisica[(b)], via Celoria 16, IT - 20133 Milano, Italy

[90]B.I. Stepanov Institute of Physics, National Academy of Sciences of Belarus, Independence Avenue 68, Minsk 220072, Republic of Belarus

[91]National Scientific & Educational Centre for Particle & High Energy Physics, NC PHEP BSU, M. Bogdanovich St. 153, Minsk 220040, Republic of Belarus

[92]Massachusetts Institute of Technology, Department of Physics, Room 24-516, Cambridge, MA 02139, United States of America

[93]University of Montreal, Group of Particle Physics, C.P. 6128, Succursale Centre-Ville, Montreal, Quebec, H3C 3J7, Canada

[94]P.N. Lebedev Institute of Physics, Academy of Sciences, Leninsky pr. 53, RU - 117 924 Moscow, Russia

[95]Institute for Theoretical and Experimental Physics (ITEP), B. Cheremushkinskaya ul. 25, RU 117 218 Moscow, Russia

[96]Moscow Engineering & Physics Institute (MEPhI), Kashirskoe Shosse 31, RU - 115409 Moscow, Russia

[97]Lomonosov Moscow State University Skobeltsyn Institute of Nuclear Physics (MSU SINP), 1(2), Leninskie gory, GSP-1, Moscow 119991, Russia

[98]Ludwig-Maximilians-Universität München, Fakultät für Physik, Am Coulombwall 1, DE - 85748 Garching, Germany

[99]Max-Planck-Institut für Physik, Werner-Heisenberg-Institut, Föhringer Ring 6, 80805 München, Germany

[100]Nagasaki Institute of Applied Science, 536 Aba-machi, JP 851-0193 Nagasaki, Japan

[101]Nagoya University, Graduate School of Science, Furo-Cho, Chikusa-ku, Nagoya, 464-8602, Japan

[102]INFN Sezione di Napoli[(a)]; Università di Napoli, Dipartimento di Scienze Fisiche[(b)], Complesso Universitario di Monte Sant'Angelo, via Cinthia, IT - 80126 Napoli, Italy

[103]University of New Mexico, Department of Physics and Astronomy, MSC07 4220, Albuquerque, NM 87131, United States of America

[104]Radboud University Nijmegen/NIKHEF, Department of Experimental High Energy Physics, Heyendaalseweg 135, NL-6525 AJ, Nijmegen, Netherlands

[105]Nikhef National Institute for Subatomic Physics and University of Amsterdam, Science Park 105, 1098 XG Amsterdam, Netherlands

[106]Department of Physics, Northern Illinois University, LaTourette Hall Normal Road, DeKalb, IL 60115, United States of America

[107]Budker Institute of Nuclear Physics (BINP), RU - 630 090 Novosibirsk, Russia

[108]New York University, Department of Physics, 4 Washington Place, New York, NY 10003, United States of America

[109]Ohio State University, 191 West Woodruff Ave, Columbus, OH 43210-1117, United States of America

[110]Okayama University, Faculty of Science, Tsushimanaka 3-1-1, Okayama 700-8530, Japan

[111]University of Oklahoma, Homer L. Dodge Department of Physics and Astronomy, 440 West Brooks, Room 100, Norman, OK 73019-0225, United States of America

[112]Oklahoma State University, Department of Physics, 145 Physical Sciences Building, Stillwater, OK 74078-3072, United States of America

[113]Palacký University, 17.listopadu 50a, 772 07 Olomouc, Czech Republic

[114]University of Oregon, Center for High Energy Physics, Eugene, OR 97403-1274, United States of America

[115]LAL, Univ. Paris-Sud, IN2P3/CNRS, Orsay, France

[116]Osaka University, Graduate School of Science, Machikaneyama-machi 1-1, Toyonaka, Osaka 560-0043, Japan

[117]University of Oslo, Department of Physics, P.O. Box 1048, Blindern, NO - 0316 Oslo 3, Norway

[118]Oxford University, Department of Physics, Denys Wilkinson Building, Keble Road, Oxford OX1 3RH, United Kingdom

[119]INFN Sezione di Pavia[(a)]; Università di Pavia, Dipartimento di Fisica Nucleare e Teorica[(b)], Via Bassi 6, IT-27100 Pavia, Italy

[120]University of Pennsylvania, Department of Physics, High Energy Physics Group, 209 S. 33rd Street, Philadelphia, PA 19104, United States of America

[121]Petersburg Nuclear Physics Institute, RU - 188 300 Gatchina, Russia

[122]INFN Sezione di Pisa[(a)]; Università di Pisa, Dipartimento di Fisica E. Fermi[(b)], Largo B. Pontecorvo 3, IT - 56127 Pisa, Italy

[123]University of Pittsburgh, Department of Physics and Astronomy, 3941 O'Hara Street, Pittsburgh, PA 15260, United States of America

[124]Laboratorio de Instrumentacao e Fisica Experimental de Particulas - LIP[(a)], Avenida Elias Garcia 14-1, PT - 1000-149 Lisboa, Portugal; Universidad de Granada, Departamento de Fisica Teorica y del Cosmos and CAFPE[(b)], E-18071 Granada, Spain

[125] Institute of Physics, Academy of Sciences of the Czech Republic, Na Slovance 2, CZ - 18221 Praha 8, Czech Republic

[126] Charles University in Prague, Faculty of Mathematics and Physics, Institute of Particle and Nuclear Physics, V Holesovickach 2, CZ - 18000 Praha 8, Czech Republic

[127] Czech Technical University in Prague, Zikova 4, CZ - 166 35 Praha 6, Czech Republic

[128] State Research Center Institute for High Energy Physics, Moscow Region, 142281, Protvino, Pobeda street, 1, Russia

[129] Rutherford Appleton Laboratory, Science and Technology Facilities Council, Harwell Science and Innovation Campus, Didcot OX11 0QX, United Kingdom

[130] University of Regina, Physics Department, Regina, Canada

[131] Ritsumeikan University, Noji Higashi 1 chome 1-1, JP - 525-8577 Kusatsu, Shiga, Japan

[132] INFN Sezione di Roma I[(a)]; Università La Sapienza, Dipartimento di Fisica[(b)], Piazzale A. Moro 2, IT- 00185 Roma, Italy

[133] INFN Sezione di Roma Tor Vergata[(a)]; Università di Roma Tor Vergata, Dipartimento di Fisica[(b)], via della Ricerca Scientifica, IT-00133 Roma, Italy

[134] INFN Sezione di Roma Tre[(a)]; Università Roma Tre, Dipartimento di Fisica[(b)], via della Vasca Navale 84, IT-00146 Roma, Italy

[135] Réseau Universitaire de Physique des Hautes Energies (RUPHE): Université Hassan II, Faculté des Sciences Ain Chock[(a)], B.P. 5366, MA - Casablanca; Centre National de l'Energie des Sciences Techniques Nucleaires (CNESTEN)[(b)], B.P. 1382 R.P. 10001 Rabat 10001; Université Mohamed Premier[(c)], LPTPM, Faculté des Sciences, B.P.717. Bd. Mohamed VI, 60000, Oujda; Université Mohammed V, Faculté des Sciences[(d)], 4 Avenue Ibn Battouta, BP 1014 RP, 10000 Rabat, Morocco

[136] CEA, DSM/IRFU, Centre d'Etudes de Saclay, FR - 91191 Gif-sur-Yvette, France

[137] University of California Santa Cruz, Santa Cruz Institute for Particle Physics (SCIPP), Santa Cruz, CA 95064, United States of America

[138] University of Washington, Seattle, Department of Physics, Box 351560, Seattle, WA 98195-1560, United States of America

[139] University of Sheffield, Department of Physics & Astronomy, Hounsfield Road, Sheffield S3 7RH, United Kingdom

[140] Shinshu University, Department of Physics, Faculty of Science, 3-1-1 Asahi, Matsumoto-shi, JP - 390-8621 Nagano, Japan

[141] Universität Siegen, Fachbereich Physik, D 57068 Siegen, Germany

[142] Simon Fraser University, Department of Physics, 8888 University Drive, Burnaby, BC V5A 1S6, Canada

[143] SLAC National Accelerator Laboratory, Stanford, California 94309, United States of America

[144] Comenius University, Faculty of Mathematics, Physics & Informatics[(a)], Mlynska dolina F2, SK - 84248 Bratislava; Institute of Experimental Physics of the Slovak Academy of Sciences, Dept. of Subnuclear Physics[(b)], Watsonova 47, SK - 04353 Kosice, Slovak Republic

[145] [(a)]University of Johannesburg, Department of Physics, PO Box 524, Auckland Park, Johannesburg 2006; [(b)]School of Physics, University of the Witwatersrand, Private Bag 3, Wits 2050, Johannesburg, South Africa

[146] Stockholm University, Department of Physics[(a)]; The Oskar Klein Centre[(b)], AlbaNova, SE - 106 91 Stockholm, Sweden

[147] Royal Institute of Technology (KTH), Physics Department, SE - 106 91 Stockholm, Sweden

[148] Stony Brook University, Department of Physics and Astronomy, Nicolls Road, Stony Brook, NY 11794-3800, United States of America

[149] University of Sussex, Department of Physics and Astronomy Pevensey, 2 Building, Falmer, Brighton BN1 9QH, United Kingdom

[150] University of Sydney, School of Physics, AU - 2006 Sydney NSW, Australia

[151] Insitute of Physics, Academia Sinica, TW - 11529 Taipei, Taiwan

[152] Technion, Israel Inst. of Technology, Department of Physics, Technion City, IL - 32000 Haifa, Israel

[153] Tel Aviv University, Raymond and Beverly Sackler School of Physics and Astronomy, Ramat Aviv, IL - 69978 Tel Aviv, Israel

[154] Aristotle University of Thessaloniki, Faculty of Science, Department of Physics, Division of Nuclear & Particle Physics, University Campus, GR - 54124, Thessaloniki, Greece

[155] The University of Tokyo, International Center for Elementary Particle Physics and Department of Physics, 7-3-1 Hongo, Bunkyo-ku, JP - 113-0033 Tokyo, Japan

[156] Tokyo Metropolitan University, Graduate School of Science and Technology, 1-1 Minami-Osawa, Hachioji, Tokyo 192-0397, Japan

[157]Tokyo Institute of Technology, Department of Physics, 2-12-1 O-Okayama, Meguro, Tokyo 152-8551, Japan

[158]University of Toronto, Department of Physics, 60 Saint George Street, Toronto M5S 1A7, Ontario, Canada

[159]TRIUMF[(a)], 4004 Wesbrook Mall, Vancouver, B.C. V6T 2A3; [(b)]York University, Department of Physics and Astronomy, 4700 Keele St., Toronto, Ontario, M3J 1P3, Canada

[160]University of Tsukuba, Institute of Pure and Applied Sciences, 1-1-1 Tennoudai, Tsukuba-shi, JP - 305-8571 Ibaraki, Japan

[161]Tufts University, Science & Technology Center, 4 Colby Street, Medford, MA 02155, United States of America

[162]Universidad Antonio Narino, Centro de Investigaciones, Cra 3 Este No.47A-15, Bogota, Colombia

[163]University of California, Department of Physics & Astronomy, Irvine, CA 92697-4575, United States of America

[164]INFN Gruppo Collegato di Udine[(a)], IT - 33100 Udine; ICTP[(b)], Strada Costiera 11, IT-34014, Trieste; Università di Udine, Dipartimento di Fisica[(c)], via delle Scienze 208, IT - 33100 Udine, Italy

[165]University of Illinois, Department of Physics, 1110 West Green Street, Urbana, Illinois 61801, United States of America

[166]University of Uppsala, Department of Physics and Astronomy, P.O. Box 516, SE -751 20 Uppsala, Sweden

[167]Instituto de Física Corpuscular (IFIC) Centro Mixto UVEG-CSIC, Apdo. 22085 ES-46071 Valencia, Dept. Física At. Mol. y Nuclear; Dept. Ing. Electrónica; Univ. of Valencia, and Inst. de Microelectrónica de Barcelona (IMB-CNM-CSIC), 08193 Bellaterra, Spain

[168]University of British Columbia, Department of Physics, 6224 Agricultural Road, Vancouver, B.C. V6T 1Z1, Canada

[169]University of Victoria, Department of Physics and Astronomy, P.O. Box 3055, Victoria B.C., V8W 3P6, Canada

[170]Waseda University, WISE, 3-4-1 Okubo, Shinjuku-ku, Tokyo, 169-8555, Japan

[171]The Weizmann Institute of Science, Department of Particle Physics, P.O. Box 26, IL - 76100 Rehovot, Israel

[172]University of Wisconsin, Department of Physics, 1150 University Avenue, Madison, WI 53706, United States of America

[173]Julius-Maximilians-University of Würzburg, Physikalisches Institut, Am Hubland, 97074 Würzburg, Germany

[174]Bergische Universität, Fachbereich C, Physik, Postfach 100127, Gauss-Strasse 20, D- 42097 Wuppertal, Germany

[175]Yale University, Department of Physics, PO Box 208121, New Haven, CT, 06520-8121, United States of America

[176]Yerevan Physics Institute, Alikhanian Brothers Street 2, AM - 375036 Yerevan, Armenia

[177]Centre de Calcul CNRS/IN2P3, Domaine scientifique de la Doua, 27 bd du 11 Novembre 1918, 69622 Villeurbanne Cedex, France

[a]Also at LIP, Portugal.

[b]Also at Faculdade de Ciencias, Universidade de Lisboa, Lisboa, Portugal.

[c]Also at CPPM, Marseille, France.

[d]Also at TRIUMF, Vancouver, Canada.

[e]Also at FPACS, AGH-UST, Cracow, Poland.

[f]Also at Department of Physics, University of Coimbra, Coimbra, Portugal.

[g]Also at Università di Napoli Parthenope, Napoli, Italy.

[h]Also at Institute of Particle Physics (IPP), Canada.

[i]Also at Louisiana Tech University, Ruston, USA.

[j]Also at Universidade de Lisboa, Lisboa, Portugal.

[k]At California State University, Fresno, USA.

[l]Also at Faculdade de Ciencias, Universidade de Lisboa and at Centro de Fisica Nuclear da Universidade de Lisboa, Lisboa, Portugal.

[m]Also at California Institute of Technology, Pasadena, USA.

[n]Also at University of Montreal, Montreal, Canada.

[o]Also at Baku Institute of Physics, Baku, Azerbaijan.

[p]Also at Institut für Experimentalphysik, Universität Hamburg, Hamburg, Germany.

[q]Also at Manhattan College, New York, USA.

[r]Also at School of Physics and Engineering, Sun Yat-sen University, Guangzhou, China.

[s]Also at Taiwan Tier-1, ASGC, Academia Sinica, Taipei, Taiwan.

[t]Also at School of Physics, Shandong University, Jinan, China.

[u]Also at Rutherford Appleton Laboratory, Didcot, UK.

[v]Also at Departamento de Fisica, Universidade de Minho, Braga, Portugal.

[w]Also at Department of Physics and Astronomy, University of South Carolina, Columbia, USA.

[x]Also at KFKI Research Institute for Particle and Nuclear Physics, Budapest, Hungary.

[y] Also at Institute of Physics, Jagiellonian University, Cracow, Poland.

[z] Also at Centro de Fisica Nuclear da Universidade de Lisboa, Lisboa, Portugal.

[aa] Also at Department of Physics, Oxford University, Oxford, UK.

[ab] Also at CEA, Gif sur Yvette, France.

[ac] Also at LPNHE, Paris, France.

[ad] Also at Nanjing University, Nanjing Jiangsu, China.

[*] Deceased.